TAMPEREEN TEKNILLINEN YLIOPISTO
TAMPERE UNIVERSITY OF TECHNOLOGY

AMIR, MEHMAN SEFAT AND DAMOON, MOHAMADI
SMALL SCALE COMPRESSED AIR ENERGY STORAGE

Master of Science thesis

ABSTRACT

Electrical Energy is what drives the modern word and storing it has always been a necessity since the source is not always available when the energy is needed. Nowadays with this boom of utilizing renewable energy sources the need is felt more than ever regarding significantly intermittent behavior of these energy sources such as wind and sunlight. Different tools have been employed for that purpose with different efficiencies and capacities. Compressed Air Energy Storage (CAES) is one of the promising technologies and being able to use it in small scales offers a lot of opportunities. In this thesis work, a Small Scale Compressed Air Energy Storage (SC-CAES) is designed, built and simulated. The steps taken to build and control this prototype as well as simulating it are reported thoroughly in this work and later on proper experiments are conducted to investigate compliance of the data acquired by the experiments with simulation results. The outcomes of the comparisons are discussed to state the possibility of using the simulation method for studying machines of the same category without building an actual prototype.

In order to measure the important features of the system including the efficiency and capacity as well as its limitations, suitable experiments are also designed and carried out. During the experiments several iterations were made in order to reach the best control algorithm for highest efficiency and agility. Ultimately the prototype proved capable of delivering efficiencies as high as 39 % which is significant for a diabatic SC-CAES. The final results and the thoroughly explained procedure can be used as guidelines for design, simulation and building of similar systems of the same category.

PREFACE

This Master's thesis is a project defined and financed by Tukisäätiö. and Tampere University of Technology.

As a part of this work a complete machine was designed and built for the target experiments. The Major challenges in this work were the numerous practical details and iterations that are usually parts of making a prototype during an R&D project. For each and every one of this challenges multiple approaches were examined in order the select the one that satisfies the criteria of this study. This document covers only the final satisfactory iterations and at the very most only reflects half of the work done to make this study possible.

This work would not be possible if it was not for the great team work between the writers of this thesis. It was impossible to work on so may weekends and those 12h days if there was only the smallest amount phase-shift in the team. We want to acknowledge that we are proud of our team and feel very lucky to have found the perfect colleague.

Also this long journey would not lead to any useful result if it was not for the presence of precious people who supported this project in different ways. The supervisors of this project Prof. Reza Ghabcheloo and Prof. Seppo Tikkanen who provided us with their unconditional support and guidance. Mr. Mats Manderbacka, who initiated this innovative idea and supported this work with his technical insight and his inspiring attitude. Mr. Juhani Tervanen the patient and helpful lab assistant who made the practicalities a whole lot easier.

Most importantly two individuals living thousands of kilometers away from their homes could not survive this much of pressure over this long period of time if it was not for the love and support of their families. A direct shout out to Amir's wife who took care of their very recent marriage matters almost single-handedly so Amir can have all of his energy for this work and also his parents who always supported their son. And kudos to Damoon's mom for keeping his son filled with energy by her constant encouragements.

We will love you till the last breath.

  Damoon and Amir Tampere, 20.06.2018

CONTENTS

LIST OF FIGURES

LIST OF TABLES

LIST OF ABBREVIATIONS AND SYMBOLS

AA-CAES	Advanced Adiabatic Compressed Air Energy Storage
CAES	Compressed Air Energy Storage
CM	Consumer Module
CoM	Center of Mass
Eq	Equation
ESS	Energy Storage System
FES	Flywheel Energy Storage
GPIO	General Purpose Input Output
HPDV	High Pressure Discharge Valve
MCP	Maximum Charge Phase
PHS	Pumped Hydrostatic Storage
P&ID	Piping and Instrumentation Diagram
PWM	Pulse Width Modulation
RPI	Raspberry Pi
ROS	Robotic Operating System
rpm	revolotion per minute
SC-CAES	Small Scale Compressed Air Energy Storage
SSI	Synchronous Serial Interface
TF	Transfer Function
TUT	Tampere University of Technology
UPS	Uninterruptible Power Supply
VBV	Vacuum Breaker Valve
a	acceleration

A_A	Chamber A effective Area
A_B	Chamber B effective Area
A_r	Piston Rod Section Area
b	Critical Back-Pressure Ratio
C	Sonic Conductance
C_v	Specifc Heat at Constant Volume
F_f	Sonic Conductance
F	force
k	the Specific Heat Ratio
m	Subsonic Index
$\dot{m}_{in}$	Input Mass Flow
$\dot{m}_{out}$	Output Mass Flow
M_L	Load Mass
M_p	Piston and Rod assembly Mass
p_A	Chamber A absolute pressure
p_B	Chamber B absolute pressure
p_a	Atmosphere absolute pressure
p_d	Downstream Pressure
p_u	Upstream Pressure
q_{in}	Input Heat (J)
q_{out}	Output Heat (J)
q_m	Mass Flow Rate
R	Ideal Gas Constant $(287 J/(kg°K)$
T	Temperature of the gas inside the Chamber
T_{in}	Temperature of the incoming gas flow
T_u	Upstream Temperature
$\dot{U}$	the change of Internal Energy
$\dot{W}$	rate of change in the work
x	Piston Position
ρ	Density of the gas inside the chamber kg/m^3
ρ_0	Mass Density in standard conditions (ANR)
Δp_c	Cracking Pressure

1. INTRODUCTION

This chapter serves as wholistic glimpse on the works done in this study by describing the driving incentive behind this work as well as the target goals. Also here a general layout of the work is provided to help the reader in understanding the sequence of steps and also the outcomes.

Storing Electrical energy have been the subject of many researches during few past years since more and more clean, cheap however not very stable renewable energy sources are being introduced to the market. With a proper storage option the excess energy produced during off-peak hours can be used for peak shaving thus reducing the total required capacity for the grid. For this purpose only two technologies has been implemented commercially so far, Pumped Hydrostatic Storage (PHS) and Compressed Air Energy Storage (CAES). As much as 99% of the world's storage capacity is done by the former with a total of 127-129 GW all around the world. The latter technology is implementable in a wide range of scales which can deliver up to 100MW+ of power per unit. [17]

A CAES plant use excessive energy of the grid to run compressors in order to compress the air and store it a reservoir. Later on during peak periods the energy of stored compressed air is returned to the grid using an expander (e.g. a turbine) coupled with a generator. Other than power-plants which use this technology, developments has been carried out in order make this type of storage possible in smaller scales for a more distributed solution. A brief introduction to present energy storage technologies followed by detailed review on developments in CAES technology in different sizes will be covered in chapter 2.

1.1   Objectives and Scope

Target objectives and questions devised by Mr. Mats Manderbacka and Tampere University of Technology (TUT) are as Follows:

- Design and build a Small Scale Compressed Air Energy Storage (SC-CAES) prototype using available standard pneumatic components.

Figure 1.1 *Magni Solidworks Assembly*

- Investigate the possibility of simulating the prototype in order to expand the scope of the study to similar machines e.g with more modules and higher capacity.

- Measure the capacity and efficiency of the proptotype.

The subject of this study is a reciprocating air compressor/expander that is consisted of three double action pneumatic cylinders in a triangular configuration, figure 1.1. This study goes through the stages of designing this machine , building and developing a control algorithm for the system. In order to prevent confusion and refrain from repeating the generic words like "machine", "motor/compressor", etc., it is named Magni[1] and is going to addressed with this name hereafter.

1.2 Road Map

The main idea of this thesis is to build an actual SC-CAES in order to experiment different scenarios of storing and recovering energy with this technology and give the reader first hand information about the possibility of having this type of storage in small scales e.g. for households or small workshops. Figure 1.2 shows the main tasks done in this study as well as their order of implementation. After reviewing current developments of CAES and SC-CAES technologies in chapter 2, the design

---

[1]Initially this machine was intended to work together with a special wind turbine so the name "Magni", god of strength and son of Thor, god of thunder in Nordic mythology was selected for it.
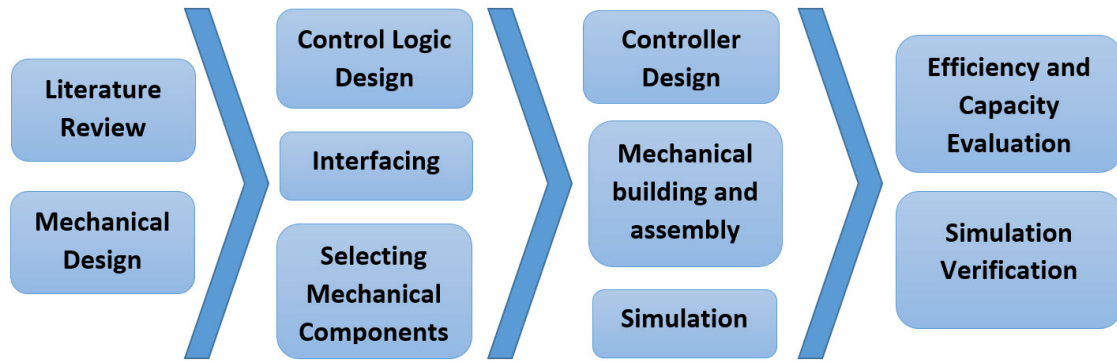
Figure 1.2 *Overview of the main tasks*

process and component selection as well as the basic control logic with which Magni is controlled are presented in chapter 3. In the same chapter implementation of the design is also covered without going through the details. Chapter 4 goes through the process of establishing a connection between the control algorithm and the actual hardware so machine states can be properly read and logged and also the logic can control the hardware based on its input data.

For any machine to work properly and have the desirable behavior, a proper controller design is necessary in addition to the basic control logic. This matter for Magni along with the goals and strategies are explained thoroughly in chapter 5. In the same chapter some basic tests are also reported to present the desirable performance of the designed controller. Process of simulating Magni, software chosen and the selected approach are reviewed in chapter 6 where some of the simulation results are compared with the test results for the purpose of validation.

In chapter 7 the efficiency of Magni is measured through multiple experiments done with different inputs and in different conditions. The same chapter evaluates success rate of this study towards its goal as well as assessing the suitability of the approach for implementing a working SC-CAES system.

2.   COMPRESSED AIR ENERGY STORAGE

The relationship of human with different resources have always followed the same path of discovering it, looking for different ways to obtain it and devising plans to store it for later use. The same process has always happened and is happening to food, water, minerals, etc. Energy as one of the most important resources, if not the most, is no exception and from the very moment of discovering, man was looking for ways to store it so they can use it at the right time. Electrical energy in particular as the most flexible form of energy, the driver of the industry and the fuel for the modern world's engine, is the main concern for technology developers researching the new, more efficient and less expensive approaches to stockpile this valuable resource.

This concern has grown into a fever during the last years as a result of recent advancements in renewable energy technologies. Energies such as wind, wave power and sunlight are provided cost-less as courtesies from our resourceful and generous environment and harnessing them is becoming more effective and abundant day by day. The main issue is that these free energy sources are not presented exactly when they are needed. For instance, high wind is not always available to wind turbines exactly during high demand periods. The other renewable sources share the same undesirable intermittent behavior which signifies the importance of man's ability to store them effectively. Further details concerning the necessity and applications of Energy Storage Systems (ESSs) is found in the works of researchers Zakeri et al. [24] and Luo et al. [16].

This chapter reviews the most common ESSs followed by thorough elaboration about SC-CAES which is the main subject of this work. Figure 2.1 shows sample pictures of these technologies.

(a) Batteries (b) PHS (c) Flywheel
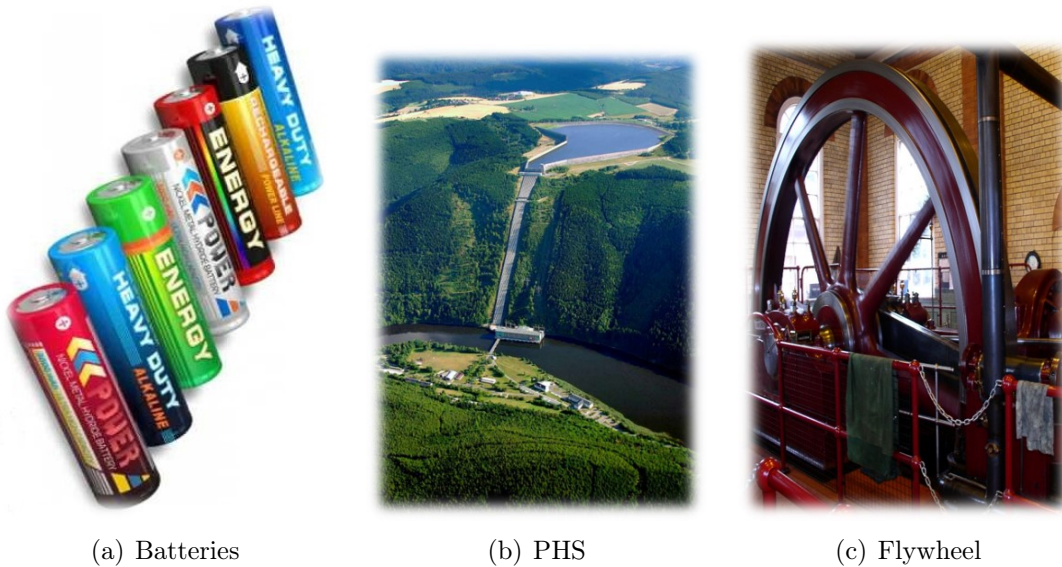
Figure 2.1 *Samples of common ESSs*

2.1 Energy Storage Technologies

Rechargeable Batteries

Batteries are energy containers that almost all the people encounter in day to day life. They are enclosures that keep chemically active substances and produce energy as their contents react to each other. Various technologies have employed this concept to develop different types of batteries each one with its own specific characteristics. The working principles of this technologies and their differences does not fit into the scope of this study therefore elaborated details can be reviewed in [7–9, 13, 18, 23]

Pumped Hydrostatic Storage

PHS has been around for many years and its technology has matured through time. By 2012, 127-129GW of this ESS was installed worldwide which translates to 99% of the total storage and 3% of power generation at the time [3, 6, 10]. The working principle is relatively simple, it consists of two large water reservoirs e.g. the ones on both sides of a dam, during the storing period the water is pumped to the reservoir with higher altitude and during the release stage the stored water is let to flow downwards to the lower tank while passing through hydro-turbines which capture its energy.

Flywheel Energy Storage

Flywheels use a very intuitive method to store energy, turning it to the inertia of a heavy rotating mass i.e. reserved kinetic energy. Nowadays using vacuum chambers and magnetic bearings have improved the efficiency of this technology significantly. [21]

Compressed Air Energy Storage

Besides PHS, CAES is the only technology until the date that has commercially provided outputs over 100MW. The main form of stored energy this technology benefits from is pressurized air. A CAES plant uses excessive energy of the grid to run compressors in order to store high pressure air in a reservoir. Later on during peak periods the energy of stored compressed air is returned to the grid using an expander, e.g. a turbine, coupled with a generator. Throughout the next sections the working principle, advancements of this technology and the operating instances are covered in detail.

2.1.1 Overall Comparison

Each of the ESS technologies has its specific features regarding, capacity, power range, efficiency, availability, capital investment, per KW cost, etc. Table 2.1 summarizes only the main technical properties based on the work done by Zakeri et al. [24] and Luo et al. [16]. Each of the technologies has its own pros and cons and limitations furthermore for different applications, situations and geographical locations certain options are more suitable.

Table 2.1 Summary of most common operational ESS technologies

Technology	Power Range (MW)	Round Trip Efficiency	Discharge time (m, h)	Life time (cycles)
PHS	10-5000	0.70-0.82	1-24 h	20,000-50,000
Batteries	Up to 100	0.60-0.95	Up to 10 h	2,000-13,0000
Flywheel	Up to 0.25	0.93-0.95	Up to 15m	20,000-100,000
CAES	3-400	0.42-0.70	1-24 h	>13,000
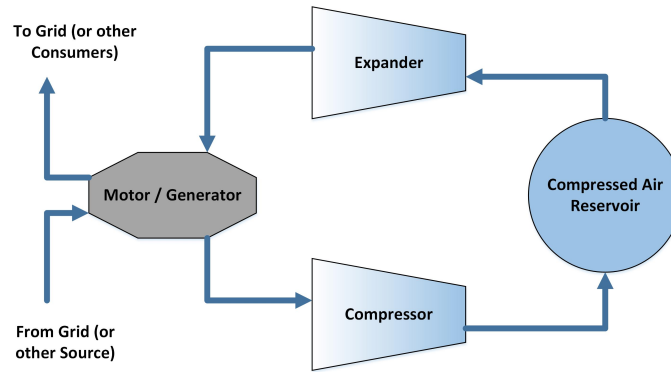
Figure 2.2 Basic working principle of a CAES

2.2 Compressed Air Energy Storage

The main idea behind energy storage with a CAES was covered in previous section. More details concerning the working principles, variations, working instances and ongoing research is explained in this part.

2.2.1 Basic Pinciples

A CAES plant uses excessive energy provided by the grid or other sources to run compressor(s) that store high pressure air in a reservoir. Later on during peak periods the energy of stored compressed air is recovered using an expander (e.g. a turbine) coupled with a generator or other type of consumer. Figure 2.2 illustrates this process in a simple manner. In some cases the expander and the compressor are coupled with different machines however the process is the same.

Current plants dissipate the generated heat during the compression mode and reheat the air for expansion mode which lowers their efficiency significantly. Furthermore a proposed improvement under the name Advanced Adiabatic Compressed Air Energy Storage (AA-CAES) is being studied which aims to store the generated heat, figure 2.3, during storage phase in special heat reservoirs and reuse it for power generation phase thus improving the total efficiency significantly. [17]

2.2.2 Working Instances

The only grid scale and commercialized CAES plants were commissioned at Huntorf, Germany in 1978 and McIntosh, Alabama, US in 1991. Both of these plants use natural gas in order to preheat the air during their power generation modes which is why their round-trip efficiencies do not exceed 42% and 54% respectively. [17]
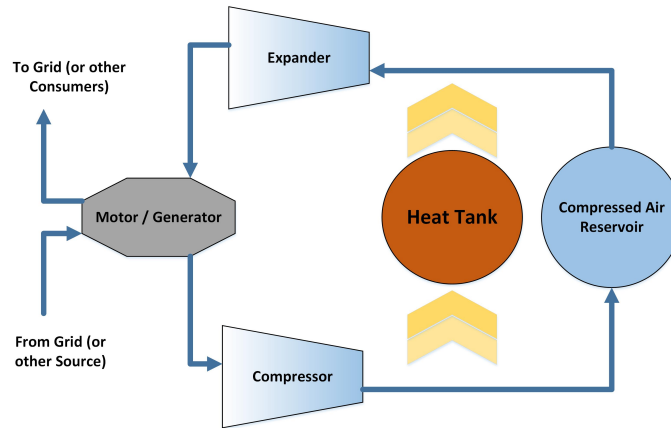
Figure **2.3** *Basic working principle of a AA-CAES*

Two Salt caverns are used in Huntorf plant as reservoirs which contain air with pressures ranging from 4.8 MPa to 6.6 Mpa [5,7,20]. This plant charges its reservoirs during an 8 hour period for each cycle and provides up to 290 MW of power for 2 hours [7].The newer McIntosh CAES uses a single salt dome cavern and the storing pressure ranges from 4.5 MPa to 7.4 Mpa [7,20,22]. The plant is able to output its full capacity of 110 MW for up to 26 hours continuously [7,22].

Both of these power-plants use centrifugal compressors to deliver the compressed air to their tanks and utilize gas-turbines which not only expand the stored air but also add heat to it via burning fuel during the power generation stage. The main difference is, in McIntosh a heat recuperator is present which employs a portion of the exhaust heat, to preheat the feed of the turbine. Figure 2.4 shows the location of these plants as well as the schematics of the one in Alabama to highlight the difference.

In addition to these high capacity plants the British Company Energetix[TM]is working on new type of small back up electricity source using a combination of a CAES and a super-capacitor pack which they call Compressed Air Battery (CAB) [17]. The Energetix group has eliminated the need for common traditional lead-acid batteries in a number of pilot telecom stations and data centers by providing them with this Air Battery Uninterruptible Power Supplys (UPSs). These systems use the utility high pressure air which is usually provided at these stations as the means to store the energy. They claim to provide a variety of UPS solutions up to 10 kW. The main component of their system is a scroll expander which converts the potential energy of compressed air to rotary motion that drives a DC generator. Using High speed valves their expander-generator starts to generate DC electricity in less than 50 ms. Since the UPS is usually used to back up sensitive equipment the 50ms interruption

(a) Huntorf CAES plant

(b) McIntosh CAES plant
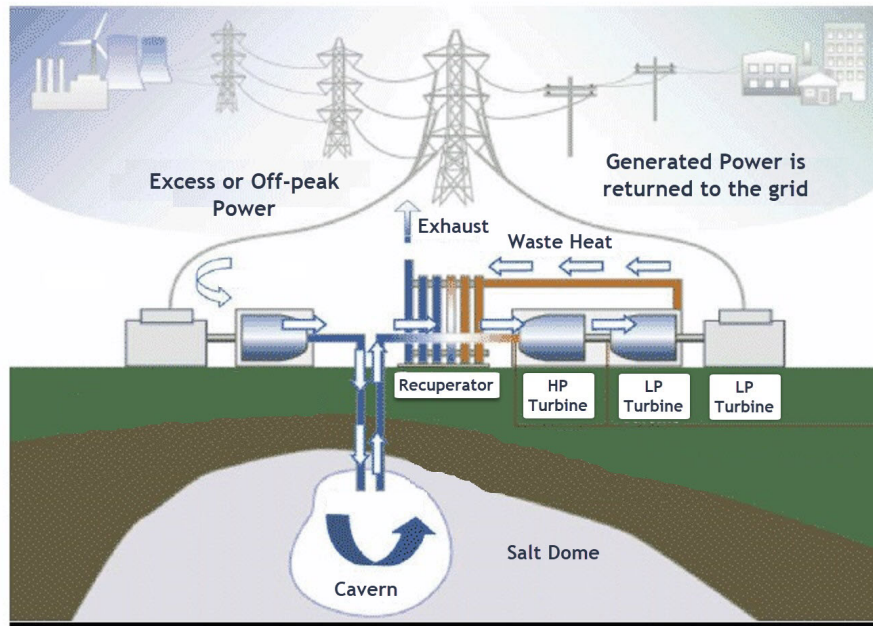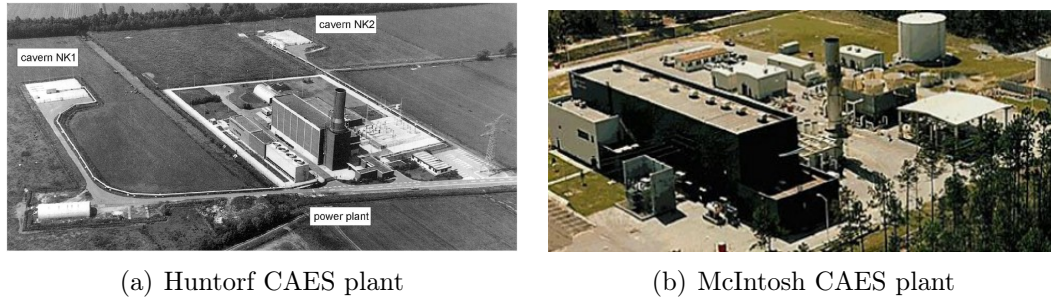
(c) Schematics of McIntosh plant

Figure 2.4 *Commissioned grid scale CAES plants*

in power supply is still too long which is why they have added enough capacitance to the system to keep the voltage high in case of power outage until the expander reaches the target speed and starts generating. [11]

The Air-Battery package is consisted of components which are far less sensitive comparing to batteries which is why the system can be stored outside without the need for expensive enclosures. To verify this theory the systems were exposed to temperature fluctuations from -40°C to +50°C for a number of weeks [11]. According to these numbers this type of batteries are far less sensitive comparing to traditional batteries. The Energetix Air-Battery is only half of a CAES system which converts already compressed air to electricity however research on making a complete CAES system with small dimensions is ongoing.

2.3   Under Development Instances

Jannelli et al. go through the design of a SC-CAES for a radio base station. They considered three rotary compressors with inter-cooling as their compression unit, and two turbines with inter-heating as their expansion unit. The design uses Heat tanks to store the heat energy separately which puts their work in AA-CAES category. Interestingly the designed system provides cool air, which is the by-product of the expansion process, for telecom systems' cooling demands. This design claim to deliver a 57% round-trip efficiency which is a high number considering the size and comparing to the operational plants. [12]

Moreover in a very interesting study Krupke et al. study a hybrid system consist of a small CAES system in combination with a wind turbine which was simulated and tested later on. This work proposes a remedy for fluctuations in electricity provided by wind turbines due to variability of wind power. The main difference of their design is they use a single generator/motor instead of a generator and an electrical-motor which will directly lead to lower costs and simpler revolotion per minute (rpm) regulation. Also the proposed solution utilizes only one scroll expander/compressor instead of individual compression and expansion units which directly contributes to lower costs and a simpler design. [14]

2.4   Future of CAES

Advent of renewable energy harnessing technologies has surely provided mankind with hopes of a cleaner and greener earth in the future however they come with their own set of challenges. One of the most important ones is that they are not available on demand. Energy Storage technologies such as CAES will cover that flaw effectively. Having CAES plants in small scales will surely provide us with the opportunity to store that cheap energy in as many nodes as necessary in a grid thus reducing the grid capacity requirements as well as lowering the transfer losses significantly.

3. DESIGN AND IMPELEMENTATION

For the purpose of this study a prototype was needed to test the possibility of storing energy in form of compressed air and recovering it with the same machine. As explained in chapter 2 there are multiple instances where such a machine is needed i.e. a wind-turbine that needs to be run at a certain rpm to deliver the highest possible efficiency. In this example fluctuations in wind power cannot be easily copped with e.g. when there is too much wind and the demand from the grid is low, firstly the generator coupled with the turbine will not provide enough resisting torque to maintain the target rpm and secondly the free wind energy cannot be fully captured. The same windmill when the wind is too slow faces a low rpm situation. A CAES system added to this turbine can both keep it from over-speeding and helping it not to fall to low rpm thus extending the operating wind speed range. This means the subject wind-turbine can operate more hours per day and captures more of the wind power.

In order to maintain the generality of the work, the energy interface of Magni with its energy source is defined as angular velocity and torque. In other words regardless of how the the main shaft is being rotated, the significant parameters to measure and evaluate are the rpm and torque. The rotation will always be in the same direction however the torque can be positive when Magni is generating power from the stored compressed air or negative when it is absorbing energy and storing it. The following abilities and conditions were defined as baselines to design this prototype:

- Can compress ambient air thus store the input energy in form of pressurized air.

- Can expand the compressed air and harness its energy in the process.

- Able to adjust its braking or driving torque according to the torque already present on the main shaft thus maintaining a certain rpm.

- Must be built using regular standard components since this machine is a prototype and time and financial resources for this study are limited.
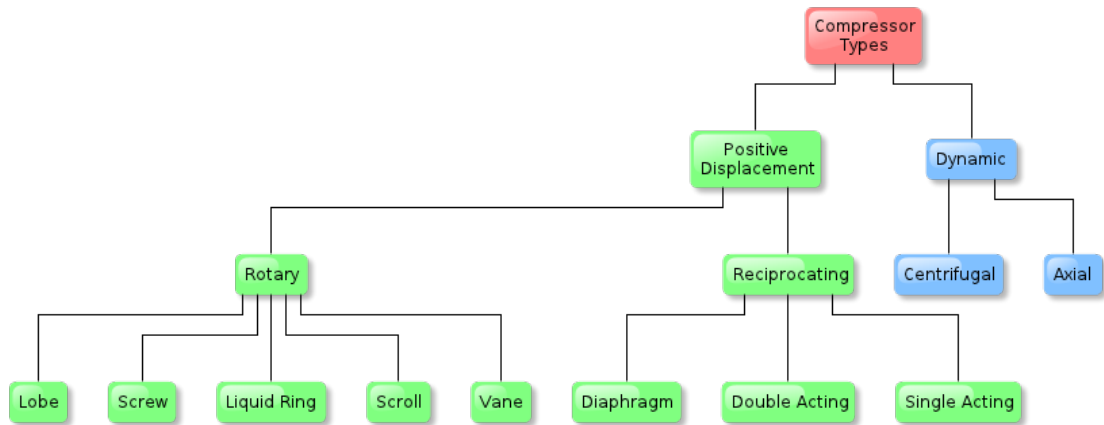
Figure 3.1 *Types of gas compressors*

Gas compressors have been around for several years and there are many types of them, figure 3.1, however for this study reciprocating type is selected for the following reasons:

- Their construction is fairly simple and building one does not need coping with too tight manufacturing tolerances.

- The basic control logic is straightforward and can be implemented by controlling the valve timings.

- The necessary components for this type are easily accessible on the market.

- This type can seamlessly switch between expanding and compressing modes if controlled intelligently enough.

3.1 Number of Cylinders and their Layout

It is decided to have three cylinders connected to Magni's crankshaft since with 120°phase[1] difference between each two of them the generated torque is distributed perfectly with this number of cylinders. later on selecting double acting cylinders with two chambers each, resulted in six chambers as sources of absorbing or generating torque.

One solution to make the phase-shifts possible was to connect all the cylinders' ends to one rod and have a crankshaft with cranks that have 120°angles with respect to

---

[1]The definition of phase is explained in detail in 3.2.1
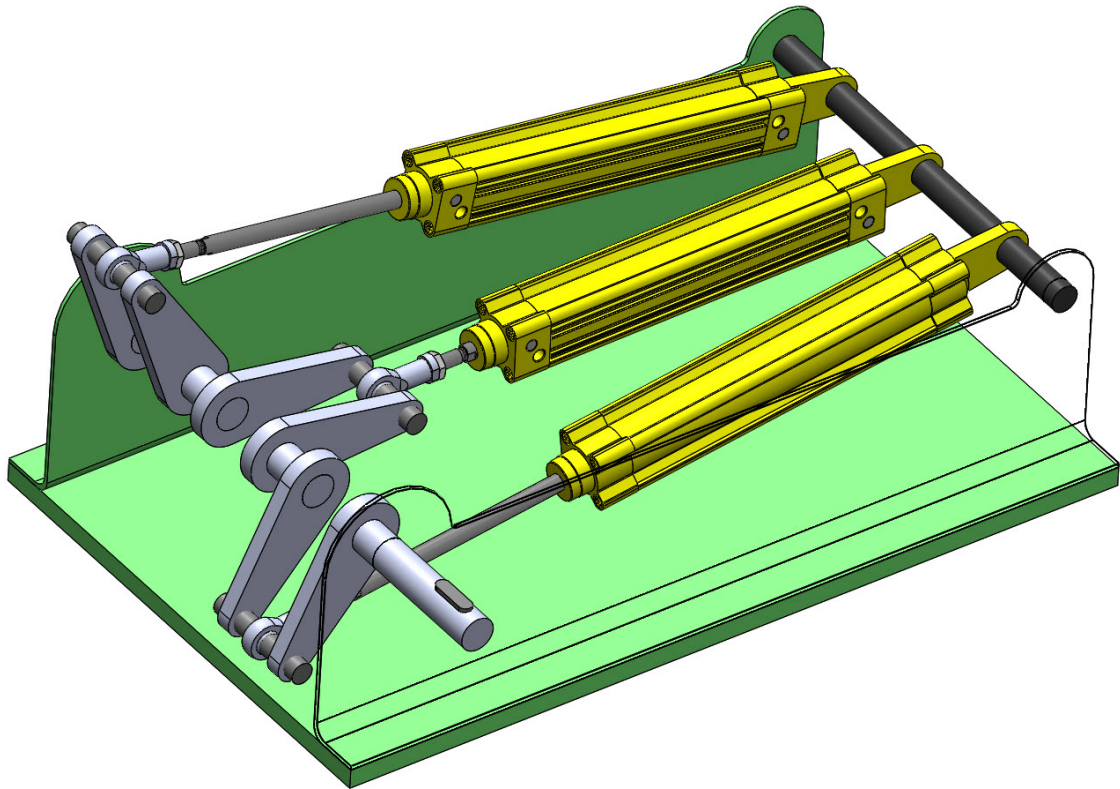
Figure **3.2** *Linear layout for cylinders*

each other as shown in the 3D model, figure 3.2. This design is very straightforward and has a minimal footprint however it requires building a complicated crankshaft with cranks that need to maintain their relative angles under moderate to high forces and torques.

The alternative layout is to have mount cylinders in a triangular design, figure 3.3 which takes more space however requires a considerably simpler crankshaft with only a single pair of cranks. This design uses a close triangular chassis that makes the assembly of different parts to some extent inconvenient however the gain because of the simpler crankshaft is more significant furthermore this design was finally chosen to be Magni's layout.

3.2   Pneumatic processes and Circuit

In order to have the desired air mass flow, a pneumatic circuit needs to be designed. This step must be done before the component selection since the type of the valves is defined by type of airflow manipulation that the circuit demands.
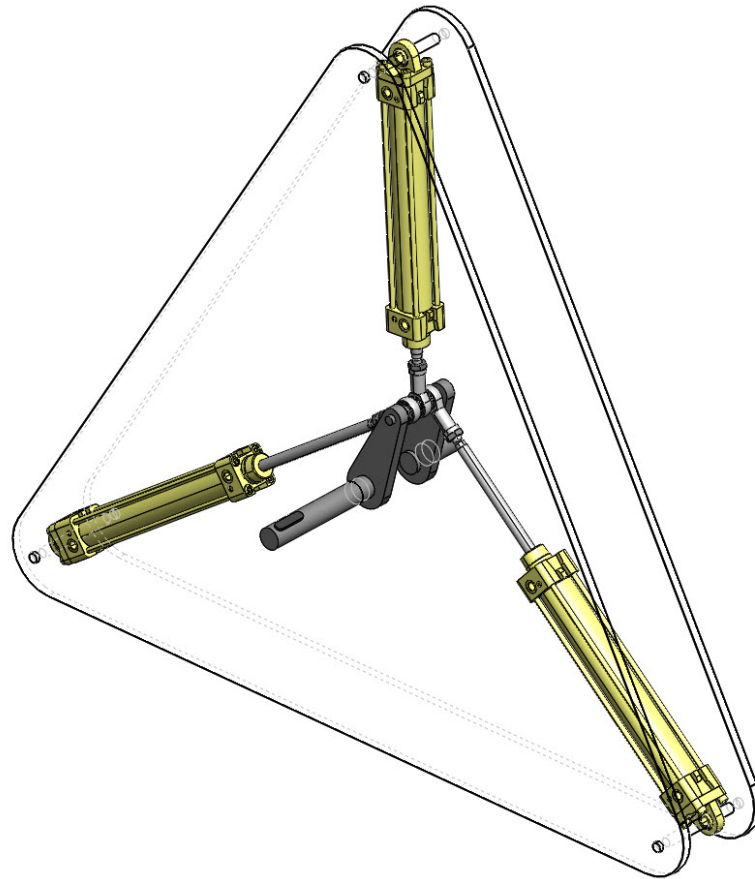
Figure 3.3 *Triangular layout for cylinders*

3.2.1   Single Chamber Circuit

Each double acting cylinder has two chambers separated by the piston. In order to determine the current state and movement direction of piston in each chamber, the concept of phase is used where the angular position of the main crank is the basis of state recognition. As demonstrated in figure 3.4, when the piston is moving away from the rodless chamber's end, the crankshaft's angle increases from zero to 180 and when the piston is moving backwards, the crank's andgle increases from 180 to 360 degrees. The opposite chamber goes through the same transition with 180 degree of phase shift.

In order to design a circuit for a single chamber, the main processes of expansion and compression need to be defined. Next subsections go through those in detail.
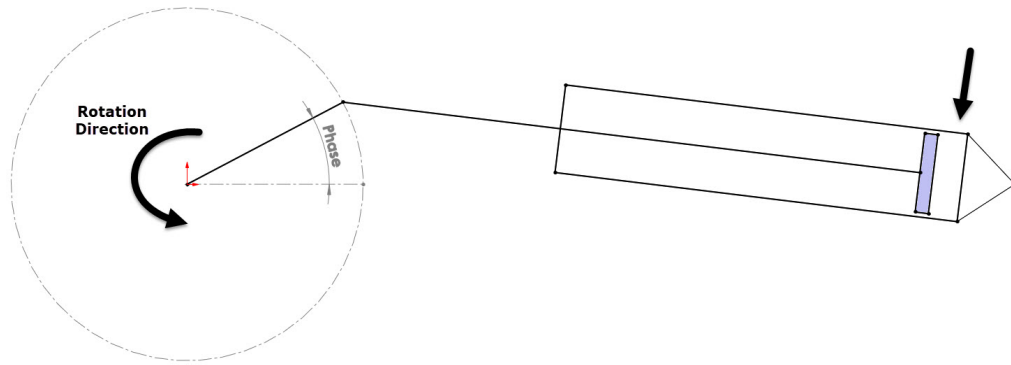
Figure 3.4 *Chamber phase definition*

Expansion in a Single Chamber

In order to generate movement from the stored energy, one of the chambers must be fed with compressed air and expanded so the resultant force in each cylinder induces a driving torque to the main shaft. The expansion process is consisted of three different stages which are shown in figure 3.5(a). During the first stage, **charge**, compressed air is let into the chamber after which the chamber is isolated again and as the piston moves, the air expands while its energy is released. When the piston reaches the end of the stroke the chamber is connected to the ambient so the piston can return to the beginning of the cycle with minimum hindrance. For such a flow control, a valve able to connect the chamber both to supply tank or the atmosphere is needed. The valve also needs to be able to isolate the chamber during the expansion stage. A closed center 3/3 (3 port with 3 positions) valve as shown in figure 3.6 is suitable to do all these tasks.

There is an intricate point during the expansion stage. The length of charge phase as will be explained in chapter 5, is the parameter by which the basic control logic adjusts the generated torque in expansion mode and in many cycles the air inside chambers will reach the ambient pressure before the piston reaches the end of stroke after which piston movement faces resistance from low-pressure air. To eliminate this issue the chamber must be connected to atmosphere after that point so air can come inside and the zero pressure is preserved. One solution is to have the pressure inside the chamber sensed so the controller makes the valve connect the chamber to the outside air when necessary. This solution is not favourable as it needs expensive pressure sensors for all the chambers. The alternative and more practical solution is to have a non-return valve (check valve) for each chamber that lets the air in once the pressure drops below the ambient pressure. This Vacuum Breaker Valve (VBV) is shown in figure 3.6 and will be recognized with this name hereafter.

(a) Expansion stages   (b) Compression stages
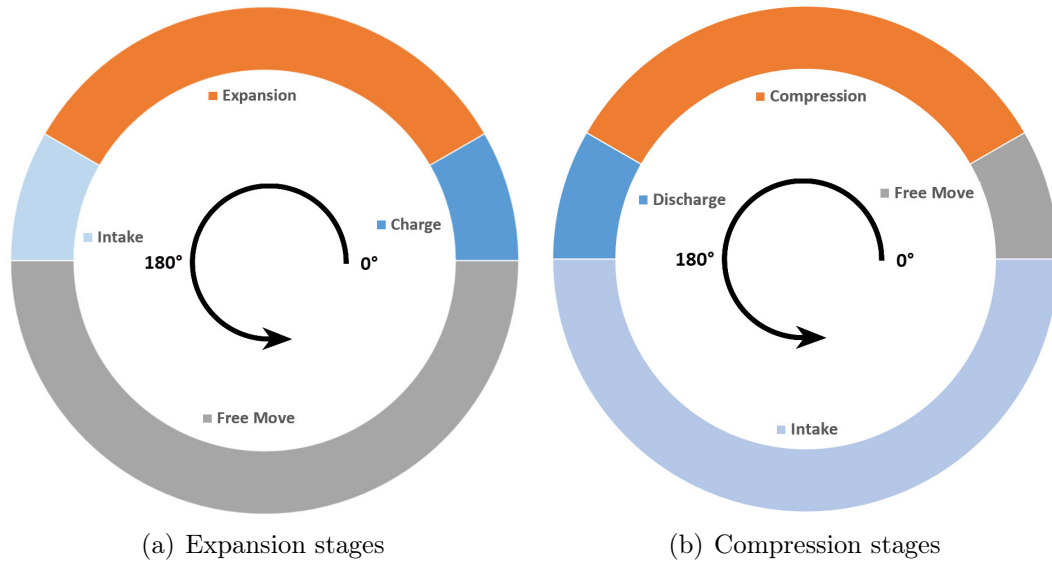
Figure   3.5 *Different stages during expansion and compression processes*
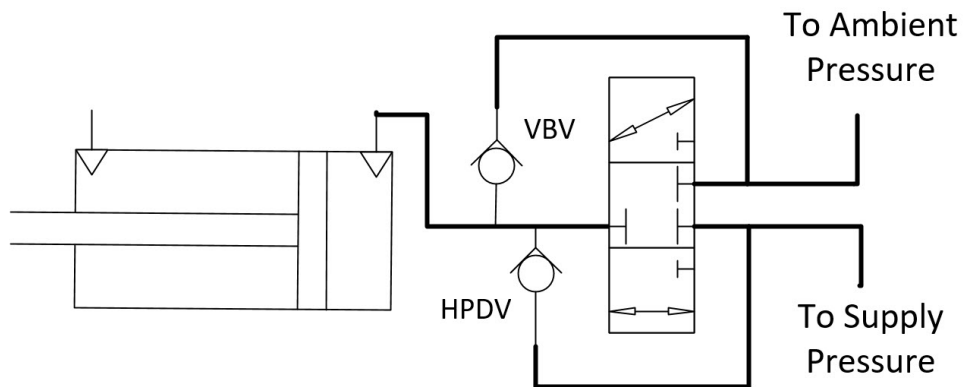
Figure   3.6 *Pinping Diagram for a single chamber*

Compression in a Single Chamber

Turning input energy which is exerted on Magni in form of torque to stored com-
pressed air requires compression process which as illustrated in figure 3.5(b) includes
sucking the environment air inside the chamber, **intake**, compressing it, **compres-
sion**, and forcing it out, **discharge**, stages. During intake the chamber must be
connected to ambient pressure while during the compression process chamber must
be isolated. After the air is compressed enough the chamber must be connected to
the reservoir tank so the generated compressed air be discharged into it. Beside these
three main stages of compression that result in compressing air with full capacity,
based on the available driving torque, the chamber isolation might need to be delayed

after the intake thus reducing the amount of generated compressed air.

These air mass flow controls are possible using the same 3/3-valve mentioned in the previous section however knowing the exact time the chamber pressure has reached the tank pressure so the valve opens and discharge can start without using sensors for each chamber is impossible. The practical solution is to use a check-valve that lets the air to the tank whenever the pressure inside the chamber rises above the tank pressure. This High Pressure Discharge Valve (HPDV) is also shown in figure 3.6 and will be referred to with this name hereafter.

3.3 Pneumatic Components Selection

The main components of Magni are the pneumatic valves and cylinders while the rest of mechanical components including chassis and crankshaft are custom made for this project. Selecting the main parts are important because the capacity of the system is directly limited by their size and operating pressure. Before proceeding to component selection the availability of compressed air at TUT labs, where building this prototype took place was also considered. The reason for this consideration is that in many cases the system reservoir must be pre-filled with compressed air or kept at a constant pressure during the test. The laboratory was equipped with 7 bar compressed air supply lines furthermore this pressure was selected as the maximum working pressure of the system.

Another important factor which affects and limits the suitable components is the target operational speed of the system. Since machines that rotate at high rpms require advanced balancing procedures and deal with tight production tolerances the target angular velocity was selected as low as 60 rpm. This decision also results in lower air flow demand from the valves and lower linear velocity of the pistons thus having broader options in selecting those components. The downside of a low rpm is lower power generation however the results from the experiments on this prototype can be extrapolated and considered as the expected results when the speed is higher.

3.3.1 Cylinder Selection

The first Criterion as mentioned in section 3.1 is to select a cylinder of double acting type. Secondly the cylinder must be able to work in pressures at least as high as 7 bars which was selected in previous section. As for sizing, there are two important sizes for each cylinder, bore diameter and stroke. The former directly affects the amount of force generated by the cylinder and the latter affects the amount of air

system can compress and or expand i.e. the capacity. Another significant factor in choosing the cylinder model is the availability so they can be sourced faster and with less complexities.

Finally considering all the conditions a cylinder made by Camozzi$^{\text{TM}}$ with the model number "60M2L032A0200" was selected. This cylinder has a $32mm$ bore diameter and $200mm$ of stroke and can operate under pressures up to $10bar$. With this stroke and the selected operational angular velocity in previous section, the linear speed can be calculated as:

$$x = \frac{200}{2}sin(\theta) \ mm \tag{3.1}$$

$$\dot{x} = \frac{d}{dt}(x) = \dot{\theta}\frac{200}{2}cos(\theta) \ mm/s \tag{3.2}$$

Based on Equation (Eq) 3.2 and the selected rpm, nominal velocity is as much as $628mm/s$ which is lower than $1000mm/s$ limit mentioned in the cylinder's catalog and leaves a margin to experiment higher speeds reliably.

3.3.2 Valve Selection and Assembly

Regarding explained processes in section 3.2.1 and as illustrated in figure 3.6 for each chamber a valve assembly including a closed center 3/3-valve and two check-valves are needed. Another criteria for selecting the valves is their size and the total assembly must be small enough so two of them can be assembled on a single cylinder. Installing the valve assembly on the chassis and connecting it to the cylinder chambers via tubes is an alternative which significantly increases the dead volume of the chambers and decreases the final efficiency consequently.

Regarding the conditions and limitations a 5/3-valve produced by SMC$^{\text{TM}}$ was selected. This valve has two ports too many however by blocking them with suitable plugs it will perfectly work as the required 3/3-valve. The check-valves were selected based on their fitting compatibility with the 5/3-valve. The valves, their model numbers and their duties are summarized in Table 3.1. The valves for each chamber are finally assembled on a cross-fitting[2] as shown in figure 3.7.

---

[2]A cross-fitting with 4 male ports were needed however since it was not found on the market a 3male-1female fitting was machined and threaded to build the desired all-male cross-fitting

Table 3.1 *Valve Models and Duties.*

Model Number	Type	Duty	Manufacturer
SY5320R-6G-01F-X406-Q	5/3-control valve	Flow Control	SMC
AKH06A	One way valve	VBV	SMC
AKH06B	One way valve	HPDV	SMC

(a) Valve Assembly

(b) Modifying the Cross-fitting
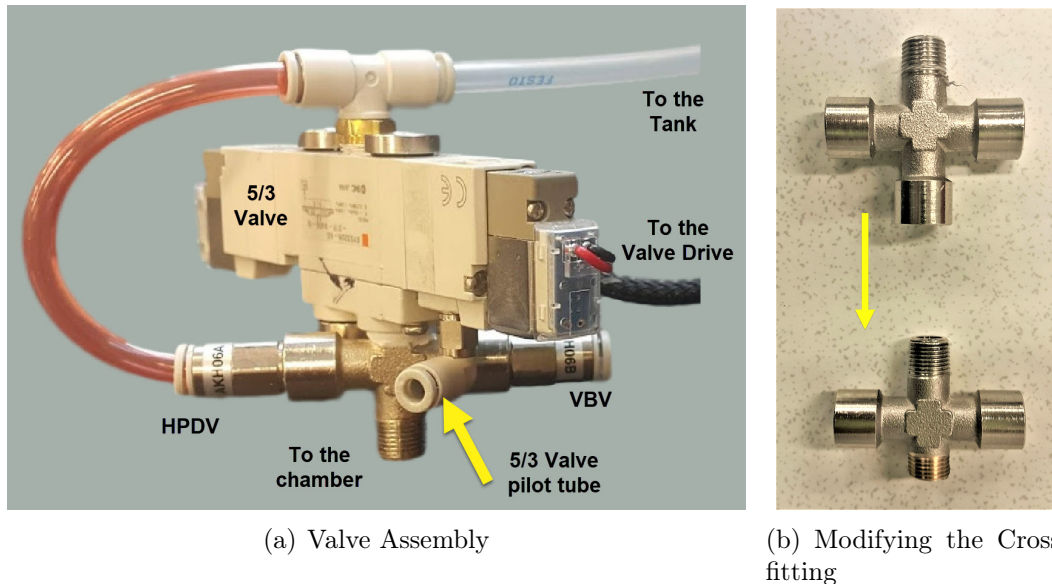
Figure 3.7 *Valve Assembly and the fitting*

3.3.3 Compressed Air Reservoir

Magni needs a tank capable of storing compressed air, as the reservoir. Selecting a bigger tank has the benefit of higher energy capacity and smoother pressure change during operation. The main limitation in selection of this tank is the footprint and the availability since most of available ready made tanks are able to withstand pressures up to $10 bars$ which is higher than the selected operating pressure. Regarding the mentioned criteria, a 45 *liter* tank has been selected which is big enough for experiments and small enough to fit in the place where Magni is put together. Figure 3.8 shows the tank during the leakage test.

3.4 Consumer Module

Magni is a machine intended to be capable of generating or absorbing torque based on the conditions. In order to test its capabilities a module is needed that can consume the generated torque or drive Magni with torque. This module is going to

Figure 3.8 Tank while being tested for possible leakges

be referred to as Consumer Module (CM) hereafter. The main idea for designing this module is to have a DC electrical motor which can also be used as a generator when driven.

3.4.1 Mechanical

The main challenge here is to convert Magni's relatively low operational rpm to within speeds in the working region of normal DC motors which is 2000 to 3000. Doing this also increases the mechanical advantage of the electrical motor over Magni making it possible to use smaller and less expensive ones with lower torque ratings. Moreover CM needs to posses high inertia to minimize the low-rpm fluctuations.

The most straightforward solution is to use a set of pulleys and belts to do the conversion and add a flywheel to one of the high speed shafts to provide the required inertia. The 3D model of this solution is shown in figure 3.9. The details of pulley

selection and their machining is not discussed here and only the resulting conversion rates are mentioned. For a single revolution on the main shaft the motor shaft and the flywheel will turn 36.3 and 66.8 times respectively. If Magni works at the 60 rpm nominal speed the motor will be rotating at 2177 rpm, slightly lower than its nominal 2800 rpm thus leaving a small margin to examine higher speeds while benefiting from nearly highest possible mechanical advantage. At the same speed the flywheel will be rotating at 4000 which results in 4500 times of the inertia it would have provided if installed on the main shaft.

3.4.2 Electrical

The electric motor within the module is the channel of energy to the whole system. If connected to a power source it will exert torque in the direction of rotation and if connected to an electricity consumer it will resist the rotation and doing so it will produce electrical current. The generated or resistance torque present on a DC motor shaft is directly proportional to the current that passes through it while the voltage between its contacts is proportional to its angular speed. In order to be able to use the motor in both modes and be able to manipulate the motor's torque a relatively simple circuit, figure 3.10, was designed. The adjustable resistance is able to change its voltage drop and consequently the total current of the circuit regardless of the mode.

DC Motor

Modern DC motors which use brushless technology have considerably higher efficiency however they cannot be used as generators conveniently, consequently it was decided to select a brush type motor for the module. Based on initial simulations Magni's power was estimated to be around 350 Watts with $10bar$ supply pressure furthermore considering the energy losses in the system and the required margin, a $1000\,W, 2800\,rpm$ DC motor, figure 3.11, was procured for the project. This motor is intended for use in electric scooters and comes with a Pulse Width Modulation (PWM) rpm control drive, however since Magni must be able to regulate the speed itself, using this drive is not desirable. More over the fluctuating nature of voltage provided by this kind of drives imposes troublesome noise on the sensors.
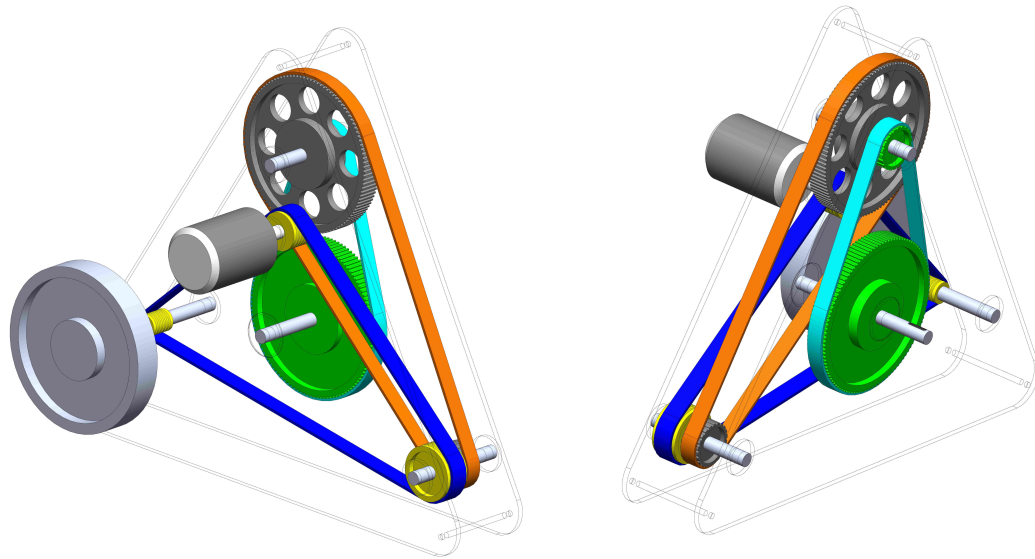
(a) Left 3D perspective

(b) Right 3D perspective
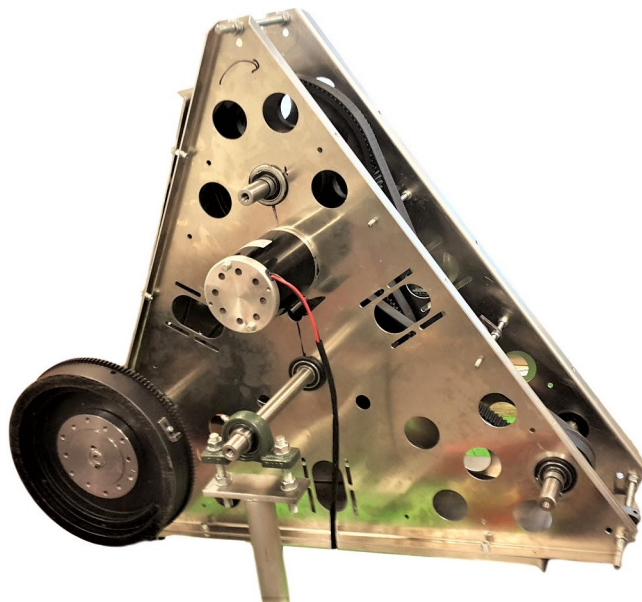
(c) Assembled Consumer Module

Figure 3.9 *Consumer module 3D model and actual assembly*

Consumer Resistance

In Generator mode with the nominal speed, 48V and 20A electricity will be produced. The 1.5Ω consumer resistance can dissipate up to 600W of it which is calculated simply from $W = RI^2$. The rest of the generated power will be consumed overcoming CM's internal friction. In order to make this electrical component,
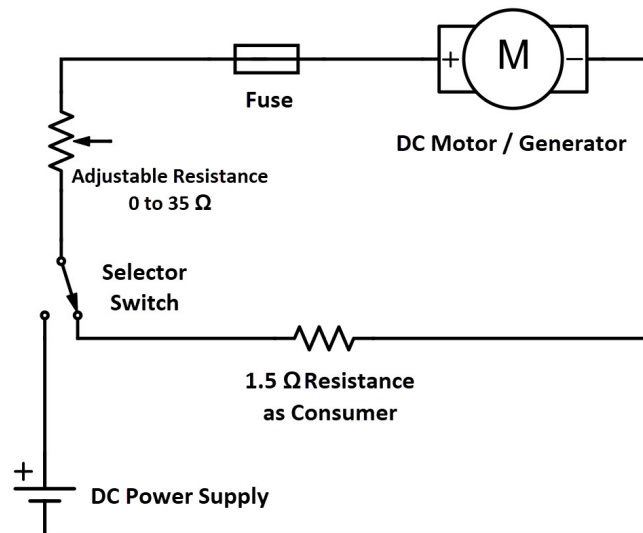
Figure   3.10 Consumer Module Electrical Circuit

Figure   3.11 DC motor box contents

3 pieces of heating element each one with 4.5Ω resistance were used in parallel, figure 3.12, and installed on top of a cooling fan to prevent it from overheating.

Adjustable Resistance

As shown in figure 3.13 the adjustable resistance is made of two main parts in series:

- Three 100Ω rheostats in parallel to form a 34Ω rheostat.

- A series of 13 0.1Ω resistors[3], each one made of 3 paralleled 0.3Ω resistors. Each of these sets have a dedicated bypass switch to reduce the resistance

---

[3]In the diagram only 4 of these sets are shown.
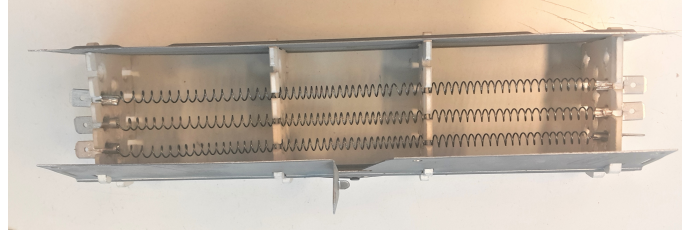
Figure **3.12** *1.5Ω resistance as electrical load*
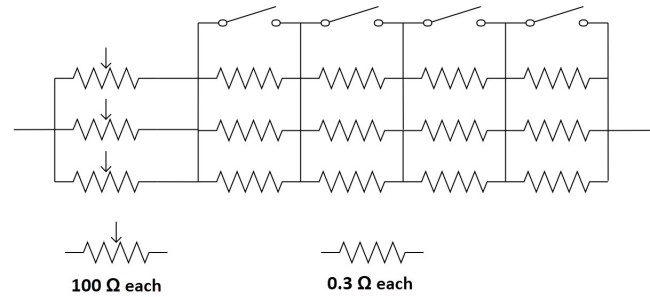
Figure **3.13** *Electrical diagram of adjustable resistance*

with fine steps. This part was fit into the same chassis as the load resistance so both of them can be cooled with the same fan.

Electrical Circuit Implementation

Parts that were used to build the electrical load and the adjustable resistance including the rheostats, the heating elements and the fan were acquired by disassembling an old electrical load made by *JJ Instruments*™. After preparing all the parts they were assembled and fit into the same casing for durability and safety reasons, figure 3.14.

3.5 Measurement and Sensors

The condition of Magni is needed to be logged in order to feed them back to the controllers and also to study the system's behavior. Within the next sections each of this parameters, their application and the way of reading them in this study are going to be explained. The details of transferring the read data from each of the sensors to the control unit including the wiring and programming are going to be covered in chapter 4.
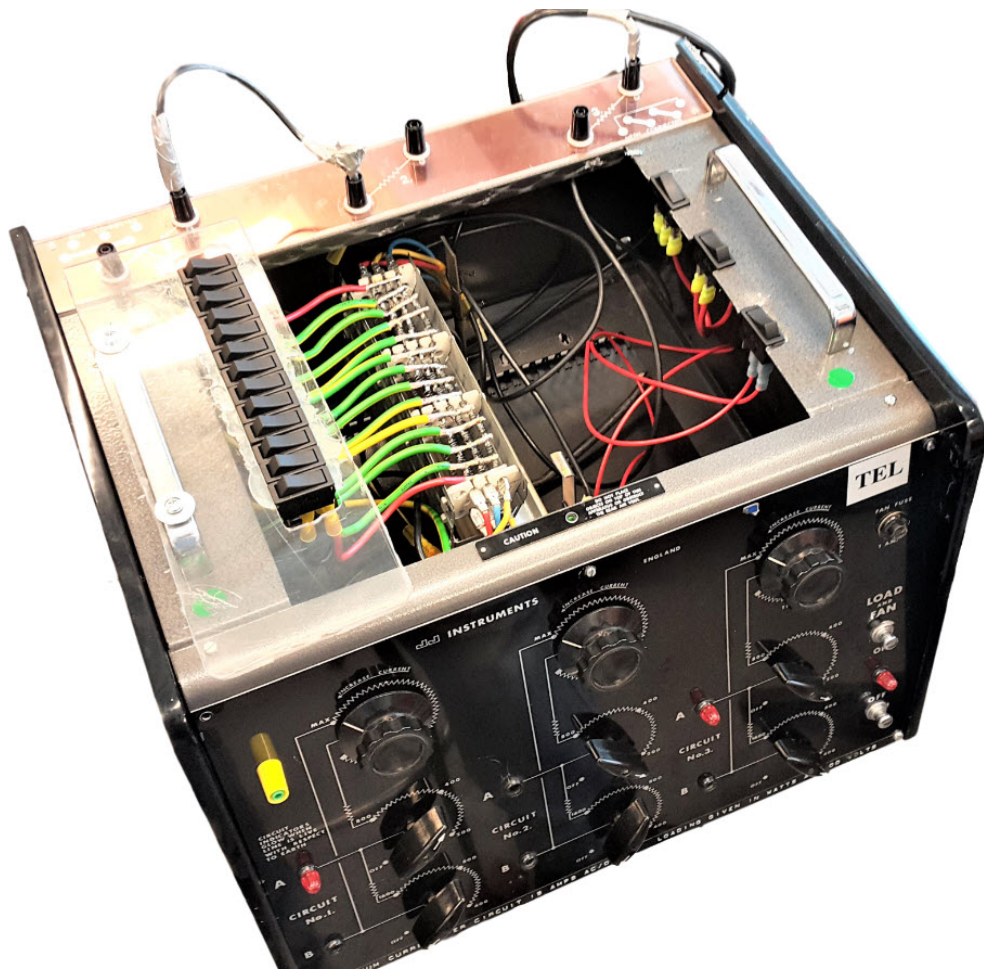
Figure 3.14 *Finished Electrical unit*

3.5.1 Angular Position

The control unit needs to know the exact phase of each chamber in order to decide when to open or close the valves. For this purpose a 12bit magnetic absolute angular encoder made by Avago$^{\text{TM}}$ with model number "AET-6012" is added to the shaft's end. As shown in figure 3.15 proper housing was machined to keep the encoder in its place thus the encoder reports the shaft phase correctly and reliably. Since the phase shift between the chambers are constant using this single reading can be used to calculate the phase for each chamber individually by implementing proper corrections.

3.5.2 Angular Velocity

Magni rotating speed is the parameter which is given to the controller as the set-point and it must be read and used as feedback so the controller can comply with

(a) Encoder as procured (b) Fixed housing (c) Rotating housing

(d) Encoder full assembly
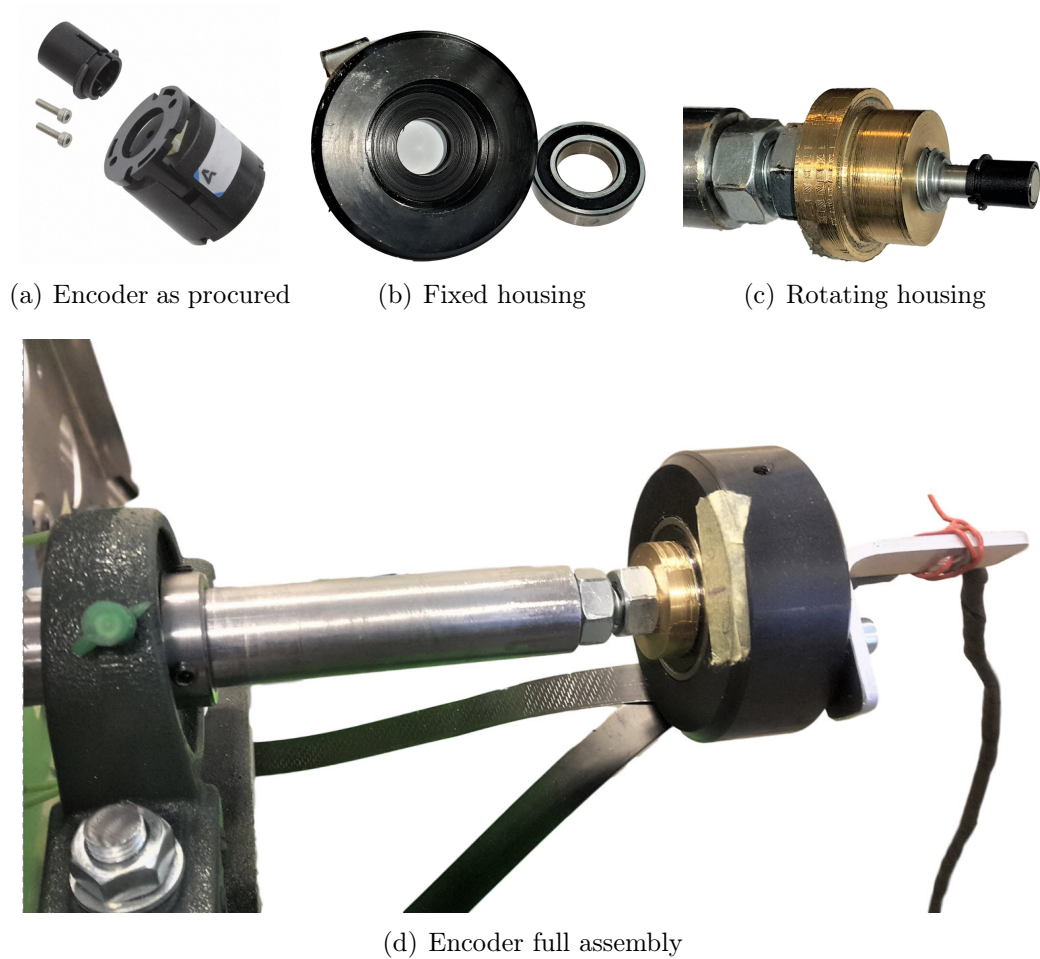
Figure 3.15 *Angular sensor and the housings*

the set-point accordingly. This parameter is calculated as the derivative of angular position with respect to time.

3.5.3 Shaft Torque

The amount of torque present on Magni's shaft needs to be measured in order to calculate the input or output power and study the system's capacity to drive in expansion mode or to brake in compression mode. The intuitive solution to measure the torque is to have a rotating torque sensor as the coupling between Magni and the CM however such sensors are very expensive and need tight alignment tolerances between the two shafts. The practical alternative is to measure one of the two systems' vertical reaction at the connecting point to the baseplate. To implement this solution, contrary to Magni which is firmly bolted to the baseplate, the CM's chassis is suspended on the main shaft. As shown in figure 3.16 the only contact point of this module's frame with the baseplate is provided by a load-cell in order

(a) Suspended CM

(b) Force sensor that measures vertical reaction
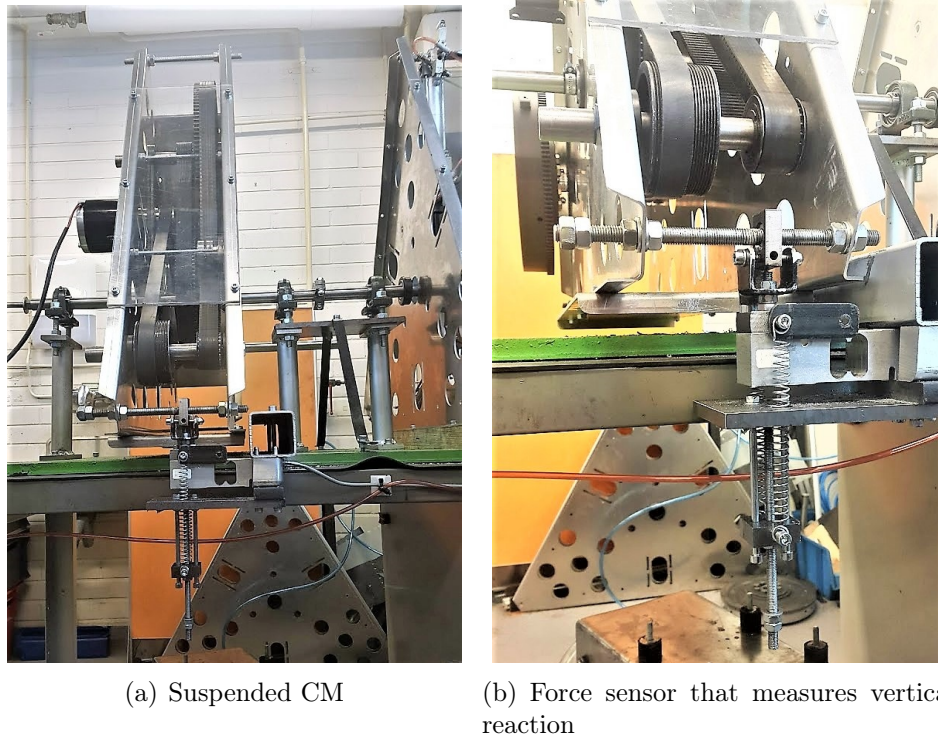
Figure 3.16 *Suspended CM and the Loadcell measuring the vertical reaction*

to measure the amount of vertical force needed to keep the module from rotating. The product of measured force and the contact point's distance to the axis of the main shaft is the torque present on the shaft.

A load-cell made bt HBM$^{\text{TM}}$ with model number *PW10 D1* is chosen for this measurement. A minor challenge here is the direction of the force since the used force sensor is only able to measure the force in one direction. To address this issue a spring mechanism was added to the sensor holder to apply pretension to the sensor. This way while the exerted force on the sensor is always downwards the changes of the readings from the neutral state can be used as the basis of torque calculation.

The selected sensor is able to measure forces up to $500N$ and a pretension as much as half of its capacity is applied on it. The contact point is $449mm$ far from the main shaft's axis. The range of torque measurement can therefore be calculated as $\pm 250N \times 0.449m = \pm 112.25N.m$.

3.5.4 System Pressures

In order to study the behaviour of compressed air inside the system and have proper data in hand to compare with simulation results, three pressure sensors are added
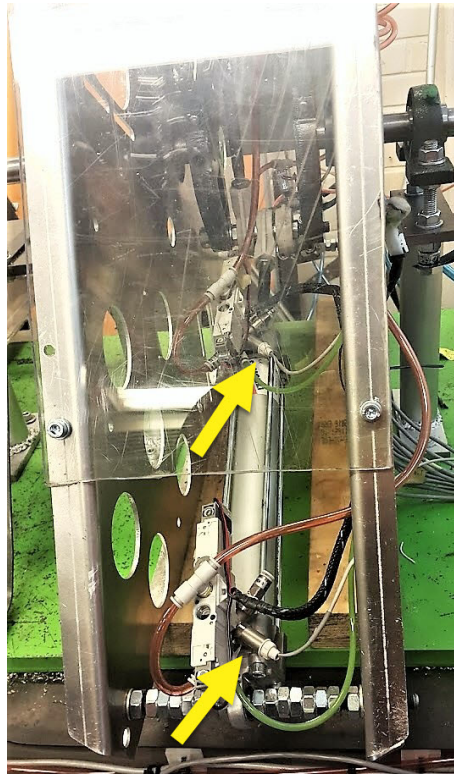
Figure 3.17 *Pressure sensors installed on cylinder 2*

to the system. Two pressure sensors were added to the cross-fittings holding the valve assemblies of two chambers of cylinder 2. As can be seen in figure 3.17 this cylinder was selected for pressure sensing because it is physically more accessible and sensor installation is more convenient on it. Another sensor of the same type was added to reservoir tank in order to read and log the pressure changes of the stored compressed air as the machine works.

3.5.5 Air Temperatures

Compression and expansion are both processes that cause significant changes in air temperature therefore two LM35 temperature sensors are added to the system to keep track of these changes. One of these sensors is added to the air tank and as shown in figure 3.18 and proper housing is made for it to keep the tank sealed while the sensor is placed $20cm$ into the tank for more accurate measurement.

Measuring the air temperature inside the chambers requires special sensors and special cylinders furthermore the other temperature sensor is put in the tube connecting chamber A of cylinder 2 to the tank. Figure 3.19 shows the housing for this sensor and its installation position. This sensor is not able to measure the

Figure 3.18 LM35 tempreature sensor for the reservoir
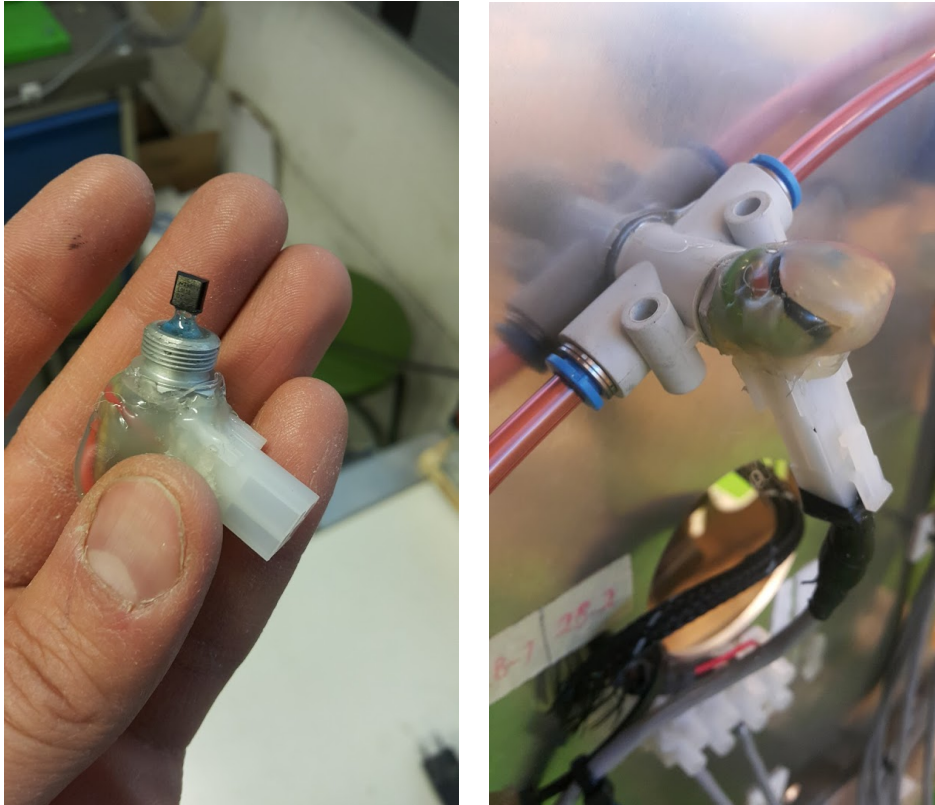
(a) C2-A temperature sensor housing

(b) C2-A temperature sensor installation position

Figure 3.19 C2-CHA temperature sensor

inside temperature accurately since the air exchanges heat on the way to the sensor however it provides the overall trend during the compression mode. In expansion mode the air temperature drops however it is vented to the atmosphere without passing through the sensor thus those changes are not captured.
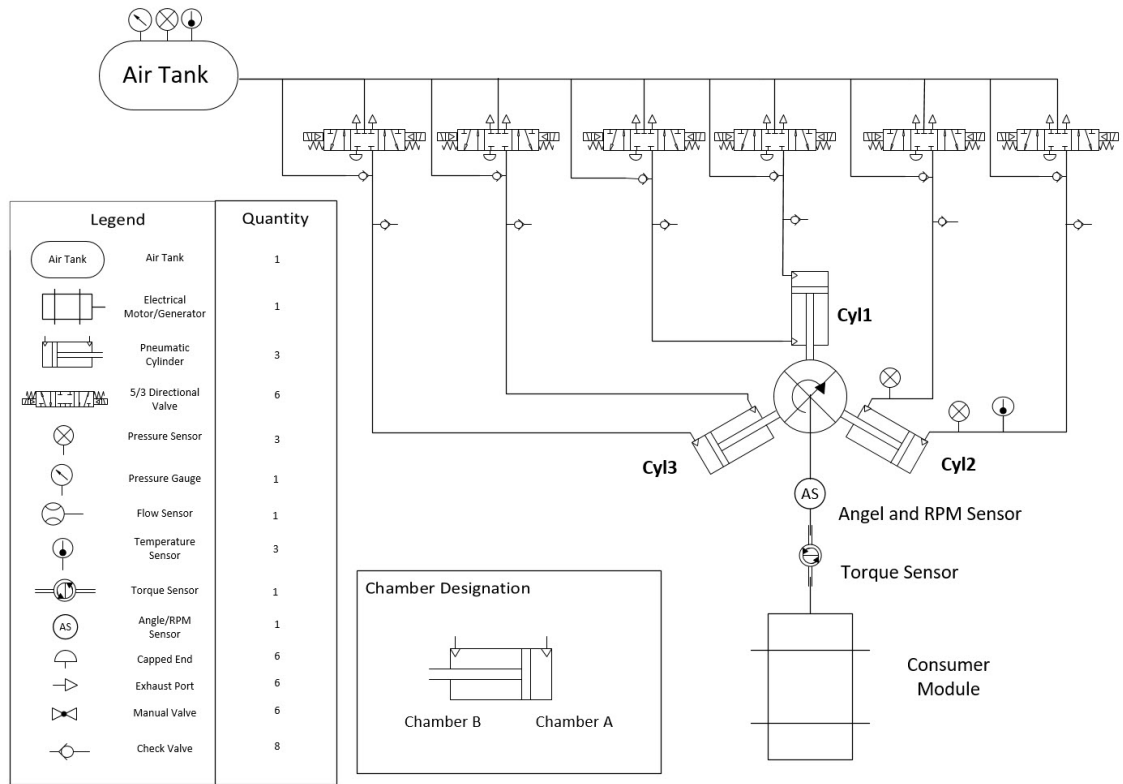
Figure 3.20 *Piping and Instrumentation Diagram*

3.6 System Final Schematics and Assembly

Using Microsoft Visio™ all the selected components and sensors are put inside a schematic blueprint which is shown in figure 3.20. This diagram helps to understand the flow destinations and the places where parameters are being measured. The actual final assembly of the system is shown in figure 3.21.
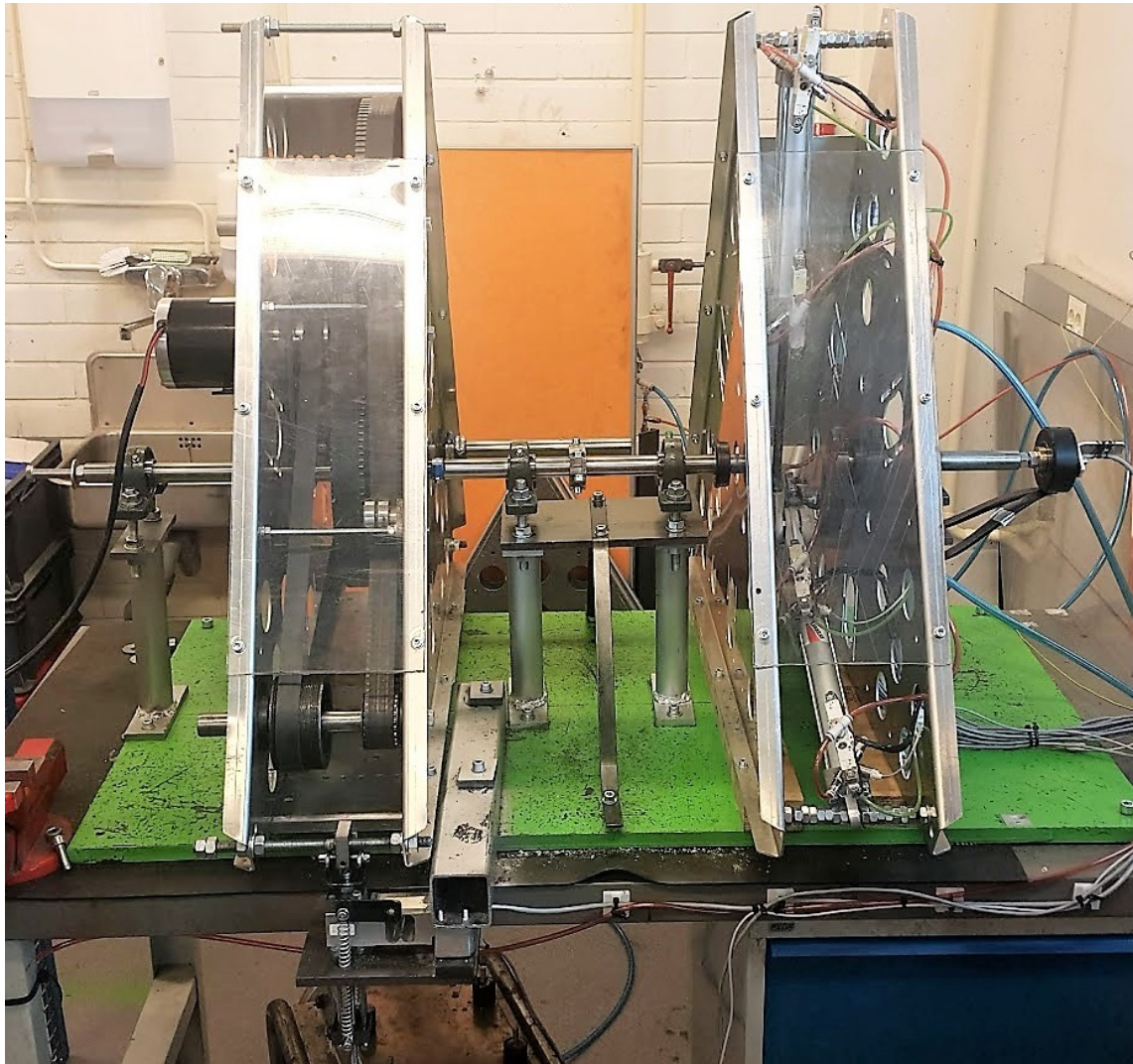
Figure 3.21 *Final assembly of Magni and the CM*

4.   HARDWARE CONTROL

It is necessary to design an interface in order to make the communication between physical and digital parts possible. The mentioned interface is a combination of versatile software and hardware that works together. Figure 5.1 illustrates how the communication between hardware and software is done in this project. The procedure of designing the interface can be put into the following categories:

1. Selecting a suitable microcontroller or computer

2. providing a suitable environment to ease the communication between hardware and software.

3. Reading sensors' data for control purposes.

4. Triggering the valves based on the received commands

Each of the above mentioned procedures requires a combination of physical components and softwares that work in parallel.

4.1   Selecting suitable microcontroller or computer

The controller unit that is used in this study is a Raspberry Pi (RPI) 3 Model B, which is chosen based on the following reasons:

- Provides as many as 26 General Purpose Input Outputs (GPIOs)

- It is supported widely by the manufacturer.

- Different codes are available by the developers.

- Fast and relatively powerful processor(1.4 Ghz)

- It is possible to take benefit of linux based OS e.g. UBUNTU

Electrical Connections
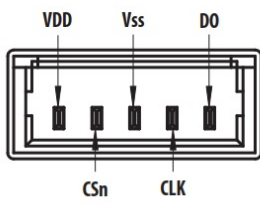
Pin	Symbol	Description
1	VDD	5V Supply Voltage
2	CSn	Chip Select – Input (See Figure 2)
3	VSS	Supply Ground
4	CLK	Serial Clock - Input (See Figure 2)
5	DO	Serial Data - Output. (See Figure 2)
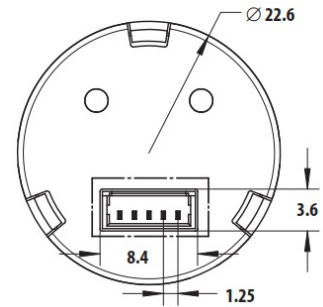
Figure 4.1 Encoder electrical connection
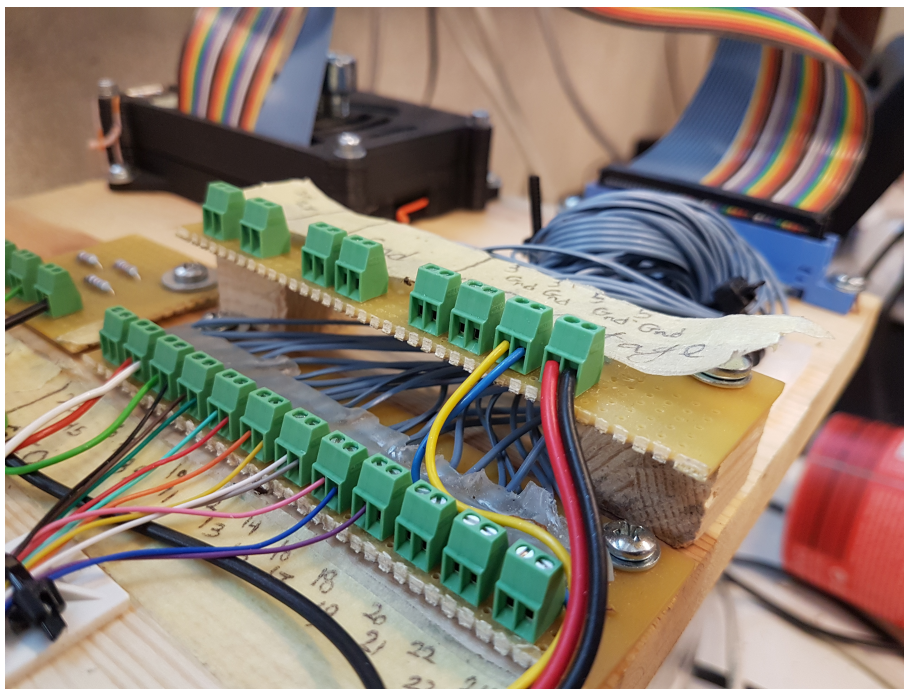
Figure 4.2 Separate GPIO board to avoid short circuit

- It is possible to develop Robotic Operating System (ROS) nodes on it that are able to Read and generate signals on its GPIO pins.

Since there are many wires connected to the GPIO pins on RPI (12 for valves and 5 for the angular sensor), a separate board is made to avoid possible short circuits when connecting the wires. Figure 4.2 demonstrates how it is done and how the GPIO pins are distributed on the board. all the 40 pins of RPI are connected to the board using a Flat(IDE) cable.
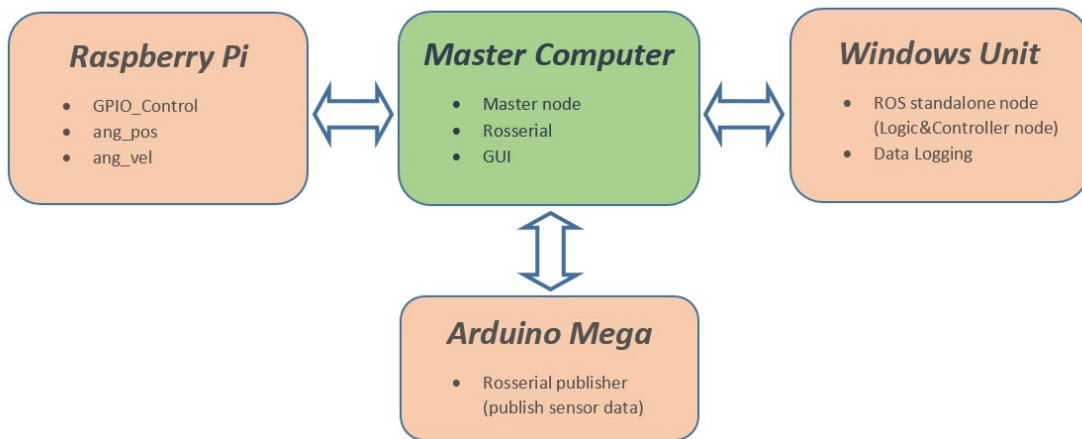
Figure *4.3 ROS network layout*

4.2 Selecting a Suitable environment

According to the fast nature of Magni, the first priority of choosing a suitable environment is the possibility of fast communication between hardware and software. This is of high importance due to the following reasons:

- Since Magni is supposed to work at 60 rpm, and the controller should be able to monitor the shaft's phase at least every 1 degree, at least 360 Hz of speed is needed to report the sensor data.

- The basic contorol logic also must be able to make decision at least with 360 Hz to acheive desired motion.

- The controller device must be able to trigger the valves with a fast response.

Different methods and approaches are examined including Simulink external mode environment, Matlab code ,C++ code on RPI and ROS in order to achieve fast communication between the RPI and the rest of system. Among the mentioned approaches, the only method that is capable of communication speed faster than 360 Hz is developing C++ code on RPI. However, this approach limits the simplicity of the work since all the controllers and data structures are needed to be developed in C++ language on RPI. ROS solves this issue by providing a comfortable environment in which different nodes in different devices can be developed and work in the same network as it is evident in the figure 4.3 and figure 5.1. The

4.3   Reading sensors' data

In order to monitor the state in which the Magni is working at, different sensors are utilized. These data from the sensors are used as a feedback to the controller node and also for data logging purposes.

Among the sensors used in this project, only the angular encoder utilizes digital signals for commiunication, which its digital outputs can be read using RPI GPIO pins. The rest of the sensors' outputs are analogue signals, consequently it is needed to read them using proper data acquisition devices capable of reading analogue data. For this purpose, an Arduino Mega is chosen which has 10 bits resolution and is able to report the data as fast as $100Hz$. Proper code is developed and transfered to the the Arduino board to read the voltages present at its analogue input pins and send the values to rosserial node running on the master computer. This node publishes these values to the ROS network so other nodes can read and use the information.

4.3.1   Absolute Rotary Encoder

As explained in chapter 3, angular position and velocity of Magni is being reported using the angular absolute magnetic encoder which its properties are summarized in table 4.1. Two ROS nodes (ang_pos and ang_vel) are developed in order to read raw data from the sensor and publish the phase and velocity of the main shaft.

Table 4.1 *Encoder Properties*

Type	Absolute Angular Encoder
Supply Voltage	5 V
Maximum Read-out Frequency	1 MHz
Resolution	12 bit (reports a number from 0 to 4095)
Max Mechanical speed (rpm)	12000 rpm*

Electrical Wiring

The encoder is utilizing Synchronous Serial Interface (SSI) protocol that uses 3 signals as illustrated in figures 4.4 for transmitting data and 2 signals as excitation. The timing characteristics and the sequence of digital signals are described in figure

Electrical Connections
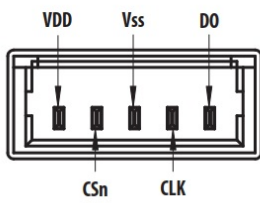
| Pin	Symbol	Description
1	VDD	5V Supply Voltage
2	CSn	Chip Select – Input (See Figure 2)
3	VSS	Supply Ground
4	CLK	Serial Clock - Input (See Figure 2)
5	DO	Serial Data - Output. (See Figure 2)
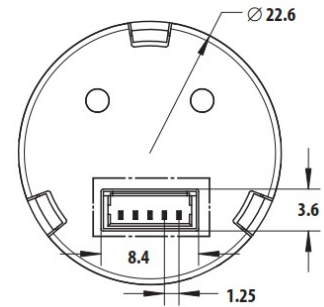
Figure 4.4 Encoder electrical connection
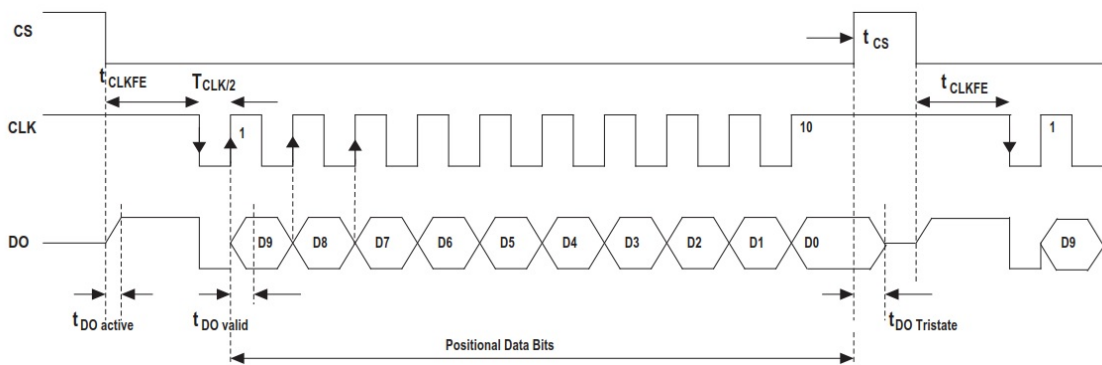
Figure 4.5 Timing characteristics of the angular encoder

4.5 and table 4.2 where the "VDD" and "VSS" are representing supply voltage and ground wire respectively. Two signals (CSn and CLK) are required to send commands continuously by changing their values between high and low. Output data "DO" is also being received continuously afterwards. The mentioned signals are being sent and received by connecting the corresponding electrical wires to GPIO pins board.

For the subject sensor there are two challenges regarding the voltage range. According to the sensor catalogue, the sensor CLK and CSn connections need to be triggered with 5V signals which is higher than the 3.3v that the Rpi is able to provide. Although the 3.3V of RPI is examined for this purpose and the sensor started working without any error. The second challenge is to read 5V digital output "DO" signal coming from the sensor since RPI is able to handle a maximum of 3.3V. This issue has been solved by making a simple circuit as shown in figure 4.6 which breaks the voltage to half.

Table *4.2 Encoder timing characteristics*

Parameter	Symbol	Condition	Values			Units	Notes
			Min	Typ.	Max		
Data output activated (logic high)	$T_{DO\ active}$				100	ns	1
First data shifted to output register	$t_{CLK\ FE}$		500			ns	2
Start of data output	$T_{CLK/2}$		500			ns	3
Data output valid	$T_{DO\ valid}$				375	ns	4
Data output tristate	$T_{DO\ tristate}$				100	ns	5
Pulse width of CSn	T_{CSn}		500			ns	6
Sampling rate for absolute output	f_{abs}		9.9	10.42	10.94	kHz	7
Power-up time	t_{CF}						8
10-bit version			-	-	50	ms	
12-bit version			-	-	20	ms	
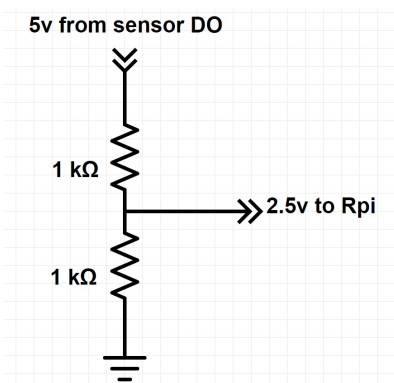
(a) 5v to 2.5v reduction circuit (b) 5v to 2.5v board
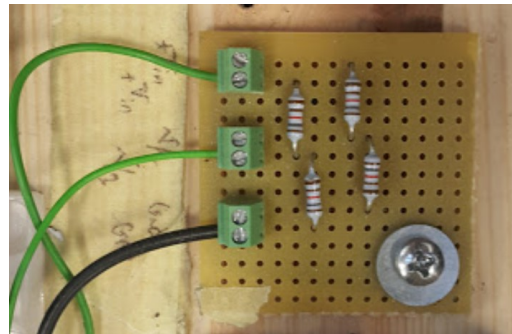
Figure *4.6 Sensor's 5v digital output to 2.5v conversion*

ROS nodes

In order to develope a C++ code that reads and generates signals on GPIO pins, "WiringPi" library is included and used in the code. Finally, a ROS node was developed to be run on the RPI and read the angular position and publish it on a ROS network which is based on the timing characteristics and sequences stated in the catalogue. The node was set to run with 1 kHz frequency and with this high frequency it occupied less than 30% of the CPU usage. The Node also calculates the angular velocity using the time function of ROS and publishes it to a different topic. The published rpm were noisy and the reason was the number rounding of the time value. Since the frequency is relatively high the rounding can cause a noticeable error and generate the noise. To remedy the problem the publish frequency of the rpm were reduced to 1/20th of the angular position.

4.3.2 Loadcell

Loadcell is using 2 wires as exitation inputs and 4 signals for transmitting output as it can be seen in the figure 4.7, The wire number 5 and 6 are called Sense signals and

Shield (yellow) = Shield connected to load cell body

Contact 1 (white) = Signal (+)

Contact 2 (red) = Signal (−)

Contact 3 (black) = Excitation (−)

Contact 4 (blue) = Excitation (+)

Contact 5 (green) = Sense (+)

Contact 6 (grey) = Sense (−)

blue marking
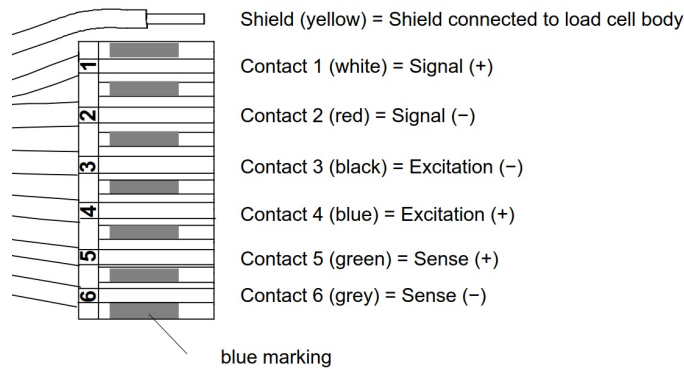
Figure 4.7 Loadcell electrical connection

are used in industries or noisy environments to eliminate the noises. Fortunately in the case of this study only wire number 1 and 2 (± Signal wires) are used to read output without reading any noisy data.

The challenges

The challenge in reading the Loadcell's data is that its output signal is in the range of 0.1 mV to 1 mV which is not recognizable by the common data acquisition devices or Arduino micro-controller. To remedy this problem, a "Zero-Span" circuit, figure 4.8, is utilized which scales up the input signal from the mentioned range to the range of (1 to V_ref). This is done by tuning the output ranges using two potentiometers on the board that adjusts the maximum and minimum of the input voltages. For the case of this project, since the analogue data is being read by the Arduino Mega which is able to read up to 5V, the output of the sensor is scaled up to the range (1..4.5V).

Calibration

With the 10 bits resolution of Arduino Mega and the output range of 1 to 4.5V (Zero-Span circuit) for 50 kg of Loadcell capacity, The highest resolution of 170 grams is achievable.
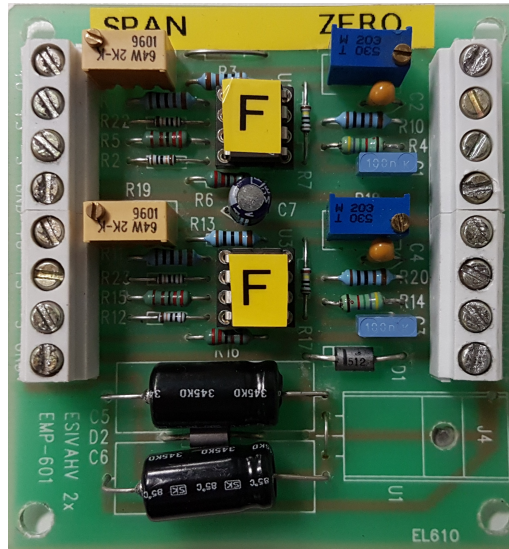
Figure 4.8 *voltage amplification using zero-span circuit*

To convert the read voltage by Arduino to mass, it is needed to find the relation between voltage and the mass. According to the manufacturer's catalogue and the experiments done, the voltage increases linearly with respect to the mass, Hence the following experiments is done to obtain the first order polynomial fitting the Loadcell's characteristics curve:

1. First the Loadcell's amplified output is read without attaching any mass and the the potensiometer is tuned to achieve 1V at 0 kg.

2. The previous step is repeated to set the maximum voltage to 4.5V for 50kg of mass hanged from the loadcell.

3. The masses from 5kg to 45kg with 5kg increments were hanged from the loadcell and the voltages were read afterwards to validate the linearity of fitted curve(figure 4.9).

The first order polynomial fitted to the measured data is as below:

$$M(kg) = V(volts) \times 14.28 - 5.774 \tag{4.1}$$

4.3.3 Pressure Sensor

According to the manufacturer's catalogue, the output of the pressure sensor varies linearly between 1V and 5V for the pressure range of 0 to 1 MPa. As it can be seen

Figure 4.9 *Loadcell calibration*

in figure 4.10(a), three wires are used for the operation of the sensor. A voltage of 12 VDC is given as excitation to the sensor and the analogue output is read using one of the analogue pins on Arduino Mega. The output is directly read by the Arduino pins since the output range of pressure sensor exactly matches the working voltage range of Arduino Mega.

The relation between pressure and voltage is given by the manufacturer in figure 4.10(b), however to calibrate the sensor more accurately, the following experiments are done:

1. two pressure gauges are used as the reference pressure in parallel.

2. The pressures inside the air tank is set to 0 and the voltage is read.

3. The voltage is read for the pressure from 0 to 10 bars with 1 bars increments.

Based on the measured data, the same slope as the one stated in data-sheet is obtained, however the distance from the origin at V=0 is slightly different for each sensor. For three pressure sensors, the following first order polynomials are obtained:

$$P(bars) = V(volts) \times 2.525 - 2.525(2.528, 2.537) \tag{4.2}$$

Internal Circuit

PSE53□
Voltage output type
1 to 5 V
Output impedance
Approx. 1 kΩ
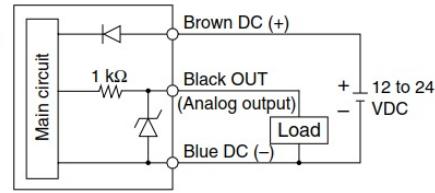
(a) Pressure sensor electrical connection

Analog Output
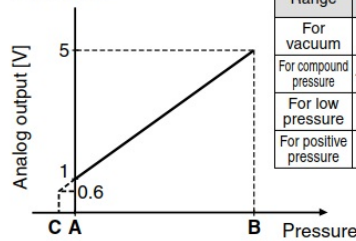
Range	Rated pressure range	A	B	C
For vacuum	0 to –101 kPa	0	–101 kPa	10.1 kPa
For compound pressure	–101 kPa to 101 kPa	–101 kPa	101 kPa	—
For low pressure	0 to 101 kPa	0	101 kPa	–10.1 kPa
For positive pressure	0 to 1 MPa	0	1 MPa	–0.1 MPa

(b) Pressure sensor analogue output

Figure 4.10 *Pressure sensor properties*

4.3.4   Temperature sensor

According to the manufacturer's catalogue, L535 series temperature sensors does not require external trimming and subtracting constant values due to inherent calibration. It means that the temperature is proportional to the output voltage. The electrical characteristics of LM35 is summarized in table 4.3. The equation for

Table 4.3 *LM35 electrical and output characteristic*

Title	Value	Description
Supply Voltage	4-30 V	5V from PS is selected
Typical curve slope	10 mV/$^{\circ}c$	-

calculating the temperature is as below:

$$T(^{\circ}C) = V(volts) \times 100 \tag{4.3}$$

The operating range of LM35 used in the study is -55 to 150 hence the maximum voltage produced by the sensor is 1.5V which is below the voltage limits of Arduino pins.

Removing noises

The challenge with LM35 despite its simplicity to work with, is that the noise from its environment can affect it easily specially when the wiring is too long. In the case of Magni since the sensor and Arduino are not close enough, the output was dominated by noise. However, this noise is eliminated by implementing the following circuit that has been proposed by the manufacturer:

Figure 4.11 *Removing noise using R-C damper*

4.4   Valve Triggering

The procedure for triggering the valves is classified as below:

- Software(gpio_control ROS node) which is responsible for listening to control commands

- Hardware (driver) which is responsible for triggering valves based on digital signals of RPI.

The commands generated based on the basic control logic and the control algorithm are explained with details in chapter 5.

gpio_control ROS node

This C++ ROS node is developed on RPI which listens continuously to the topics advertising the control commands and generates voltage signals based on the messages it receives. For this purpose,"wiring pi" library is utilized which makes it possible to read and generate signals on GPIO pins.

Driver

The valves that have been utilized in this project need 12v signals as excitation which can not be provided by RPI pins. So the signals must be amplified by the

means of relays or amplifier circuits. Using relays impose a delay to the system due to the mechanical slow response. As a result a simple transistor board, figure 4.12, is made that triggers 12V of power supply when a weaker signal is generated by RPI.
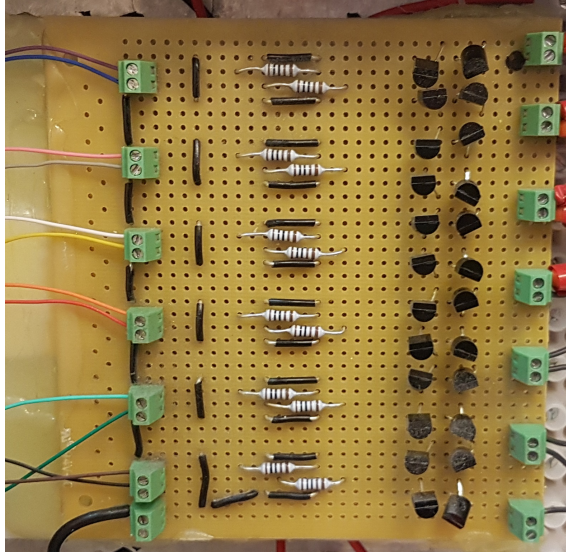
Figure 4.12 *Transistor Board*

The "base" pin of the transistors used in the circuit is connected to RPI pins corresponding to each valve, the -VDC from the valves is connected to GND of power supply and the +VDC wire of the valve is connected to supply voltage. Whenever the RPI triggers a valve, The transistors complete the line between GND and valve -VDC. The diagram of the mentioned circuit is demonstrated in figure 4.13.
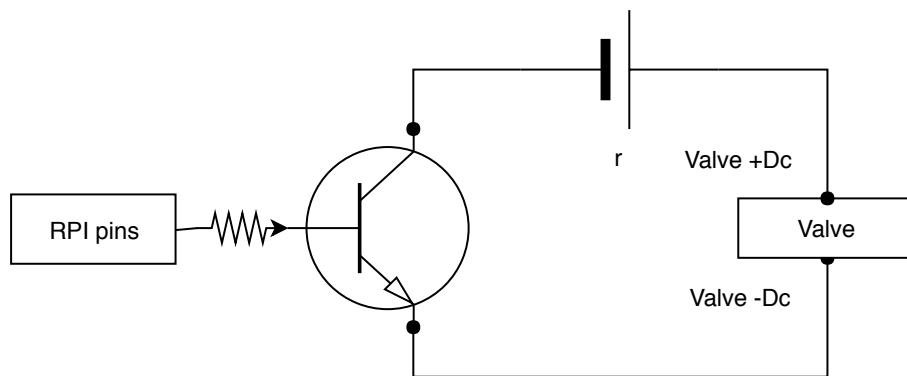
Figure 4.13 *Amplifier circuit using NPN transistor*

5. CONTROL

Different controllers are utilized in order to acheive desired motion by Magni. The main controller, Basic control logic, controls the timing of the valves and expansion and compression controllers control the intake and discharging period of the main controller to keep the magni work at a certain rpm.

As it is explained in the chapter 4, nodes are developed in ROS environment in order to achieve a fast and reliable communication between hardware and software. The following nodes are developed for being able to trigger the valves at the right time and acheive desired motion:

- Controller node which is responsible for collecting information from other nodes and making decisions.

- ang_pos which is responsible for reporting the shaft's angular position.

- ang_vel which is responsible for reporting the shaft's angular velocity.

- gpio_control which is responsible for receiving commands to manipulate GPIO pins on RPI.

- AI_Read which is the node that reports the status of Arduino analogue pins.

The above mentioned Nodes must work together in order to control magni based on the current state of Magni. Figure 5.1 demonstrates how these nodes are working in a loop. To develop the Controller node, the following approaches are possible:

- Using Simulink Environment and Robotics Systems toolbox

- Matlab Code

- Developing ROS nodes using C++ or python programming languages

- Generating Standalone nodes from Simulink environment
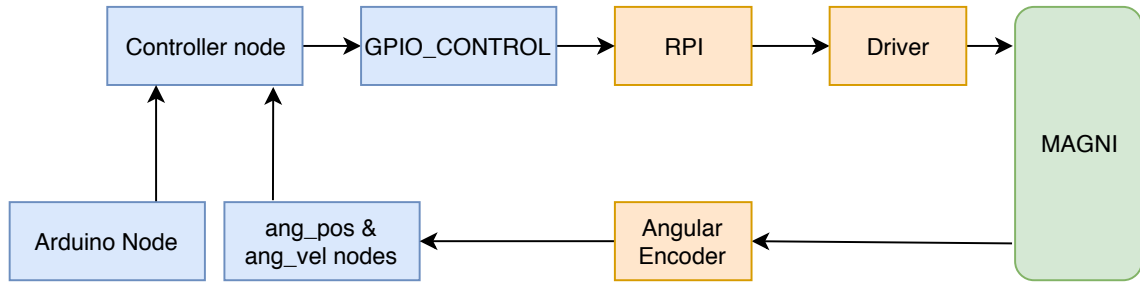
Figure 5.1 *Overall Layout*

Simulink is an environment in which the algorithms and logic of the controller can be implemented conveniently. Utilizing Simulink libraries alongside "Robotics systems toolbox" makes it possible to manipulate and control parameters and also to receive and log sensor data. However at the very first attempts, a simple Simulink model consist of only 2 "subscribe" and one "publisher" block was developed. The maximum frequency achieved by this method was 50 Hz which is not suitable for control purposes since at least 360 Hz is required as mentioned previously.

Matlab Code another approach is to develop a Matlab code and subscription to the topic published in ROS network. Same as Simulink environment, the code can only reach maximum of 50 Hz with simple subscriptions hence, it is not suitable for the purpose of this study. Aside the low speed, the complexity of developing long scripts in order to control, log and manipulation of parameters is not of interest.

C++ or python codes developing codes with C++ or python programming languages is the obvious solution to achieve fast response and communication speed in ROS network. A code consisting of subscribers and publishers can reach more than 5000 Hz easily with this approach since they are lower level programing languages. One of the major drawbacks of this approach alongside the developing of a suitable node is that recognition of possible errors, bug fixing and implementing different control logics are difficult and time consuming.

Simulink Stand Alone ROS Nodes another approach is to use code generation method in Matlab. Due to the convenient environment of Simulink, Simulink code generation is of interest in this study. Fortunately, Mathworks has added this feature to Simulink environment to convert Simulink models to stand alone C++ ROS nodes. As a result, developers are not required to get engaged with converting C++ codes to ROS nodes. Using this approach, developers and researchers can benefit from all the features of low-level programming languages as well as convenient and user friendly environment of Simulink.
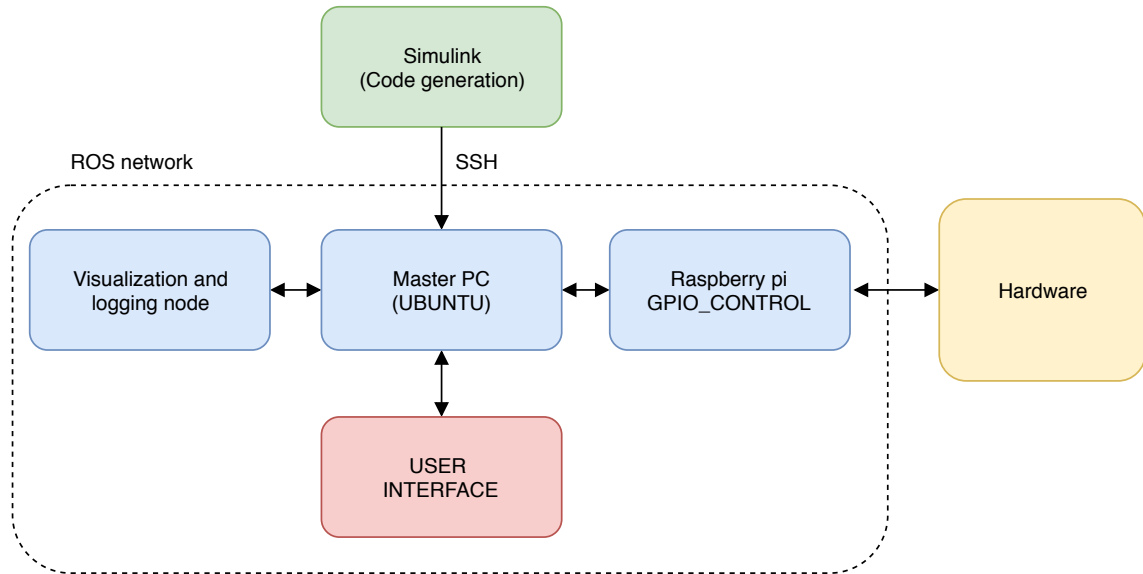
Figure 5.2 *ROS standalone node*

5.1 Magni Controller using ROS Stand Alone Code Generation feature

Magni controller node is being developed in Simulink environment and Simulink code generation has been used to build a standalone ROS node in a target computer. The operating system of the mentioned target pc is Ubuntu which is a necessity to run ROS nodes. figure 5.2 demonstrates how the nodes are connected together and how is it possible to monitor and log data in Matlab.

The configuration needed for generating standalone node is described with details in Mathworks website.

The controller node is responsible for receiving sensors' data over ROS network, processing the data and sending commands to "gpio_control" node based on the operating mode. For each mode, a certain logic is implemented to control the timing of valve openings to achieve the desired motion and behavior of Magni module. Moreover, since the desired working condition of Magni is at 60 rpm, a P-controller is designed and implemented for each mode to adjust the charging and compression phases respectively.

As it can be seen in the figure 5.3, 7 different modules inside the simulink model with different roles are developed in order to achieve the desired control commands that are explained below:

Subscribers The controller node makes its decisions based on the data reported
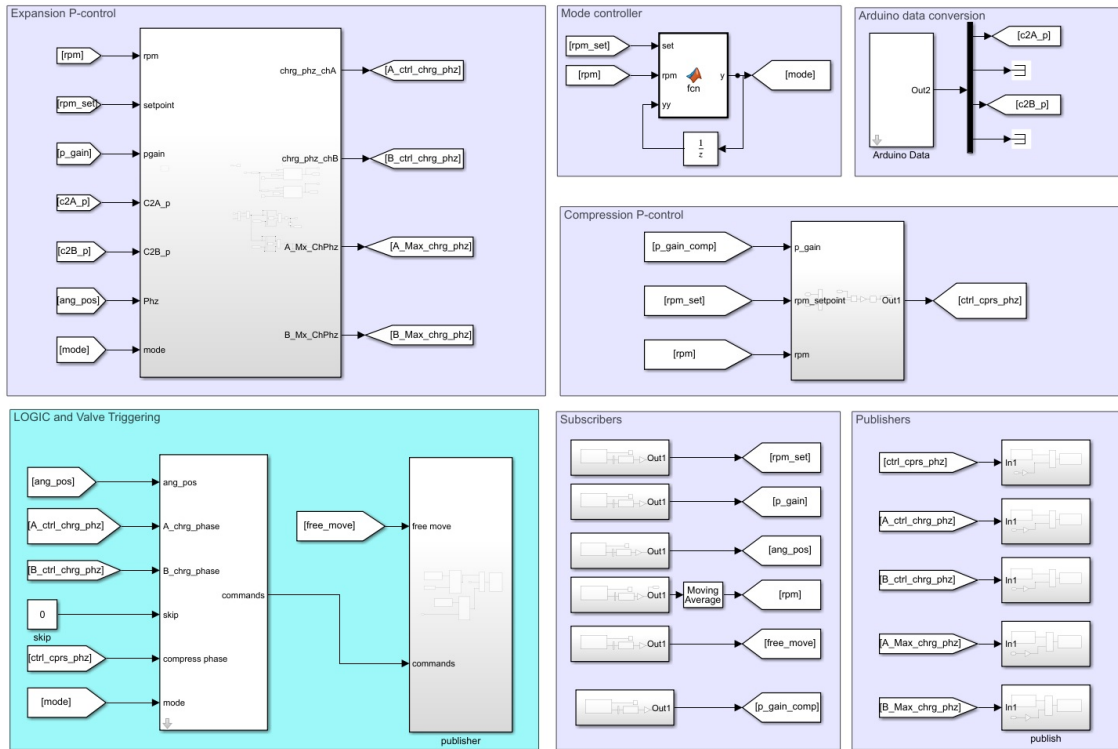
Figure 5.3 *controller node modules*

by the sensors and also the user commands. This parameters and data can be categorized as below:

- User defined parameters that are controlled and manipulated during execution of the controller node. rpm set point, proportional gain of the controllers and the operating mode are of this type.

- Sensor data that are being published over ROS network. Arduino analogue data and angular position and velocity from RPI are of this type.

Publishers: This module is being used to publish and report the decisions made by the controller node for further processing and visualization including charge phase of both chambers, compress phase, and upper limit of charge phase.

Basic control logic and valve triggering: Logic module is responsible for sending the trigger commands according to the phase, needed charge or compression phase and operating mode. Cycle characteristic parameters including charge starting phase, exhaust starting phase, exhaust start and ending phase and angular position calibration values are set in the mask of this subsystem.

As there are 6 chambers with 60 degree phase-shifts in Magni module, Logic module
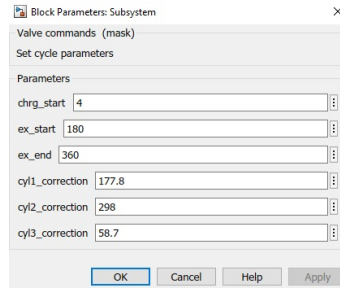
Figure   5.4 *Logic mask*
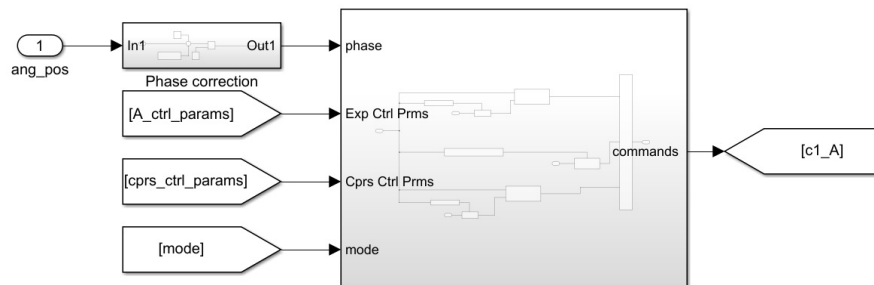
Figure   5.5 *control logic for each chamber*

has to make the decision for each chamber separately based on the phase in which the piston is at. As it can be seen in the figure 5.5, the inputs to the logic subsystems are phase, cycle parameters for either compression or expansion mode and the operating mode itself.

As it can be seen in the figure 5.6, control parameters and mode is being updated at specific phases:

- Control parameters for expansion and compression are only being updated at the beginning of each chamber cycle. This is due to the face that the control parameters will change continuously by the rpm regulating controllers which causes undesired valve openings during each cycle.

- The mode also is being updated every 180 degrees. This is a measure to avoid mode transition during the cycles and avoid releasing the pressurized air release into the ambient.

The logics for each operating mode is different in Valve timings. For expansion mode, as it can be seen in the figure 5.7, three conditions are possible:
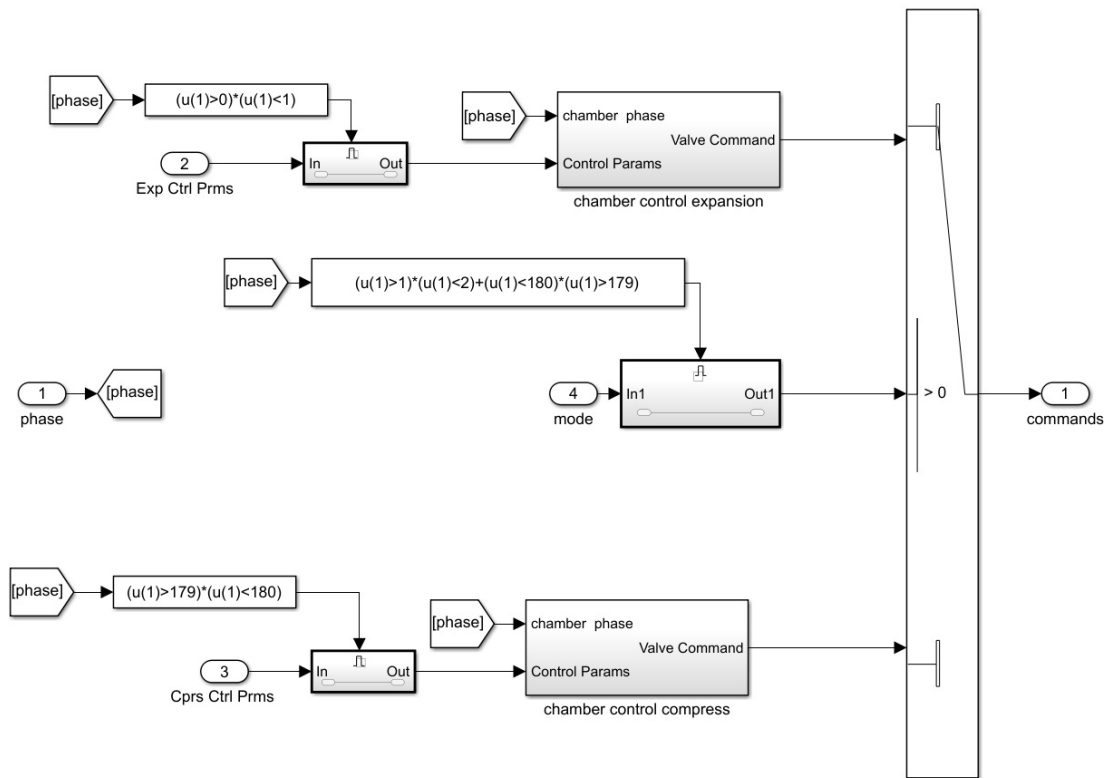
Figure 5.6 *updating cycle characteristic at certain phases*

- Chamber connected to supply line: "chrg_start" < phase < "chrg_start"+"chrg_phase".

- Chamber connected to exhaust: "ex_start" < phase < "ex_end".

- Valves off: other phases

For the compression mode, as it can be seen in figure 5.8, two conditions are possible:

- Chambers connected to exhaust (intake mode): 90<phase<360-"cprs_phase"

- Valves off: other phases

The compression in this mode occurs when the valves are not connected to exhaust or supply line. In fact, in the phase between 0 and 90, the chamber is expanding and the VBV does not let the pressure to go below ambient pressure, and when the phase is between 360-"cprs_phase" and 360, the pressure inside the chamber will begin to increase until it overtakes the pressure of supply line. At this stage, the HPDV will let the compressed air to the air tank.
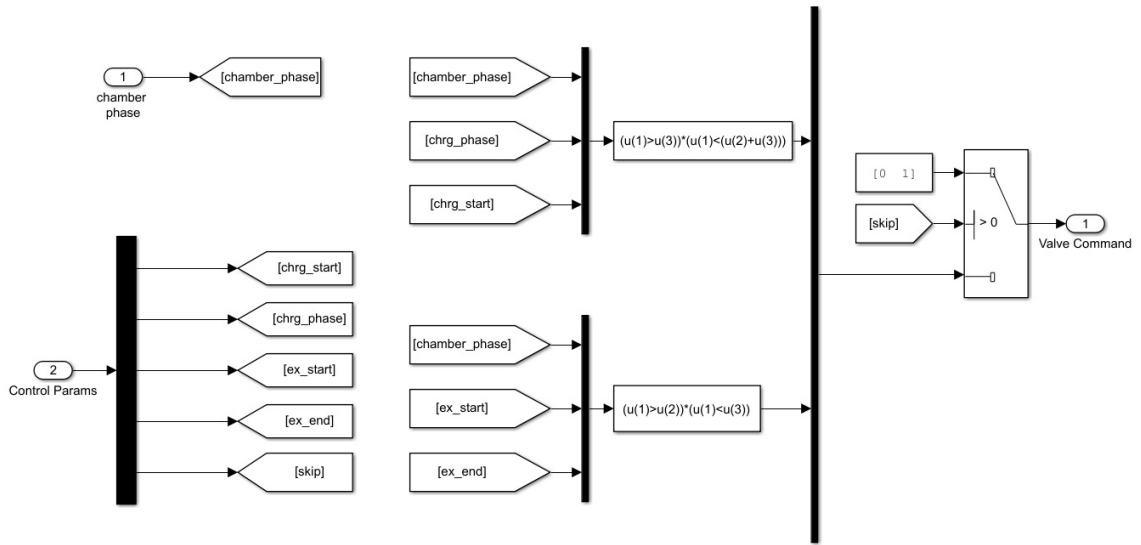
Figure **5.7** *valve timing logic in expansion mode*
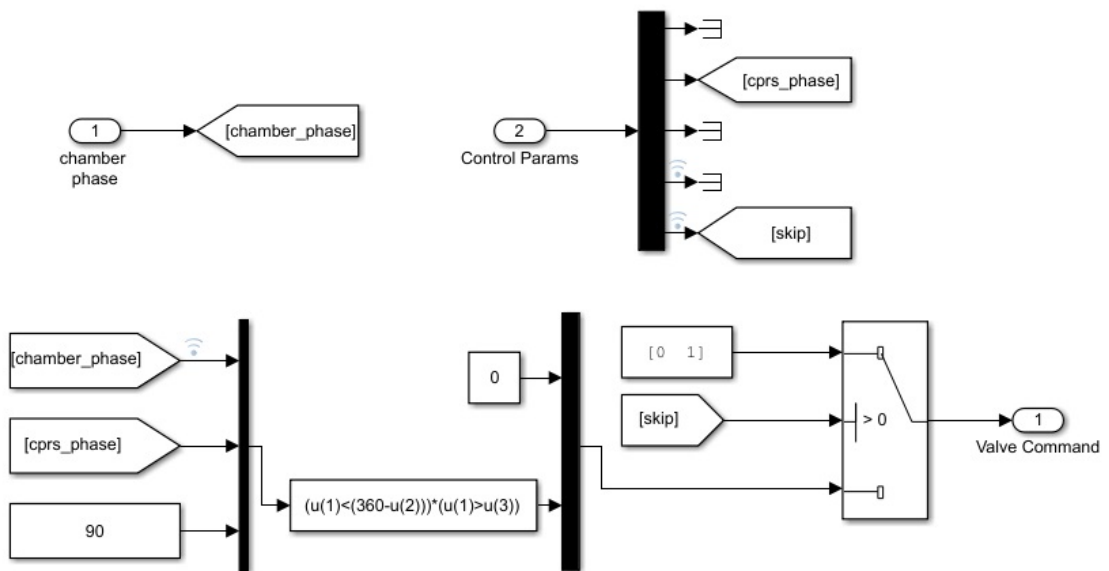
Figure **5.8** *valve timing logic in compression mode*

Expansion P-controller module

This module is responsible for determination of charge phases in both A and B chambers of the cylinders separately. The controller increases the charge phase with respect to error proportionally. The procedure of designing a P-controller will be elaborated through the next section.

Figure 5.9 in fact is illustrating a P-controller for a closed loop system in which rpm, that is reported using the encoder, is the feedback to the system. The output of the controller is saturated using "Upper limit" and "saturation" blocks respectively. The reason for overriding the saturation block with Upper limit block is that the maximum charge phase is being controlled in order to achieve the most efficiency.
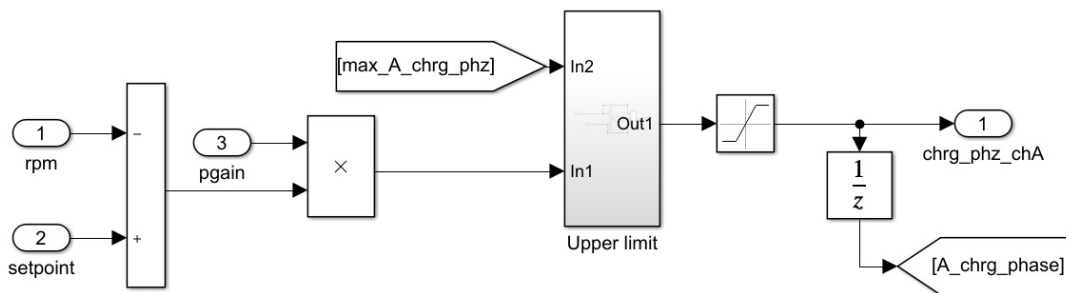
Figure 5.9 *Expansion mode P-controller for rpm regulation*

As mentioned previously, maximum charge phase is being changed during the execution. This is done for each chamber using separate controllers. The objective is to find the optimum max charge phase which can guarantee the most delivered torque as well as least waste of energy (no pressurized air at the end of cycle). However, this is only being used in efficiency tests or when higher efficiencies are of interest. In the cases when torque generation is of interest, it will not override the fixed "saturation" block. The procedure of designing controller will be elaborated in the next sections.

Compression P-controller module

As it can be seen in the figure 5.10, the P-controller for compression mode has similar structure to the expansion mode. The difference between the controllers is only in saturation blocks. There is no need to override the saturation block since it does not affect efficiency. The fixed saturation block is set to 20 and 180 as minimum and maximum respectively in order to ensure the controller will determine proper

compression phases. In this case, with the growing error, compress phase increases
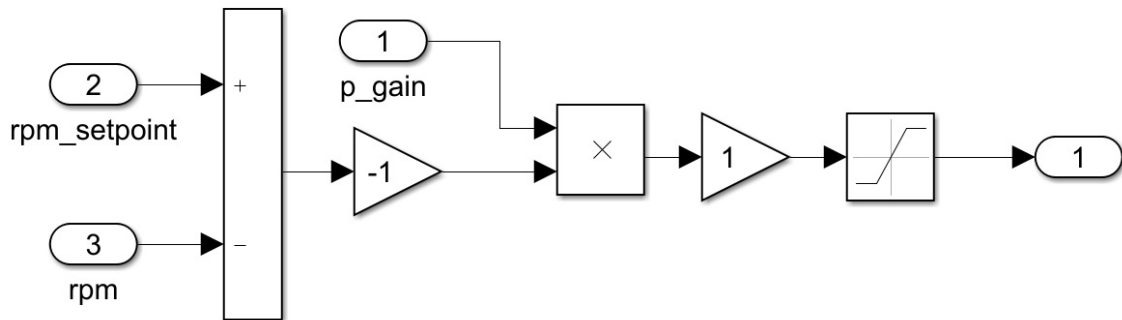
Figure *5.10* *Compression mode P-control for rpm regulation*

in order to decrease rpm since the compression impose resisting torque to the system.

Mode controller

Mode controller is responsible for maintaining the rpm set point. When the rpm is increasing by the external torque, it will enable compression mode and when the rpm is decreasing due to external torque, it will enable expansion mode. In fact, this Controller is utilized in the situations when the external torque is disturbing the system. The logic can be seen in the code below:

Table *5.1* *Mode definitions*

Mode 0	Mode 1
Compression	Expansion

mode controller

```
function y = fcn(set,rpm,yy)
u=yy;
if yy>2
u=1;
elseif yy==1 && rpm>set+1
u=0;
elseif yy==0 && rpm<set-1
u=1;
end
y=u;
end
```

The first condition "yy>2" is for the first step where the mode value is initially set

to 10 in order to start with expansion mode. A Unity delay block has been used to feed the subsystem with the previous cycle's mode.

Arduino Data Conversion

This subsystem is receiving 10 bit Arduino analogue output and converts sensor's raw data to corresponding decimal data. As it can be seen in the figure 5.11, three pressure sensors, two temperature sensors and one load cell are being converted to meaningful data based on the sensors' characteristics and using proper coefficients. Since the resolution of Arduino is 10 bits (0 to 1023), the inputs are divided by 1023
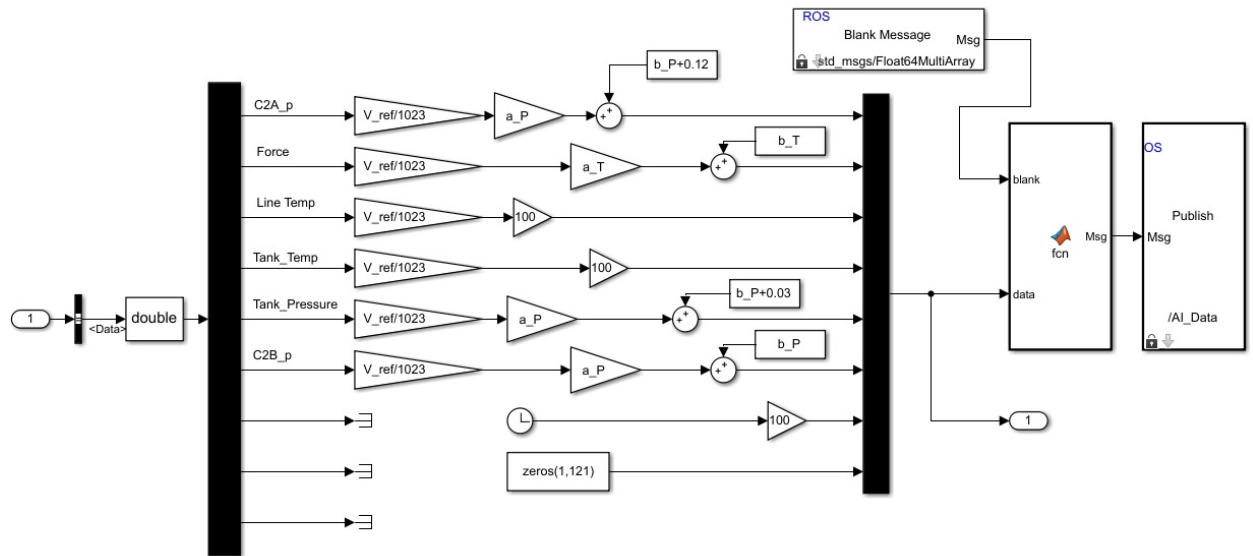
Figure   5.11 Arduino data conversion module

and multiplied by reference voltage which is given to Arduino Mega to calculate the sensed voltage. The converted signals are used inside control node for making decisions. The same Data will be published under "AI_Data" topic in order to be able to monitor the sensors' data over ROS network.

5.2   rpm regulation

Since Magni is supposed to work at a constant rpm, using rpm controller is inevitable. In order to obtain a suitable controller, it is necessary to have a mathematical model of the system to study its characteristics including steady state error and stability margins. The desired approach to control the rpm is to manipulate the charge or compress phase in compression or expansion modes.

5.2.1 Mathematical model of the system

In order to reach this goal, a mathematical model representing the behavior of the system to the generated torque is needed. Two approaches are possible:

1. Mathematical modelling of each part of the system, finding relation between them and deriving state space model of the whole system.

2. by assuming the whole model as black box and using System Identification for Control method and deriving a mathematical model representing the system using experimental data.

In this study, since deriving the exact mathematical model of the machine requires complicated setups and it is not in the scope of this project and deriving the characteristics of Magni is possible by doing experiments, the latter approach is selected.

Experimental model

Since the working speed of Magni is 60 rpm, the experiments for deriving suitable transfer function from charge phase to rpm were done at this speed. Once the relation between charge phase and generated torque is obtained, the relation between dynamics of the system and torques imposed to the consumer module can be derived using Newton's second law.

Table 5.2 torque samples in different charge phases at 60 rpm

Charge phase	10	15	20	25	30	35	40	45	50	55
Torque	14.9	18.3	22.5	29.9	34	39.1	45.4	50.1	54.1	59
Charge phase	60	65	70	75	80	85	90	95	100	
Torque	63.6	68.3	72.9	75.8	78.9	83.3	84	85.7	87.6	

Plotting the generated torques versus charge phase, a linear trend is evident. The fitted first order polynomial to the sampled data is derived using Matlab "polyfit" function. The coefficients for the first order polynomial are shown in table 5.3. The relation between the Torque imposed to the consumer module and the dynamics of system can be represented as below:

$$\tau_{magni} - \tau_{CM} = I_{CM}\alpha \qquad (5.1)$$

Table 5.3 first order polynomial coefficients

a	b
0.86	8.21
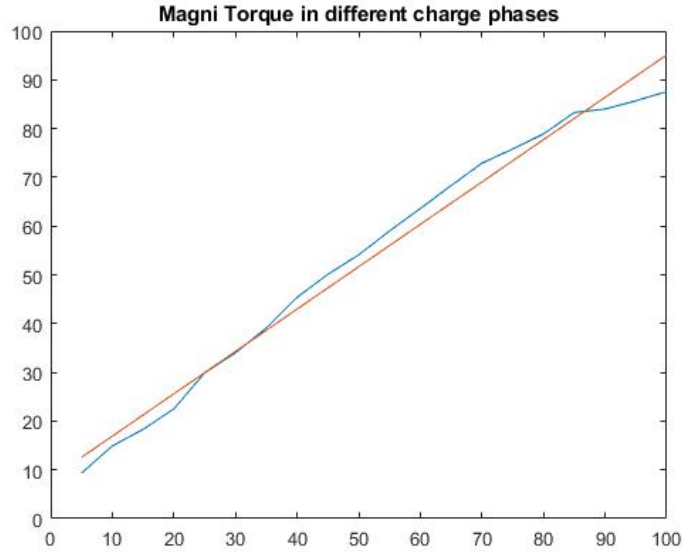
Figure 5.12 *generated torque in different charge phases*

$$\alpha = \frac{\tau_{magni} - \tau_{CM}}{I_{CM}} \tag{5.2}$$

In Eq 5.2, the torque terms in the nominator are derived from the data collected by experiments.

$$\tau_{magni} = 0.86 \times chrg\_phz + 8.21 \tag{5.3}$$

$$\tau_{CM} = 0.86 \times rpm + 12.6 \tag{5.4}$$

Subtituting Eqs 5.3 and 5.4 into 5.2 along with the integral of acceleration, the angular velocity is obtained. Figure 5.13 is the block diagram of mentioned model in matlab simulink. As it can be seen in the figure 5.13, the constant part of torque
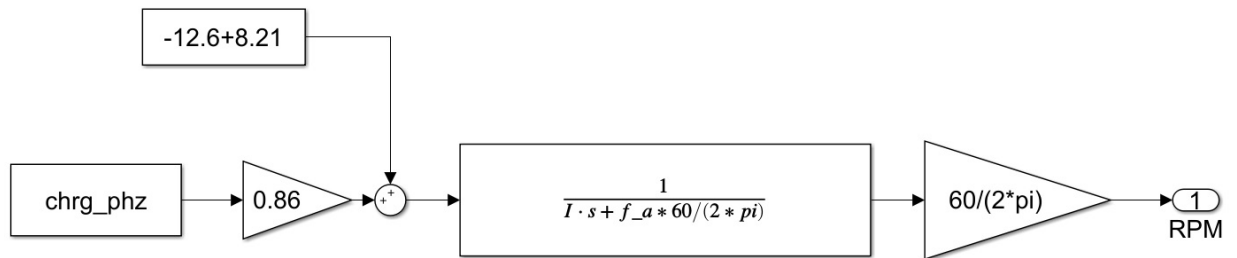
Figure 5.13 *Block diagram of Magni from charge phase to rpm*

equations are added to the system as disturbance since they can be assumed as a constant torques affecting the system. The term f_a in the block diagram is the sum of Magni and CM module viscous coefficients.

Adding rpm feedback for rpm regulation

Having the Block diagram from charge phase to rpm, the block diagram of the desired feedback loop can be represented as in figure 5.14
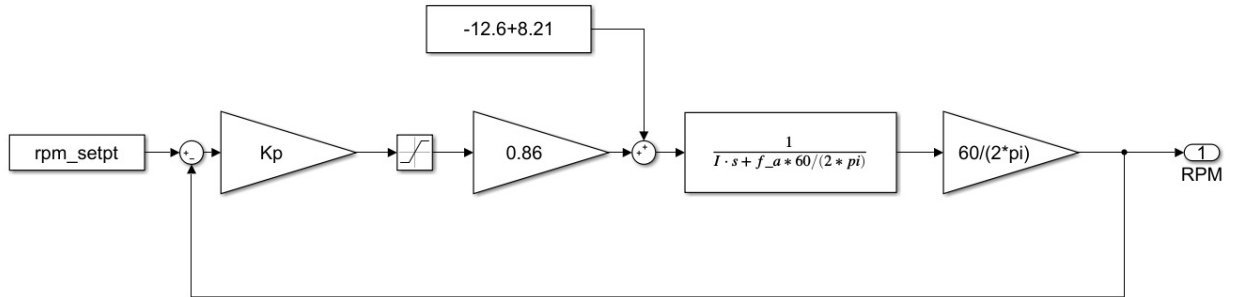
Figure 5.14 *Magni closed loop transfer function with rpm feedback*

According to figure 5.14 and assuming Kp equal to 1, the open loop transfer function from rpm set-point to output rpm of the system is as below:

$$TF_{openloop} = \frac{0.86 \times \frac{60}{2\pi}}{Is + \alpha_{friction} \times \frac{60}{2\pi}} \tag{5.5}$$

Using Matlab function Damp(TF), the following information about the system is derived:

damp(TF)=

Table 5.4 *dynamic characteristics*

Poles	Damping factor	Frequency(rad/sec)	Time constant(sec)
-8.2e-3	1.00e+00	8.2e-3	1.22e+02

As it can be seen, the model is over damped and it reaches a steady final value by a constant charge phase input. This is also seen in the figure 5.15 which is the result of the mentioned TF to the constant input.

The model is reaching 60 rpm in approximately 140 secondsconds. Similar behavior has been observed in real experiments where Magni reached 60 rpm in the same duration with 100 degree of charge phase.
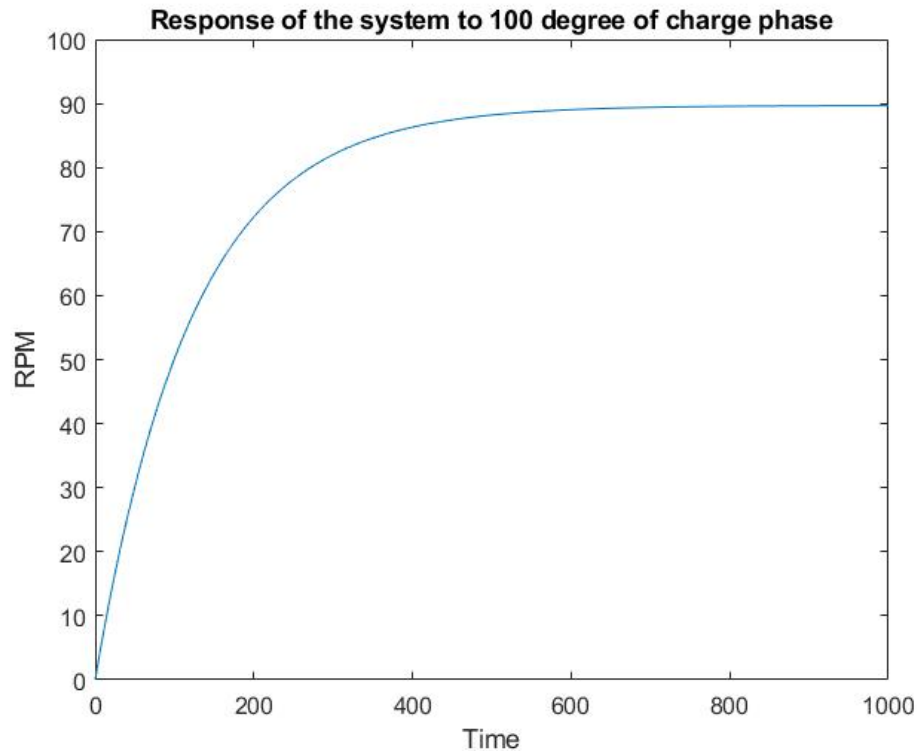
Figure 5.15 *Response of openloop TF to 100 degree of charge phase*

5.2.2 P-controller

In order to find suitable gain for proportional controller, it is needed to study maximum allowed error and stability margins since these two factors specify maximum and minimum gain limits.

Stability margin limitations

For the purpose of finding maximum gain limitations, Nyquist diagram and bode diagram of the openloop TF are plotted. (See figures 5.16 and 5.17)

By increasing the loop gain, the nyquist circle's diameters grows, however it still lies to the right side of imaginary axis and by increasing the loop gain, the phase margine decreases down top 90. From figures 5.16 and 5.17, it can be concluded that the transfer function never become unstable by increasing the loop gain. So there is no limit in the case of choosing proportional gain.

Maximum error limitations

In order to design an accurate controller, a minimum gain limit must be considered. This can be calculated using the relation between steady state error and the
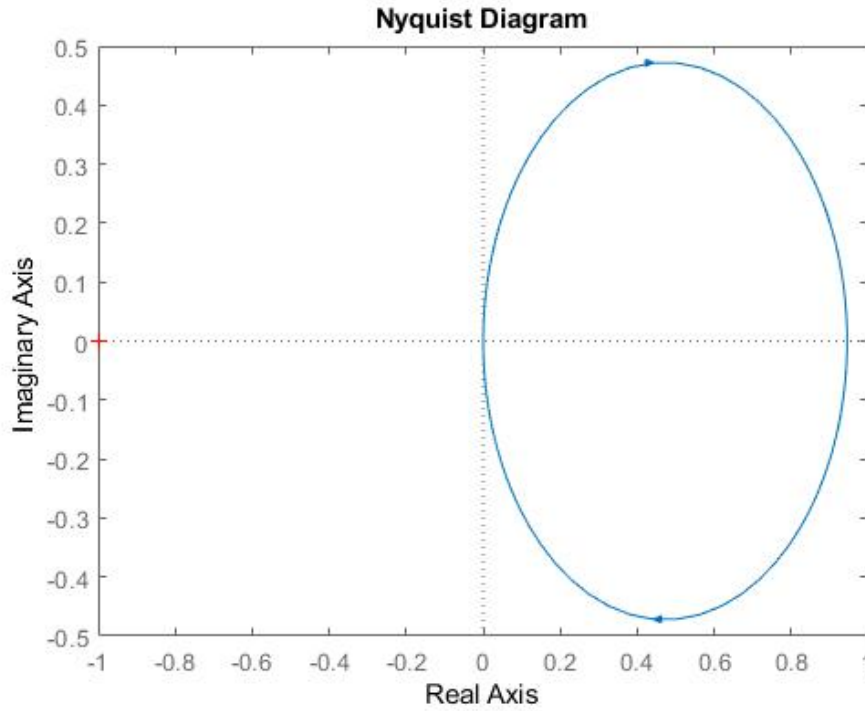
Figure 5.16 *Nyquist diagram*

proportional gain. From the block diagram we have:

$$E(s) = R(s) - Y(s) = \frac{R}{s} . \frac{1}{1 + Kp.TF_{openloop}} \tag{5.6}$$

where R(s) is rpm set point, Y(s) is the output rpm and E(s) is the error Transfer Function (TF). Using final value theorem, the steady state error can be calculated as below when **s** is approaching zero:

$$E(s)_{ss} = sE(s) = R\frac{1}{1 + Kp.TF_{openloop}} \tag{5.7}$$

Assuming maximum of 2 rpm error and substituting values in the equation 5.7 the gain "Kp" must be bigger than 18.

Conclusion

As it is calculated in this section the minimum and maximum gains are 18 and ∞. So any Kp greater than 18 is desirable and will improve the response time and reduces the error. However, a maximum of 120 degree charge phase is forced to the system using a saturation block.
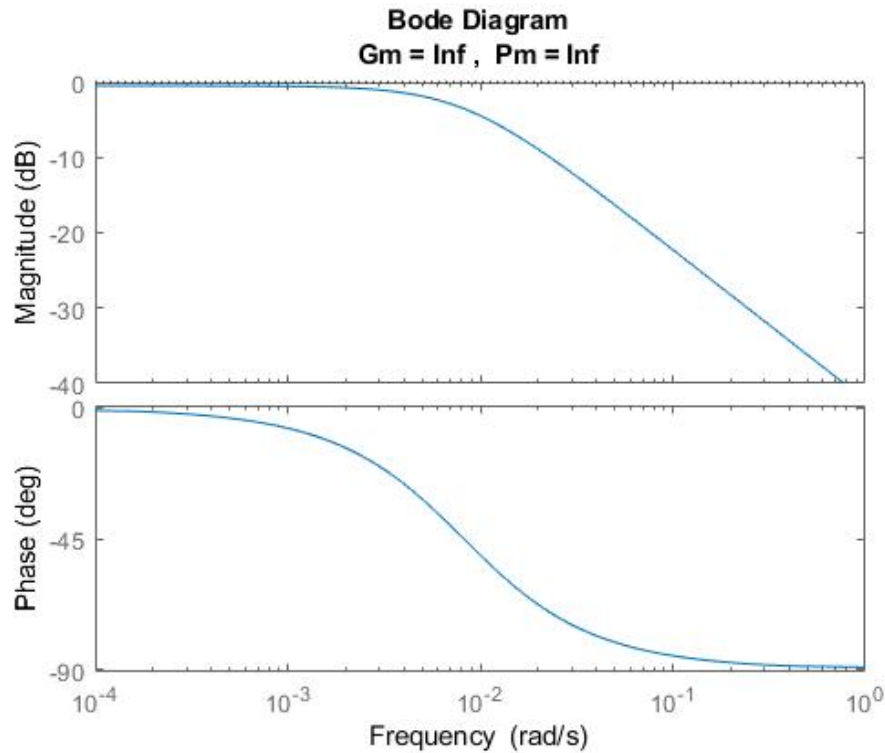
Figure 5.17 *Bode diagram*

5.3 Controller for highest efficiency

One of the main factors in evaluating Magni's performance is its efficiency beside its torque generating capacity. The maximum available torque is produced at full charge cycles, however at this condition, efficiency is not desirable since the pressurized air is released into ambient at the end of stroke. Consequently, to study the efficiency, charge phase must be controlled in a way that the pressure at the end of stroke be as close as possible to ambient pressure. To avoid pressurized air at the end of stroke, it is necessary to monitor the pressure inside chambers during the cycles. By monitoring the pressure, it is possible to decide whether to increase or decrease the charge phase accordingly. However, since the rpm regulating controller is changing the charge phase continuously to maintain the set point, the maximum charge phase, figure 5.9, is being controlled instead.

5.3.1 Maximum charge phase Controller

The logic behind the controller is to decrease the upper limit of charge phase if pressurized air exists at the end of stroke or if the chamber reaches ambient pressure earlier than the phase of 180°. As a result, an upper limit saturation is overriding

the saturation block using switch as it can be seen in figure 5.18.
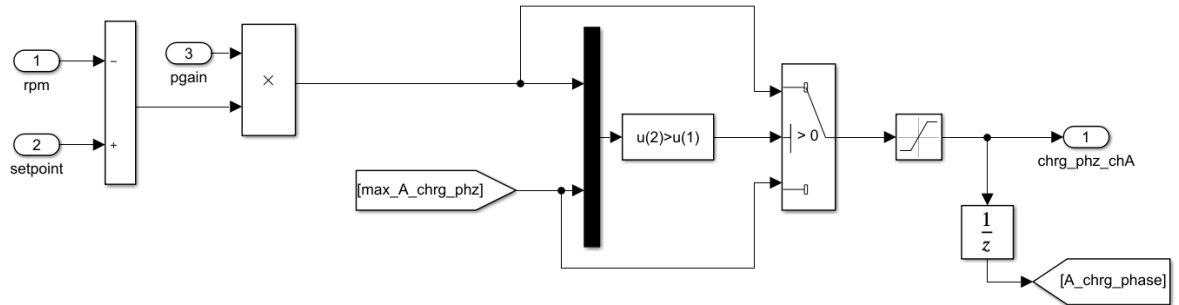
Figure 5.18 Manually forced upper limit
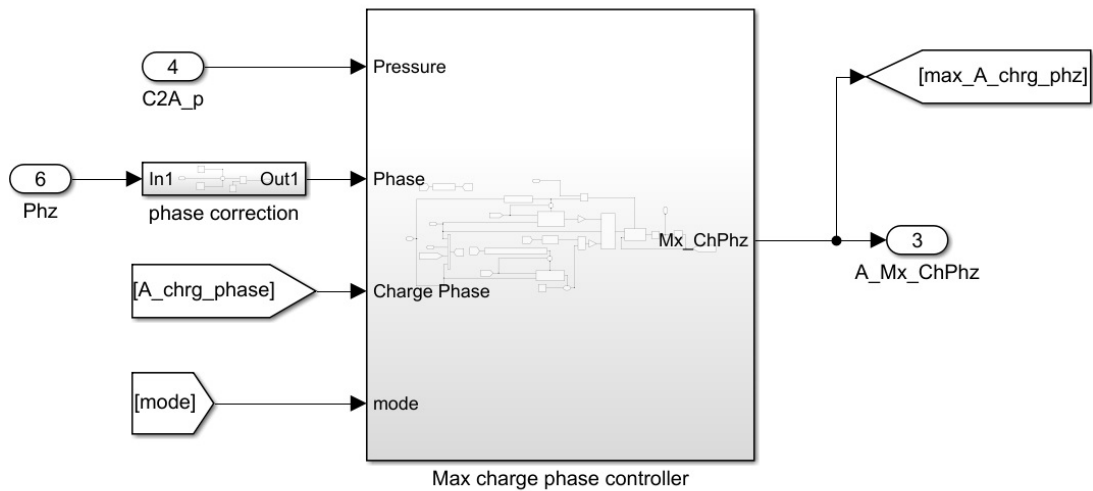
Figure 5.19 Maximum charge phase controller block

As it can be seen in the picture 5.19 and figure 5.20, controller is utilizing shaft phase, chamber pressure, charge phase at previous cycle and the working mode to make decision about the maximum charge phase.

There are two different criteria to switch between increasing or decreasing maximum charge phase. In either of the cases as it can be seen in figure 5.20 the generated error will be multiplied by suitable gains and the resulting deviation will correct the maximum charge phase of the previous cycle.
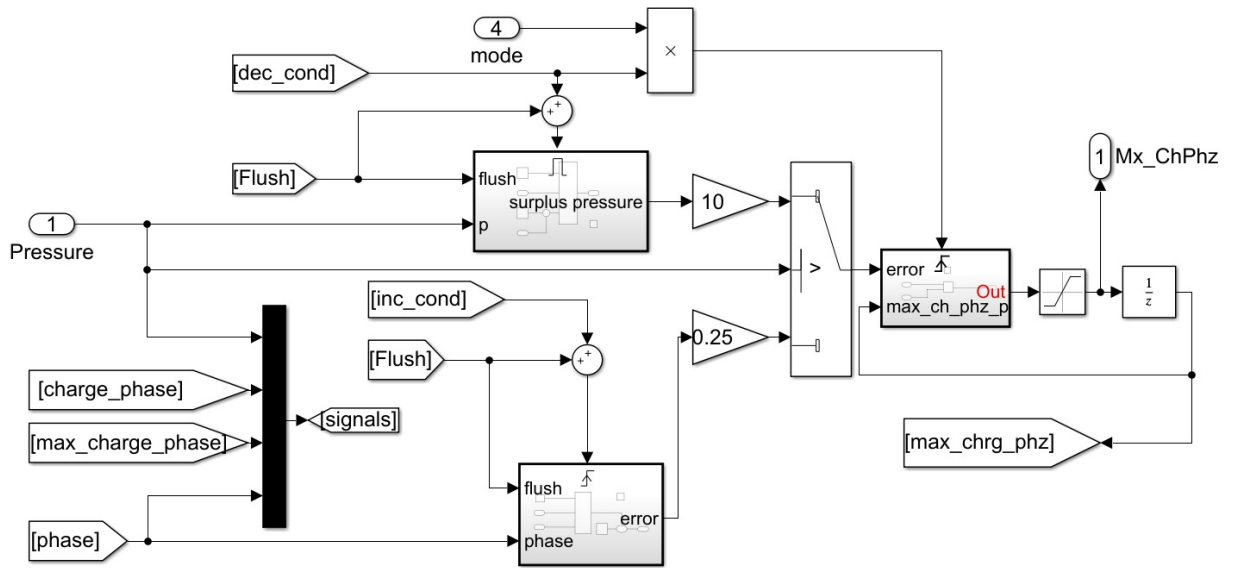
Figure 5.20 *MCP control logic*
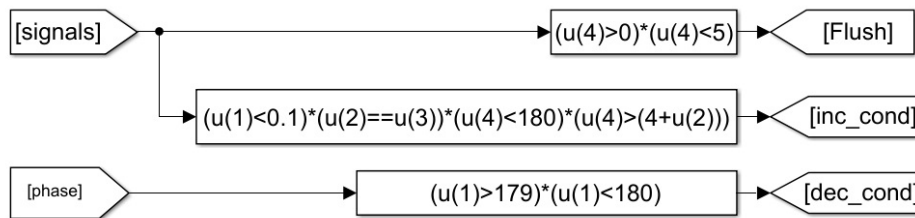
Figure 5.21 *controller conditions for updating error and flushing it*

Decreasing upper limit

The controller decreases the MCP when the pressure is above zero and the chamber is at a phase between 179 and 180. (See figure 5.21)In this situation, the pressurized air exists at the end of stroke which must be eliminated. Since the controller monitors the pressure at the end of stroke and the desired pressure is ambient pressure, the set point is ambient pressure which is being read by the pressure sensor.(See figure 5.22)

Increasing upper limit

As it can be seen in the figures 5.20 and 5.21, The controller increases the upper limit when all the following conditions are met:
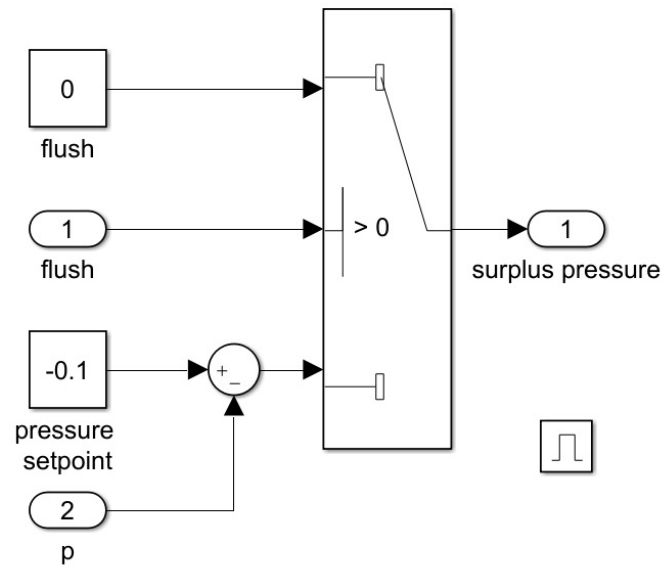
Figure 5.22 *Error when the chamber is in higher pressure than ambient at the end of stroke*

- The pressure is approximately zero

- The piston has passed the previous cycle's charge phase and is still not reached the end of stroke.

- The charge phase of rpm controller is equal to the maximum charge phase. This condition is added since the rpm controller might reduce the charge phase that causes the same situation, however in these cases, there is no need to correct the upper limit. In other words, the torque is limited by the controller to maintain rpm, not by the saturation block.

In this case, controller attempts to find and control the phase in which the above conditions are met. Since it is desired to have ambient pressure at the end of stroke, the set point of error subsystem is 180.(See figure 5.23)

When the controller updated the controlled MCP, a flush signal will clear the previous error found by the system so it will not change the controlled signal when the conditions are not satisfied.
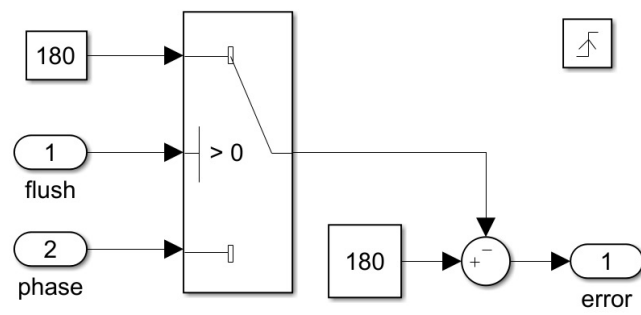
Figure 5.23 *Error when the chamber is in ambient pressure before the end of stroke*

6. SIMULATION

Simulation is a very important part of this study since it provides a way to extend the scope of this study to similar machines without the need to build a separate set-up. Simulation consists of generating mathematical models which provide the same outputs as the actual machine when given the same input parameters. For the purpose of this study, Matlab Simulink and its additional packages were used to generate this model. The simulation file include the following parts:

- Multi-body Modeling: this part is where the movement of the mechanical components are modeled and visualized using "Simscape Multi-body" package.

- Valves Modeling: the mass flow through all the valves of the system are modeled in this part using pure mathematical models which are fed with upstream and downstream pressures of each valve.

- Cylinder Modeling: this model calculates the pressure and generated force by each cylinder using the piston positions provided by "Multi-body Model" and mass flows provided by "Valve Models"

Figure 6.1 shows the highest level of simulation block diagram in which the inputs and outputs of the subsystems and the signal flow among them is evident. Eventually the simulated model is going to be controlled with the exact same control algorithm that is used to control the actual machine. Throughout the next sections, each of these parts are going to be explained in detail.

6.1 Multibody Modeling

In order to simulate the physical movements of the system, Matlab-Simulink Package, "Simscape Multi-body" is used which provides a suitable way to model such movements as well as relatively detailed 3D representation of the components and the assembly. Three main jobs were done in order to model each component:
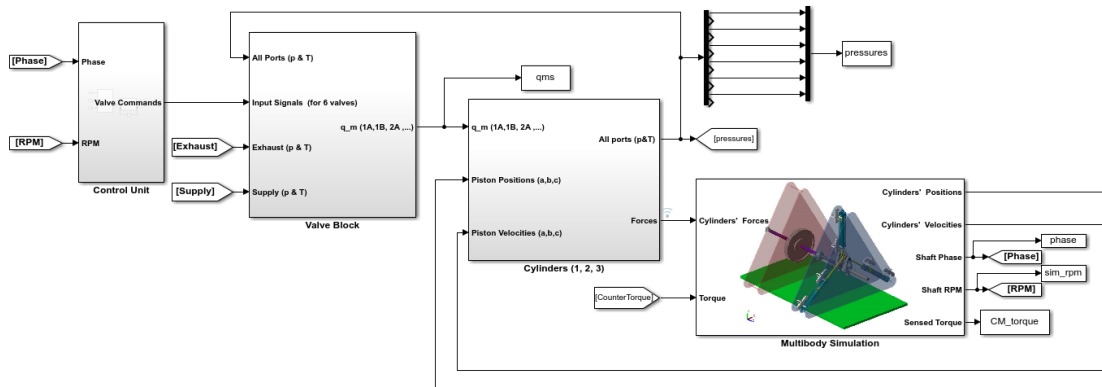
Figure 6.1 Full Simulation Diagram

- Adding Solid Blocks representing each component and setting corresponding physical parameters such as weight, inertia and center of mass inside every block. For this study, most of the parameters were set as variables and matrices and their values were later set inside Matlab code files.

- Making a 3D visualization of the component. This makes the user able to see a 3D representation of the whole model after the simulation is done and observe the apparent behavior of the system. Furthermore, Simscape can use the same 3D model to calculate the inertia properties of the components if provided with mass or density information. In order to visualize the mechanics of the subject system, Simscape offers some rudimentary 3D modeling features. The other alternative is importing 3D CAD models from another 3D modeling software. In this study both of the options were used depending on the complexity of the part.

- Using transforms and joints to define the connections and relations of the components with respect to each other. Most of the parameters of this part were also given to the model as variables and were later set inside the code.

Figure 6.2 illustrates the top level view of the multi-body modelling diagram which contains various subsystems that simulate different components of the machine. The process of modelling each part and setting the parameters and defining the relations are going to be explained throughout the next sections. In order to have more consistent and homogeneous model the following Conventions were followed which make the model easier to understand and modify:

- Parts which do not move relative to each other were put in subsystems and were connected to each other using "Rigid Transfer" blocks to form sub-assemblies.
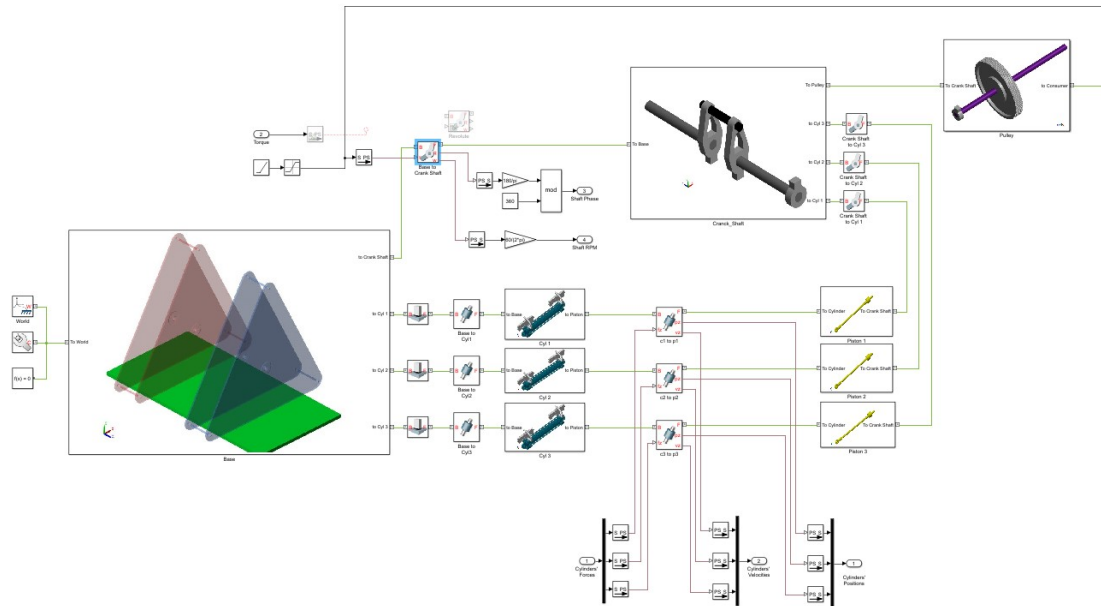
Figure 6.2 *Multibody Top Level Diagram*

The subsystems' icons were set to an image that includes all the solid bodies inside the sub-assembly.

- All the joints that make movements of sub-assemblies relative to each other possible, were put on the physical model root.

6.1.1 World

For a multi-body physical model to works, there must be a world frame, a Mechanism Configuration and a Solver Configuration Block inside the model. The 1st provides the connection of the model to the ground, the 2nd allows setting the gravity parameters and the latter is where physical simulation solver parameters are set as figure 6.3.

6.1.2 Base

Base is the sub-assembly immediately connected to the world and all other sub-assemblies are connected to it directly or indirectly. Parts forming the Base and their properties are explained in table 6.1

Figure 6.4 shows the base assembly block diagram and the resulting 3D model.
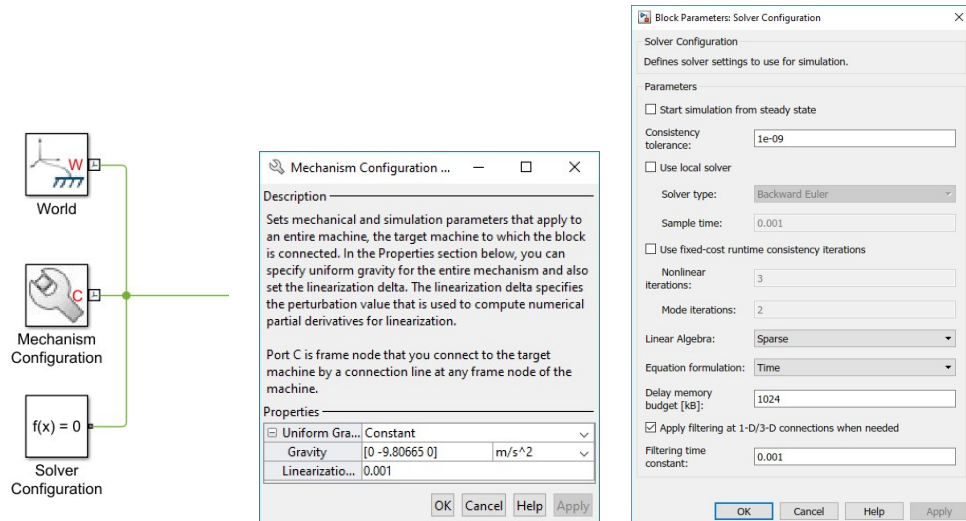
Figure 6.3 *World Diagram, Mechanism and Solver Parameters*

Table 6.1 *Base components and their properties.*

Part Name	3D Model Type	Inertia Parameters	Connected to
Magni Base	Imported STEP file Created in Solidworks	None of these parts are moving therefore the inertia parameters were left to default since they do not affect the simulation at all	• Three Cylinders on the three rods on the corners via Cylinderical Joints • Crank Shaft in the middle • Base Plate • Consumer Base
Consumer Base	Imported STEP file Created in Solidworks		• Magni Base
Base Plate	Simscape Basic Primitives		• Magni Base

6.1.3 Cylinder

There are three Cylinder sub-assemblies in the model each one including a cylinder model and two valves as shown in figure 6.5. Each one of them is connected to the Base separately and to their corresponding piston.

Parts forming the cylinder assembly, their properties and their connection are stated in table 6.2.

The cylinder used for Magni is made by Camozzi™ with the part number "60M2L032A0200". The mass properties were not provided in product's catalogue or on the manufacturer's website. As a result, in order to measure mass and Center of Mass (CoM)
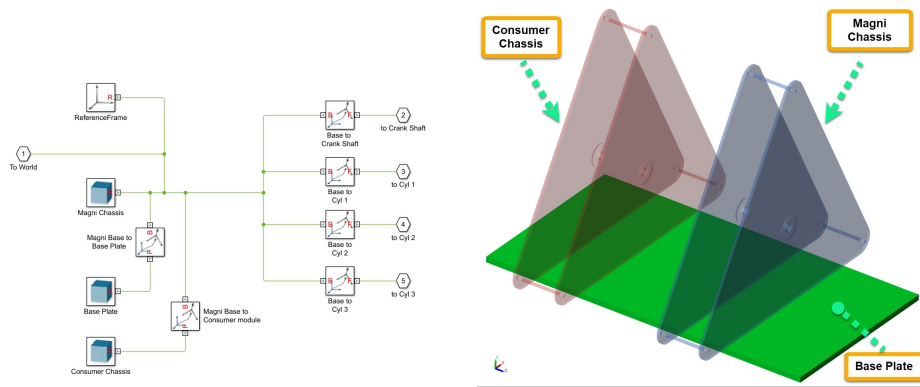
Figure 6.4 *Base block diagram and 3D model*
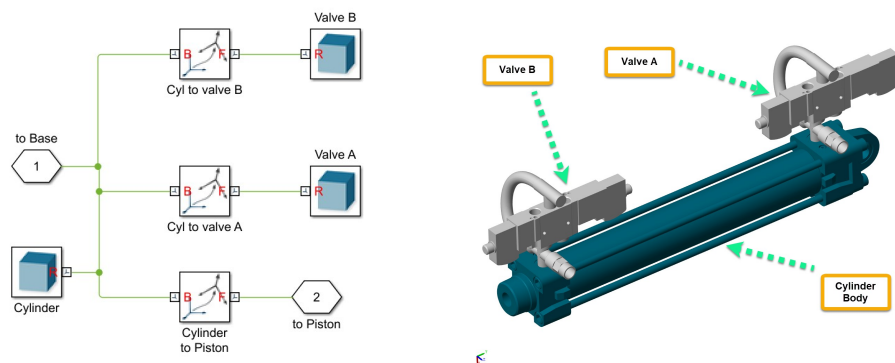
Figure 6.5 *Cylinder block diagram and 3D model*

of the cylinder body separately from the piston, it was disassembled and weighed then suspended and balanced on a thin edge as shown in Figure 6.6(a). The CoM in the 3D model provided by Camozzi was slightly different with the actual measured value, therefore it was manipulated using Solidworks in order to make the CoM be at the right location as shown in figure 6.6(b). With this strategy, there is no need to enter the inertia matrices as parameters in the Simscape model and the model was given the mass of the body, *cyl_mass*, and was set to calculate the inertia from the geometry.

The Valve 3D model is the body representing the valve assembly for each chamber including a 5/3-Valve, a cross fitting, two check-valves and a short tube. The 5/3-valve 3D model was downloaded from the manufacturer's website, SMC^{TM}to which the rest of the assembly was added using Solidworks. Since this assembly's mass is not significant comparing to other parts its inertia properties was approximated with a rectangular cube big enough for the valves and the cross fitting to fit and the CoM for this model was calculated from the mass and position of the sub-parts.

Table 6.2 *Cylinder components and their properties.*

Part Name	3D Model Type	Inertia Parameters	Connected to
Cylinder	Downloaded STEP file from the Manufacturer website and modified in Solidworks	Calculated by Geometry with provided mass value* Cyl_mass =0.664 kg	• Base via Cylinderical Joint • Piston via Cylinderical Joint • Two Valves at the to ports
Valve A and Valve B	Downloaded STEP file from the Manufacturer website and modified further in Solidworks	Approximated** with a rectangular cube of size 117*46*15 mm and measured Vlv_mass=0.155 kg And Calculated Vlv_COM=[0,28,11.5] mm	• To the Cylinder
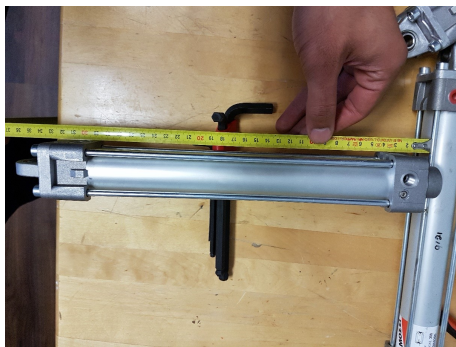
(a) Cylinder CoM measurement
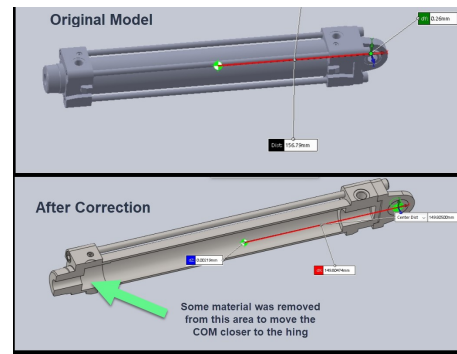
(b) Cylinder CoM Correction

Figure 6.6 *Measuring Cylinder Body CoM and Correcting cylinder 3D model accordingly*

6.1.4 Piston

There are three pistons in the physical model each one connected to their corresponding cylinder and to the crankshaft. The properties and connections are shown in Table 6.3. This part consists of the piston and the hinge that connects to the crankshaft. For determining the mass and CoM of the piston, it was weighed after the cylinder was disassembled and also suspended and balanced over a thin edge as shown in figure 6.7(a). The CoM of both parts assembled is calculated based on their measured masses and CoMs.The 3D model provided by Camozzi is not sufficiently representative of the actual part so more details are added in Solidworks and the model is tuned so that the CoM position matches the measured value as shown in figure 6.7(b). Similar to the cylinder body with this accurate enough 3D model, only mass of this part is given to the simulation as *pstn_mass* and the solid body block is set to calculate the inertia from the geometry. The corresponding block diagram and 3D model are shown in figure 6.8.

(a) Piston CoM measurement
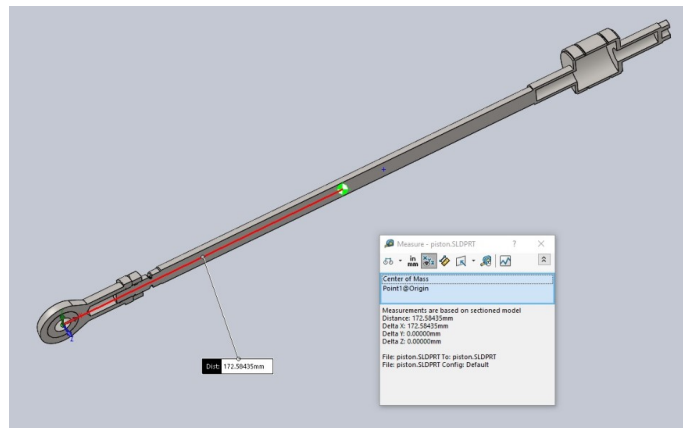
(b) Piston CoM Correction

Figure 6.7 *Measuring Piston CoM and correcting the 3D model accordingly*
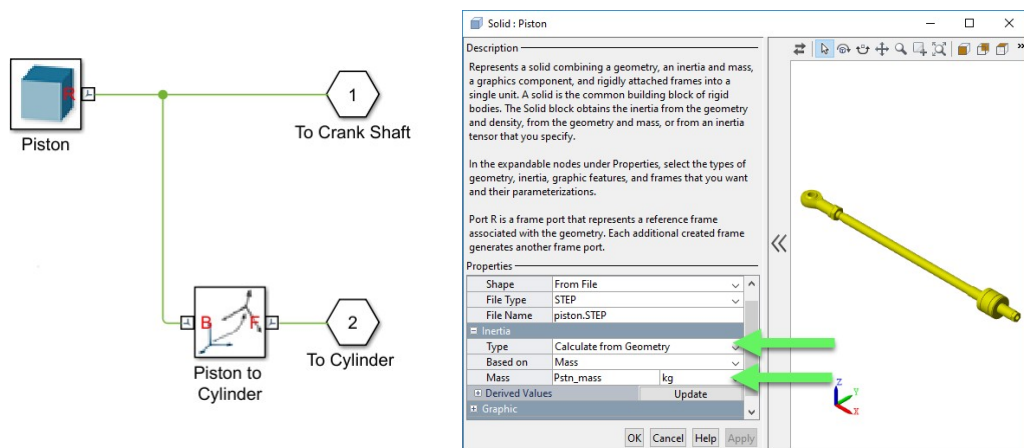
Figure 6.8 *Piston block diagram and 3D model*

Table *6.3* *Piston properties and connections .*

Part Name	3D Model Type	Inertia Parameters	Connected to
Piston	Downloaded STEP file from the Manufacturer website and modified in Solidworks	Calculated by Geometry with provided mass value Pstn_mass =0.38 kg	• Cylinder via cylinderical joint • Crankshaft via Revolute joint

6.1.5 Crankshaft

The crankshaft sub-assembly is the part that converts the linear forces and movements of the pistons to torque and rotation respectively. The parts forming this sub-assembly, their properties and connections are stated in Table 6.4 and the corresponding block diagram and 3D model are illustrated in figure 6.9.

Table *6.4* *Crankshaft parts and their properties and connections*

Part Name	3D Model Type	Inertia Parameters	Connected to
Cranks	STEP file Created in Solidworks	Calculated from geometry based on density=7800 kg/m³	• There are two cranks both connected to crank rod and each connected to one of the 240 mm shafts. • Crank 1 is connected to the base via a Revolute joint
Crank Rod	Simscape primitive, cylinder		• To both cranks rigidly
240 mm shafts	Simscape primitive, cylinder		• Each one connected to onr of the cranks rigidly • One connected to the coupling and the pulley rigidly
Coupling	STEP file Created in Solidworks		• To one of the 240 mm shafts

6.1.6 Pulley

Pulley sub-assembly is responsible to transfer the torque and motion to the Consumer module. Table 6.5 shows parts in this assembly along with their properties and connections. In figure 6.10 the block diagram of this assembly and the resulting 3D model are illustrated.
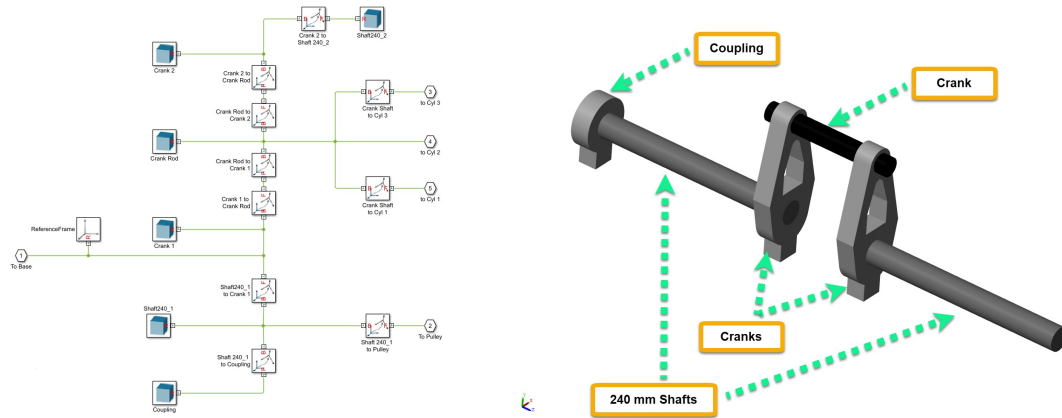
Figure 6.9 *Crankshaft block diagram and 3D model*

Table 6.5 *Pulley parts and their properties and connections*

Part Name	3D Model Type	Inertia Parameters	Connected to
Pulley	STEP file Created in Solidworks	Calculated from geometry based on density=7800 kg/m³	• To the shaft rigidly
600 mm shaft	Simscape primitive, cylinder		• To the pulley and the coupling rigidly • To the Crankshaft Rigidly • To the consumer rigidly
Coupling	STEP file Created in Solidworks		• To the shaft rigidly

6.1.7 Consumer Module (CM)

As explained in 3.4 the actual CM is consisted of various mechanical parts including different pulleys and belts, each one with inertia and friction characteristics of its own and modeling them in detail is neither simple nor necessary. Instead CM's inertia as a whole is simulated with an equivalent inertia block, figure 6.11(a) and the friction was simulated using an external torque which is a function of rpm exerted on the shaft revolute joint, figure 6.11(b). In reality the torque is applied to the pulley however since the parts along the shafts are connected rigidly and the simulation does not take the axial flexibility of the bodies into account, it does not generate any error. In order to measure these values, two experiments were conducted which are going are explained in next two sections:
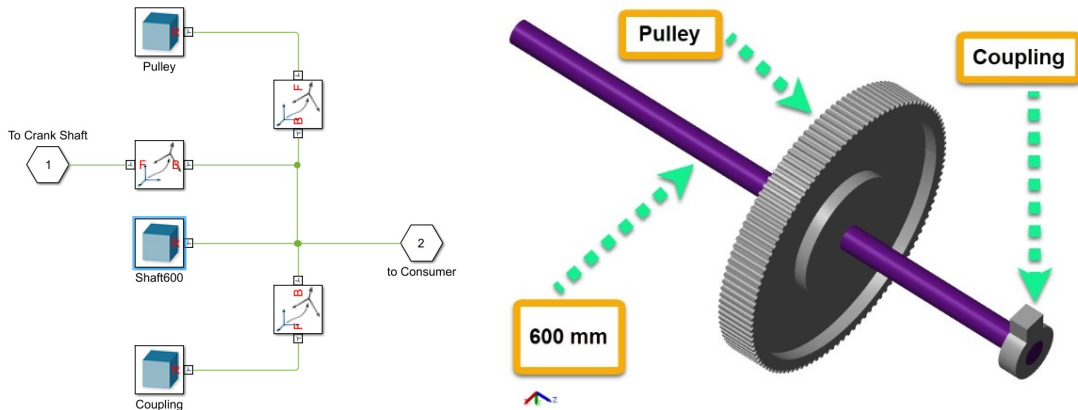
Figure 6.10 *Pulley block diagram and 3D model*

(a) Consumer module inertia block

(b) Input torque
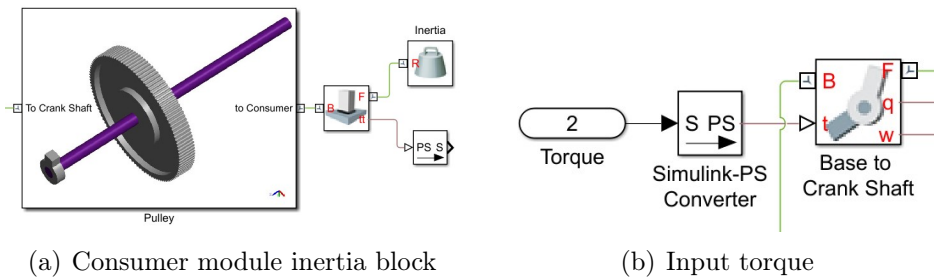
Figure 6.11 *Pulley block diagram and 3D model*

CM Friction Measurement

Magni was controlled with a P-controller in order to bring up the CM speed to various set points with 5 rpm intervals. The reason for doing the measurements at settled set-points is to eliminate the effect of torque needed to overcome the inertia. As it is evident in figure 6.12 the amount of torque required to keep the system rotating at each rpm setting grows as the speed increases. Using 11 points from 20 to 66 rpm, table 6.6, a first order polynomial was estimated to calculate the friction, Eq 6.1.

$$Friction = 0.86 \times \text{rpm} + 12.6 \tag{6.1}$$

In figure 6.13 the calculated and measured data are compared in order to examine the accuracy of the obtained model.
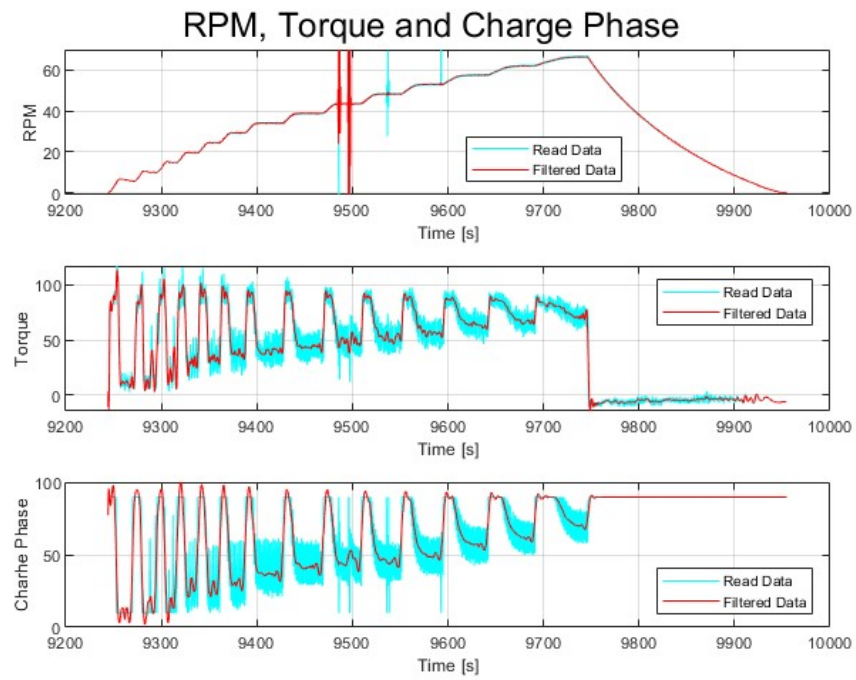
Figure ***6.12*** *Measuring CM friction*
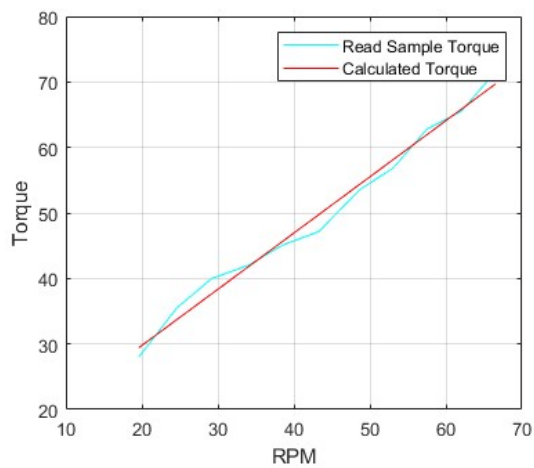
Figure ***6.13*** *Calculated and Measured CM friction*

Table 6.6 *CM friction measurement*

	1	2	3	4	5	6	7	8	9	10	11
rpm	19.6	24.6	29.2	34	38.5	43.3	48.3	53.1	57.5	62	66.5
Torque [N.m]	28	35.5	40	42	45.1	47.2	53.5	56.9	62.8	65.5	71.5

CM Inertia Measurement

In order to measure the inertia properties of the CM an experiment was conducted with high positive and negative rotational accelerations. First Magni was used to accelerate the whole system up to 65 rpm with a constant charging phase of 100. Afterwards all the valves were turned to closed state which means compression with compress phase of 180 which generates highest braking torque that Magni can produce. Speed and torque changes during this experiment are depicted in figure 6.14.

As shown in tables 6.7 and 6.8 , data from 11 points in Acceleration phase from 10 to 60 rpm and 9 points in deceleration phase, from 60 to 20 rpm with 5 rpm steps were read. Using Eqs 6.2 to 6.5, after deducting τ_{fr}, the previously calculated friction torque of the CM corresponding to the average rpm between two steps from τ_i, the measured torque, the value of remaining torque, τ_I, was used to calculate the inertia, I, for each two steps. After calculating the inertia based on all the data, an average equal to $1060 kg/m^2$ was accepted as the amount to be used in the simulations since there is only a narrow divergence (min 930 and max 1160).

$$\overline{rpm} = \frac{rpm_i + rpm_{i+1}}{2} \tag{6.2}$$

$$\tau_i = \tau_I + \tau_{fr} \tag{6.3}$$

$$\bar{\alpha} = \frac{\omega_{i+1} - \omega_i}{t_{i+1} - t_i} \tag{6.4}$$

$$\tau_I = I \times \bar{\alpha} \tag{6.5}$$
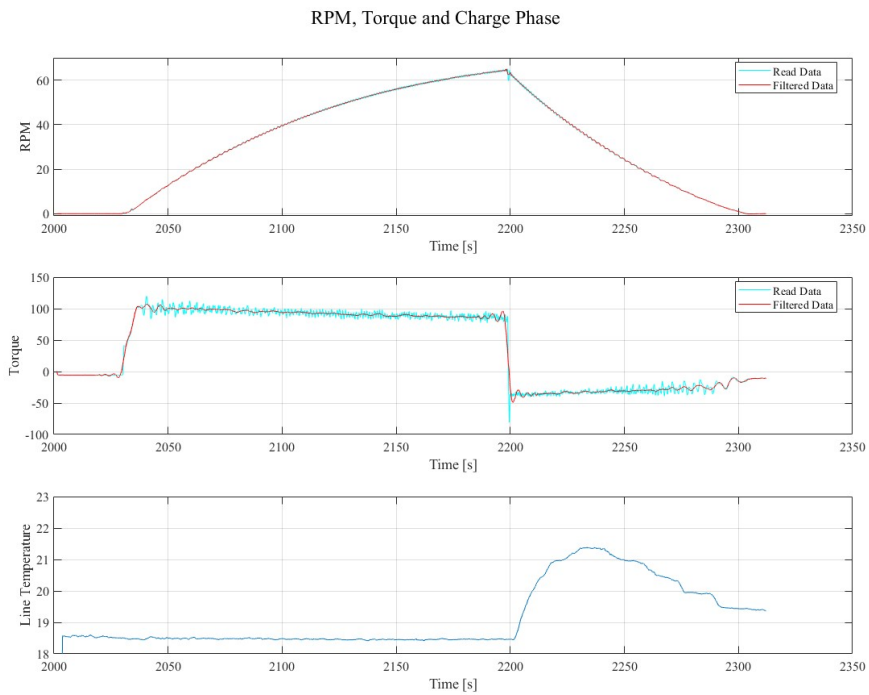
Figure 6.14 *Acceleration and Deceleration test to measure CM inertia*

Table 6.7 *CM Inertia measurement, Acceleration Test*

Acceleration Data Set								
	Average Torque	**rpm**	**Torque [N.m]**	**Time Difference [s]**	**Angular Acceleration [rad/s²]**	**Average rpm**	**CM Friction [N.m]**	**Inertia [kg/m²]**
1		10	105					
2	102.3	15	99.5	7.5	0.0698	12.5	23.4	1130
3	99.6	20	99.7	8	0.0654	17.5	27.7	1099
4	99.4	25	99	8.5	0.0616	22.5	32	1094
5	96.7	30	94.3	10	0.0524	27.5	36.3	1154
6	94.7	35	95	10	0.0524	32.5	40.6	1033
7	94.5	40	94	11	0.0476	37.5	44.9	1043
8	93.5	45	93	13	0.0403	42.5	49.2	1101
9	91.7	50	90.3	15	0.0349	47.5	53.5	1094
10	89.1	55	87.8	17	0.0308	52.5	57.8	1016
11	87.9	60	88	23.5	0.0223	57.5	62.1	1160

6.1.8 Actuation and Sensing

The Multi-body Subsystem has input and output signals which it receives and sends to the rest of the simulation. The inputs are given to a number of joints as actuations and the outputs are read from the sensing ports of other corresponding joints. These signals are shown in the subsystem mask figure 6.15 and their summary is stated in the table 6.9

Table *6.8* CM Inertia measurement, Deceleration Test

Deceleration Data Set								
	Average Torque	rpm	Torque [N.m]	Time Difference [s]	Angular Acceleration [rad/s²]	Average rpm	CM Friction [N.m]	Inertia [kg/m²]
1		60	-35					
2	-35	55	-35	5	-0.1047	57.5	62.1	927
3	-35.3	50	-35.6	6	-0.0873	52.5	57.8	1066
4	-35.7	45	-35.7	6	-0.0873	47.5	53.5	1021
5	-34.9	40	-34	7	-0.0748	42.5	49.2	1123
6	-32.7	35	-31.4	7	-0.0748	37.5	44.9	1037
7	-31.7	30	-32	7	-0.0748	32.5	40.6	966
8	-31.5	25	-31	8	-0.0654	27.5	36.3	1035
9	-30.3	20	-29.5	8.5	-0.0616	22.5	32	1010
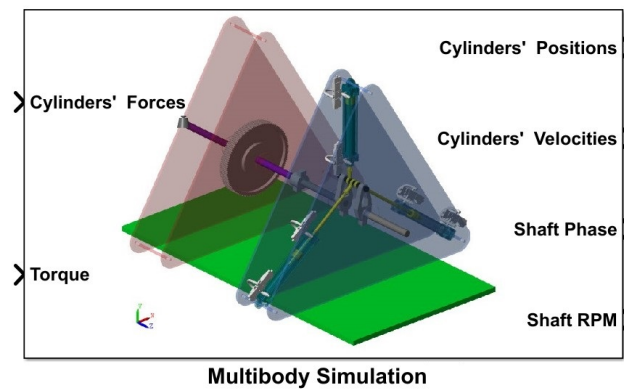
Figure *6.15* Multibody Subsystem mask

6.1.9   Friction
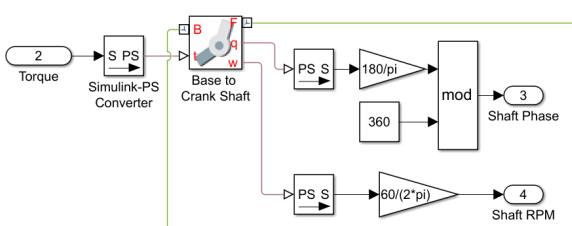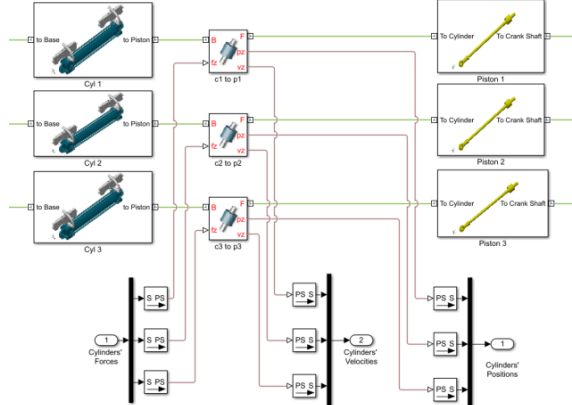
Magni friction is not modeled inside the Multi-body model. The friction of the system is calculated in other Simulink subsystems and applied to the multi-body assembly in form of external torque.

6.2   Modeling of Valve Flows

The Valve Block subsystem, figure 6.16, is consisted of six valve sets each one responsible for calculating the flow in and out of each chamber. This subsystem receives vectors containing the temperature and pressure information of chambers, ambient and supply tank as well as the valve control signals and calculates the mass flow rate of the chambers and exports it as a vector of size 6.

Three types of valves have been used to control the flow in and out of Magni cylinder.

Table 6.9 *Summary of Multibody input and output signals*

Signal Name	Type	Unit	Corresponding Joint	Image
Torque	Input	Nm	Base-Crankshaft Revolute	
Shaft Phase	Output	Degrees		
Shaft rpm	Output	rpm		
Cylinders' Forces	Input	N	Cylinder-Piston Cylindrical	
Cylinders' Positions	Output	m		
Cylinders' Velocities	Output	m/s		

Their model numbers and types as well as their manufacturer are stated in table 6.10.

Table 6.10 *Valve Model numbers, types and Manufacturers*

Model Number	Type	Manufacturer
SY5320R-6G-01F-X406-Q	5/3 control valve	SMC
AKH06A	One way valve	SMC
AKH06B	One way valve	SMC

Each valve set includes a 5/3-control valve and one of each check-valve types. The 5/3-control valves are controlled using the control algorithm allowing the control of the charge and compress phase of Magni thus adjusting the generated driving or breaking torque. AKH06A is a check valve that opens whenever the pressure inside the chambers fall behind ambient pressure and is going to be called VBV hereafter. AKH06B on the other hand is a check valve that opens whenever the pressure inside the chamber become higher than the supply line and is going to be regarded as HPDV. The Simulink model of a complete valve set, figure 6.17, receives the command signals and the temperature and pressure information at its ports and calculates the final mass flow rate which is the sum of the flow that passes
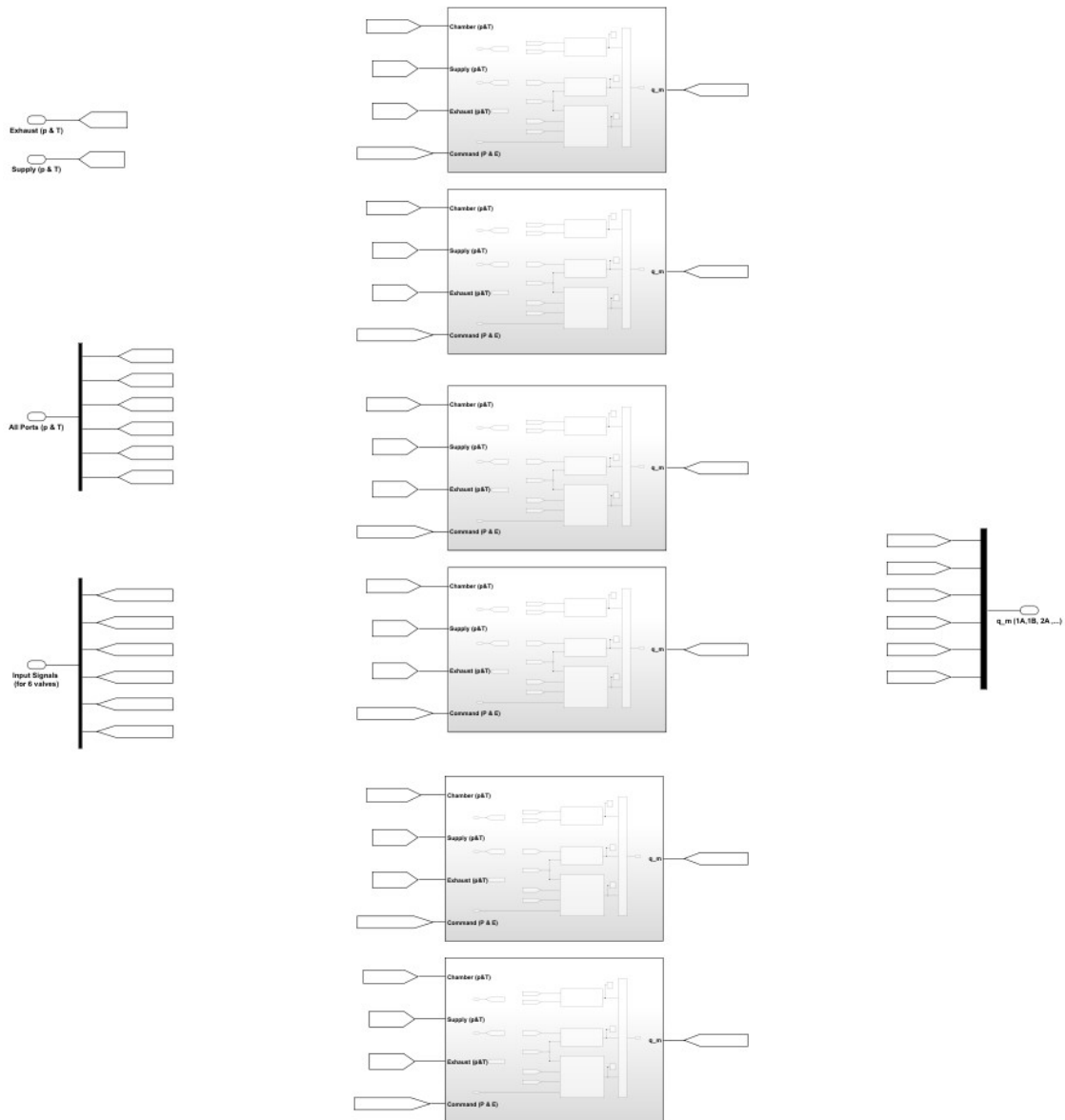
Figure 6.16 *Multibody Subsystem mask*

through all of the three valves. The flow that exits the 5/3-valve and VBV and enters the chamber is considered as positive flow and the flow that exits the chamber and goes to either 5/3-valve or HPDV is accounted as negative flow. The signals of this subsystem are summarized in table 6.11.

The mathematical models for these valves are developed based on ISO6358-1 standard [1] and the provided information by the manufacturer's data-sheet. This standard defines certain parameters to quantify the pneumatic flow characteristics of different pneumatic components while providing precise instructions for experiments to measure these parameters. The parameters and their definitions exactly as they
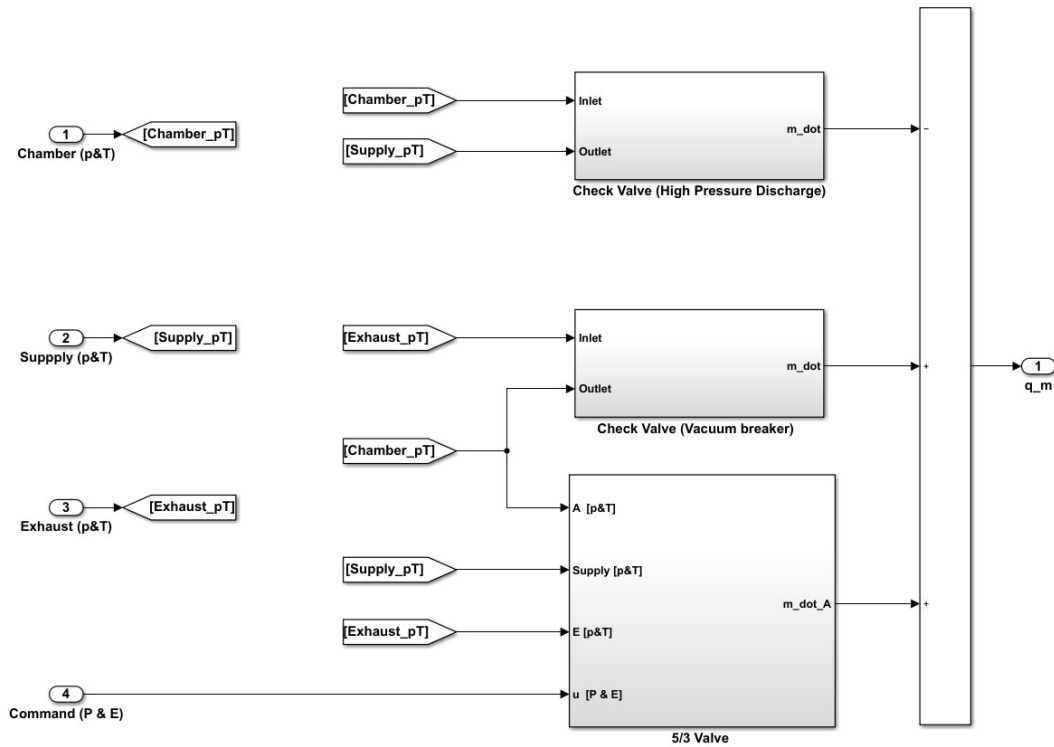
Figure 6.17 *Valve Assembly Model*

Table 6.11 *Valve assembly signal summary*

Signal Name	Type	Description and unit
Chamber (p&T)	Input Signal	Pressure and Temperature of the chamber [pa , °K]
Supply (p&T)	Input Signal	Pressure and Temperature of the Supply source [pa , °K]
Exhaust (p&T)	Input Signal	Pressure and Temperature of the Exhaust [pa , °K]
Command (P & E)	Input Signal	Vector of size 2 that opens the 5/3 valve to presser or exhaust [0/1, 0/1]
q_m	Output Signal	Mass flow out of the valve assembly [kg/s]

are in the standard are as follows:

- The sonic conductance, C, corresponding to the maximum flow rate (choked) is the most important parameter. This parameter is defined by the upstream stagnation conditions.

- The critical back-pressure ratio, b, representing the boundary between choked and subsonic flow is second in importance. Its definition differs here from the one in ISO 6358:1989 because it corresponds to the ratio of downstream to upstream stagnation pressures.

- The subsonic index, m is used if necessary to represent more accurately the

subsonic flow behaviour. For components with a fixed flow path, m is distributed around 0.5. In these cases, only the first two characteristic parameters C and b are necessary.

- The parameter $\boldsymbol{\Delta pc}$ is the cracking pressure. This parameter is used only for pneumatic components that open with increasing upstream pressure, such as non-return (check) valves or one-way flow control valves.

The standard in its Annex E provides equations to calculate the mass flow rates for different flow types which are stated in table 6.12 where p_u and T_u are the upstream pressure and temperature and ρ_0 and T_0 are the mass density and Temperature of air in standard conditions.

Table 6.12 *Massflow rate calculation based on ISO-6358-1*

Flow Type	Condition	Calculated Mass Flow rate [kg/s]
Subsonic	$b < \dfrac{p_d}{p_u} \leq 1 - \dfrac{\Delta p_c}{p_u}$	$q_m = C p_u \rho_0 \sqrt{\dfrac{T_0}{T_u}} \left\{ 1 - \left(\dfrac{\dfrac{p_d}{p_u} - b}{1 - \dfrac{\Delta p_c}{p_u} - b} \right)^2 \right\}^m$
Sonic (Chocked)	$\dfrac{p_d}{p_u} \leq b$	$q_m = C p_u \rho_0 \sqrt{\dfrac{T_0}{T_u}}$
Closed Check Valve	$1 - \dfrac{\Delta p_c}{p_u} < \dfrac{p_d}{p_u} \leq 1$	0

Throughout the following subsections, modelling of the flow in each of the subsystems that form a complete valve assembly are going to be explained in detail.

6.2.1 5/3-Control Valve

SMC, SY5320R-6G-01F-X406-Q has 5 ports designated as P, A, B, EA and EB and has three different positions. While in the middle position, all the ports are closed, in left position port A is connected to port P (supply pressure) and port B is connected to EB (exhaust) and in right position the connections are the reverse of left. Regarding the requirements of this project the ports B and EB are unused therefore they were blocked with proper plugs and the corresponding flow paths will not be modelled and simulated. The valve simulated model includes the dynamics and two flow paths, figure 6.18. The input and output out signals to this model can be reviewed in the table 6.14. The flow that travels out of port A is considered to be positive regardless of the source (EA or P) and the reverse is accounted as
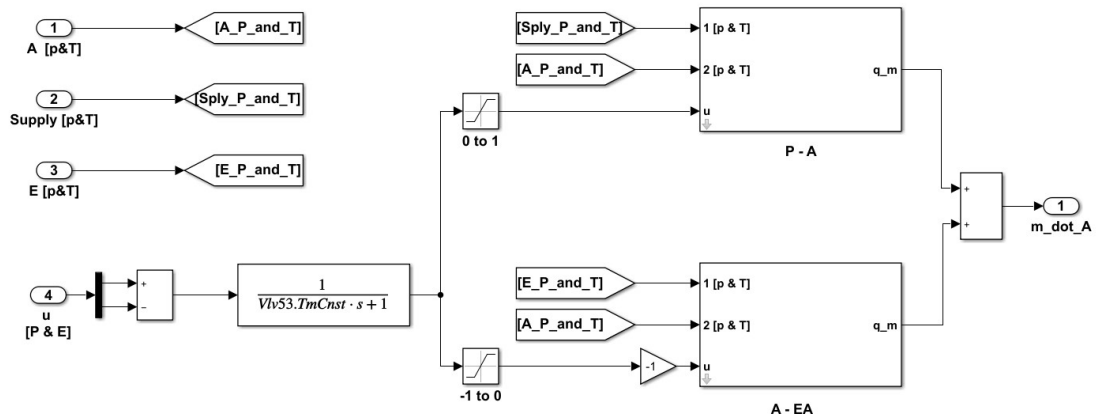
Figure   6.18 *5/3-Valve flow simualtion model*

negative regardless of the destination. Consequently the final calculated mass flow rate of the valve is the sum of flow rates of two paths, P→A and A→EA. Based on the product's catalogue the flow characteristics through these paths , table 6.13 ,are slightly different consequently their flow are calculated using two of the same flow-path model however with different parameters. Modelling a single path flow will be explained in the following subsections.

Table   6.13 *5/3-Valve flow characteristics*

Flow Path	C (dm³/s.bar)	b	Valve Symbol
1→4/2 (P→A/B)	1.7	0.43	(A) (B) 4 2
4/2→5/3 (A/B→EA/EB)	1.8	0.35	5 1 3 (EA) (P) (EB)

Table   6.14 *5/3-Valve flow simulation input and output signals*

Signal Name	Description	Type	Value and Unit
A [p&T]	Vector of pressure and Temperature at port A	Input Signal	[Pa , °K]
Supply [p&T]	Vector of pressure and Temperature at port P	Input Signal	[Pa , °K]
E [p&T]	Vector of pressure and Temperature at port EA	Input Signal	[Pa , °K]
u [P & E]	Vector of the valve commands	Input Signal	[0/1 , 0/1]
m_dot_A	ANR Mass Density	Output Signal	[kg/s]

Modelling of the Dynamics

This valve has an external pilot meaning that it uses high pressure air provided by a dedicated tube (not the supply line) to move the spool to the desired position.The product catalogue provides the valve dynamics data by stating the response time as much as 32 milliseconds or less when the pilot pressure is 5 bars. Throughout all the experiments in the scope of this study the pilot pressure is kept at 7 bars and as a result all the real responses are going to be consistently at least as fast as the mentioned value or faster. Taking this measure helps the simulation conform with the actual experiments regarding the valve dynamics.

As shown in Figure 6.18, opening of the valve is modelled using a 1st order transfer function with a time constant equal to 0.015 which leads to 90% of valve opening in 32ms, Figure 6.19. Modelling the 5/3-valve dynamics more accurately requires disassembling it and measuring the mass of the spool and the bore of the miniature cylinder which moves the spool via pilot pressure. Regarding the fact that this valve is considerably faster comparing to the dynamics of the rest of the machine, the accuracy using the 1st order transfer function is accepted as accurate enough.

The Valve is of 3 position type and have two coils. Each of the coils when energized will move the spool to one of the directions. When either both or none of the coils are energized, the spool will return to the center position. In order to model the case where the spool travels from one direction all the way to the other direction one of the signals is negated then the sum of two is given to the transfer function as the input, Figure 6.18. Using this strategy makes the simulated model compatible with the exact same control subsystem which is used for controlling the actual machine.

Modelling of the Flow

In order to model the flow rate of a path i.e. from port 1 to port 2 (P to A) a Simulink subsystem was developed to implement the formulas mentioned in table 6.12. The flow pathway model and the parameters and signals used in it are stated in figure 6.20 and table 6.15 respectively. This subsystem selects the higher pressure as upstream pressure and the corresponding temperature as upstream temperature. The other port's pressure is therefore selected as downstream pressure. Flow from port 1 to port 2 is considered to be positive flow and the reverse negative flow.

The product of calculated mass flow and the valve opening forms the final output of the flow path in order to take the dynamics of the valve into account. Here a
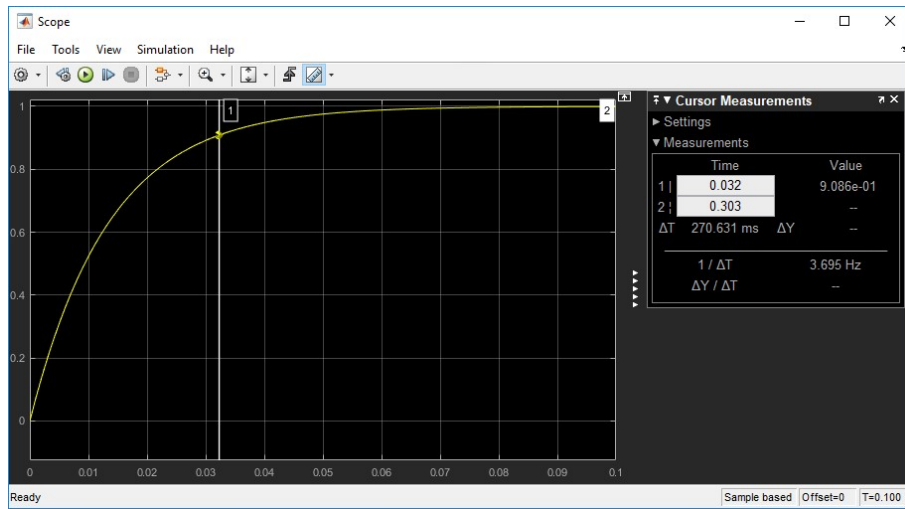
Figure 6.19 5/3-Valve Response Time
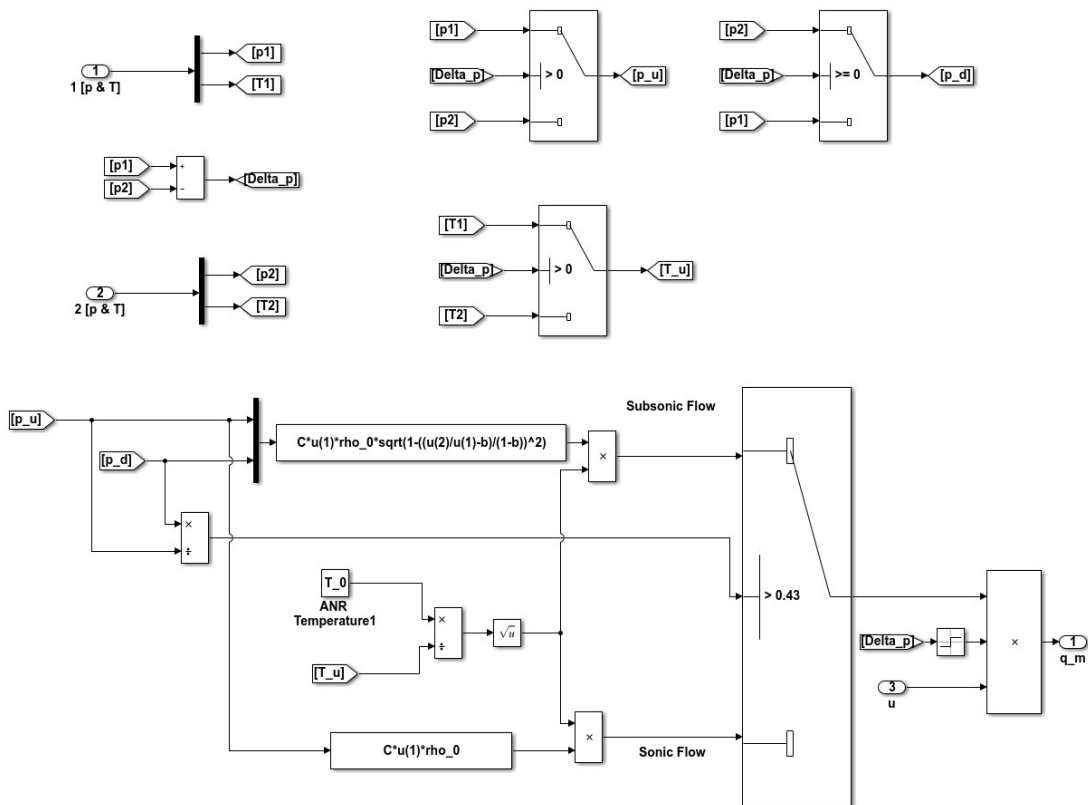
Figure 6.20 Valve single path flow simulation diagram

Table 6.15 Valve single path flow simulation parameters

Parameter Name	Description	Source	Value/Parameter Name and Unit
p1	Pressure at port 1	Input Signal	[pa]
P2	Pressure at port 2	Input Signal	[pa]
u	Valve opening	Input Signal	0 to 1
T_0	ANR Temperature	Workspace	293.15 [°K]
rho_0	ANR Mass Density	Workspace	1.185 [kg/m^3]
C	Sonic Conductance	Entered in Subsystem Mask	1.7×10^{-8} [dm³/s·bar]
b	Critical Back-Pressure Ratio	Entered in Subsystem Mask	0.43

simplifying assumption was made that the flow of the valve increases linearly with the value of valve opening. This assumption is not entirely accurate however taking into account the fast response of the valve and the minimal magnitude of the caused error, the result of this simplification is accepted as accurate enough.
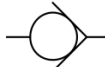
Leakage

Regarding the relatively low working pressure of the system, the short period that pressured air stays in each chamber of the cylinders and rubber seals of the valves, the 5/3-valves' leakage is assumed to be close to zero thus its not modelled.

6.2.2 Check Valves

There are two types of check valves in the system which both have the same flow characteristics and are only different in the direction of the flow. The flow characteristics of these valves were stated by the manufacturer as shown in table 6.16.

Table 6.16 Check Valve Flow Characteristics

C (dm³/s.bar) Sonic Conductance	b Critical Pressure Ratio	Δp_c[pa] Cracking Pressure	Valve Symbol
1.3	0.35	500	

Each of the check valves is modelled using the same path-flow model used in the 5/3-valve and a function that decides the opening of the valve based on the upstream
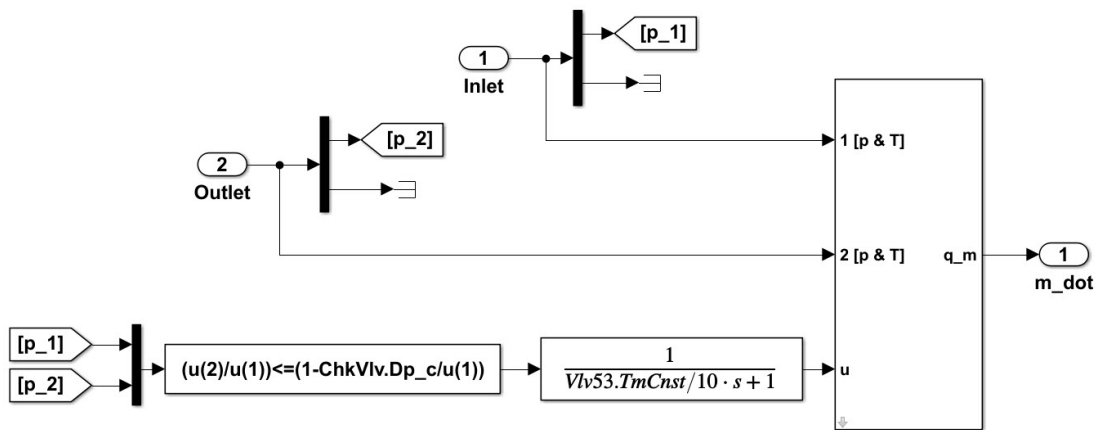
Figure 6.21 Check valve simulation diagram

and downstream pressures, the value of cracking pressure and the formulas in table 6.12. The diagram is shown in Figure 6.21.

Modelling of the check-valve has some limitations which along with their workaround are listed below:

- According to the products catalogue, the valve does not fully open at cracking pressure however since modelling this behaviour requires knowing the spring constant which is not provided by the manufacturer, it is assumed that the valve is fully open at cracking pressure.

- Modelling the dynamics of the valve requires knowing both the spring characteristics of the valve as well as the mass of the spool which weren't provided by the manufacturer. Regarding the small size of the valve and the light spool an assumption was made that the valve opens almost instantly to fully open at cracking pressure. (The 1st degree transfer function that models the dynamics uses a time constant equal to 1/10th of the one for 5/3-valve)

- As a result of the previous two assumptions, the flow is assumed to be only in the valve directions and the reverse flow during the closing period of the valve were not modelled and assumed to be zero.

The check-valve subsystem used parameters similar to ones used in the 5/3-valve model. The details of these parameters are stated in table 6.17.

Table 6.17 *Check Valve model parameters*

Parameter Name	Description	Source	Value and Unit
p1	Pressure at port 1	Input Signal	[pa]
P2	Pressure at port 2	Input Signal	[pa]
u	Valve opening	Calculated based on differential pressure and Δp_c	0 or 1
T_0	ANR Temperature	Workspace	293.15 [°K]
rho_0	ANR Mass Density	Workspace	1.185 [kg/m^3]
C	Sonic Conductance	Entered in Subsystem Mask	1.3×10^{-8} [dm³/s·bar]
b	Critical Back-Pressure Ratio	Entered in Subsystem Mask	0.35
Δp_c	Critical Back-Pressure Ratio	Entered in Subsystem Mask	5000 [pa]

6.3 Modelling of Cylinders

Cylinders block, figure 6.22 consisted of three cylinder subsystems and it is responsible for calculating the forces generated by each one as well as their pressures. Those values are calculated using the mass flow rates coming from valve block and piston positions and velocities sent from multi-body simulation.

6.3.1 Cylinder mathematical Modeling

The cylinders used for this project are of double action type and they have two chambers separated by the piston. The chamber through which the piston rod passes is called Chamber B hereafter and the rod-less one is called chamber A. the schematics of a single cylinder is illustrated in figure 6.24.

In order to model a cylinder the force equilibrium equation can be written as

$$(M_L + M_p)\ddot{x} + F_f + F_L = p_A A_A - p_B A_B - p_a A_r \tag{6.6}$$

The parameters used in Eq. 6.6 are described in table 6.18. As described in chapter 6.1 the dynamics are modelled by the Simscape-Multi-physics and friction of Magni as a whole is simulated as a function of rpm. As a result only the right side of Eq 6.6 which is the force generated by the cylinder is simulated in this section. This is done by modelling the pressure of each chamber individually using a dedicated chamber subsystem for each one, figure 6.23. The only difference is that for chamber B piston speed is negated and piston position is negated and added by stroke of the cylinder.
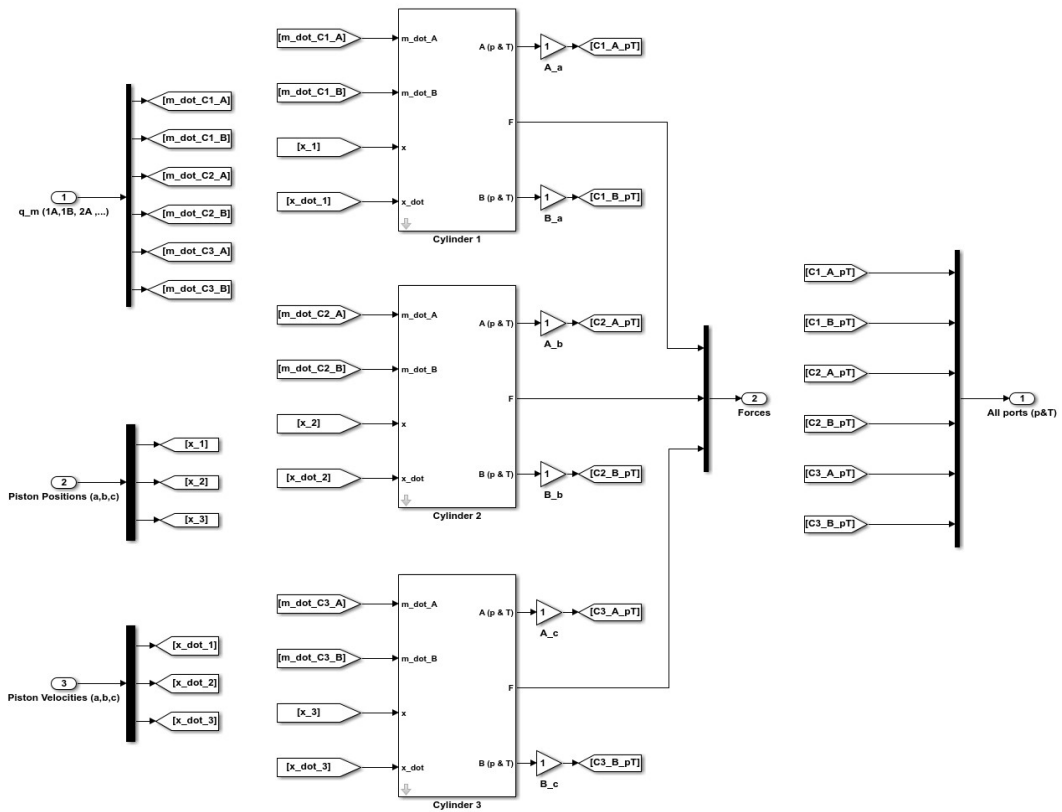
Figure 6.22 *Cylinders block simulation diagram*

Table 6.18 *Force Equilibrium parameters*

Parameter	Description	Parameter	Description
A_r	Piston Rod Section Area	M_L	Load Mass
A_A	Chamber A effective Area	M_p	Piston and Rod assembly Mass
A_B	Chamber B effective Area	x	piston position
p_A	Chamber B absolute pressure	F_f	Friction Force
p_B	Chamber B absolute pressure	F_L	External Force
p_a	Atmosphere absolute pressure		

6.3.2 Chamber Modelling

Pressure changes in a chamber can be mathematically modelled using the physical laws governing the behaviour of gases. The main intricacy of this model is the thermodynamics of gas during different states since the gas has different sorts of energy exchange with the cylinder body and the environment depending on weather the gas is entering or leaving the chamber or during the volume change as a result of piston movement.

Edmond Richer and Yildirim Hurmuzlu in their work [19] derive a general mathe-
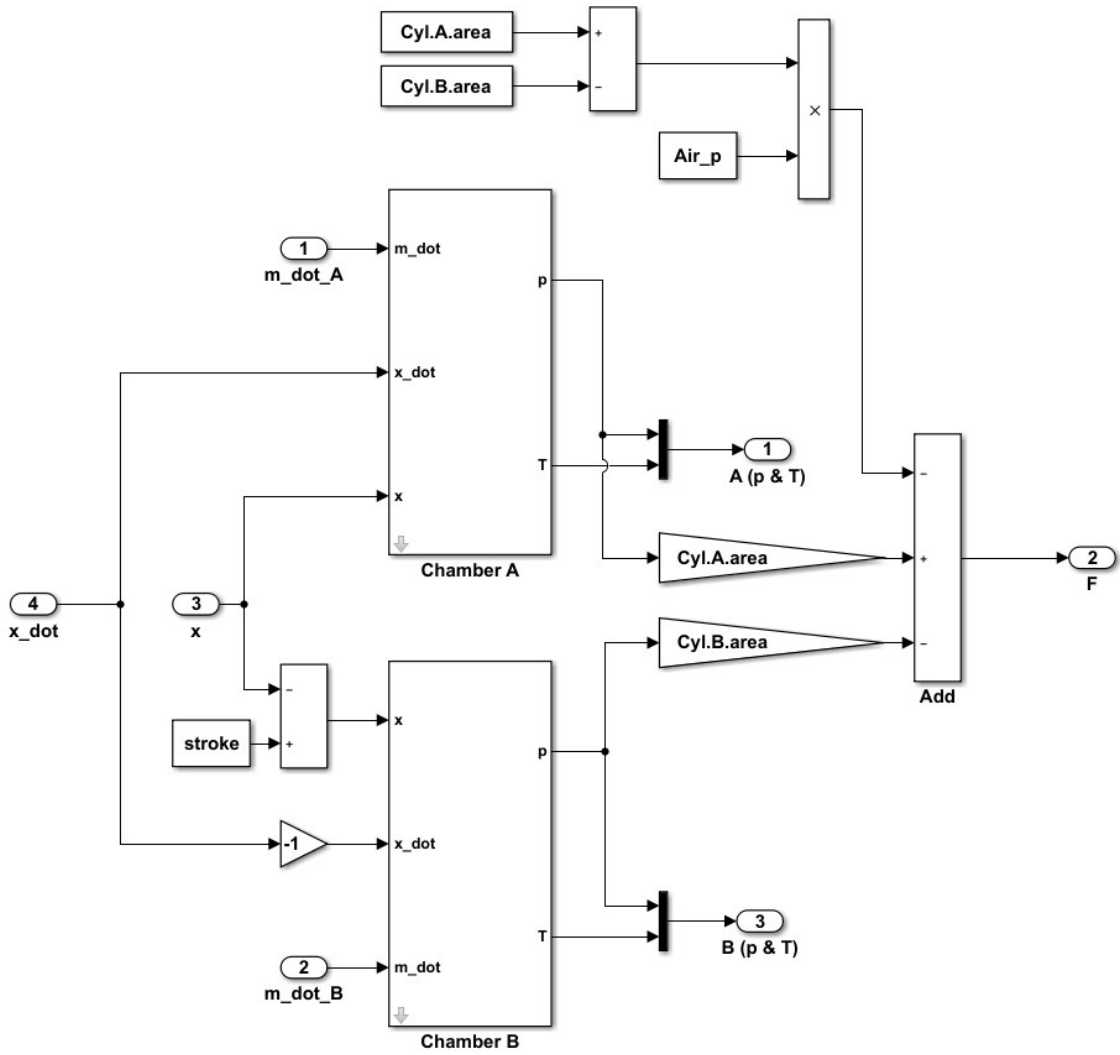
Figure 6.23 *Single cylinder force calculation digram*
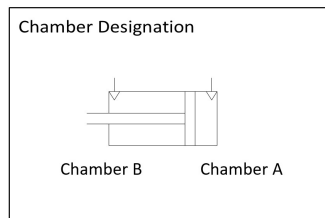
Figure 6.24 *Single cylinder schematics and chamber designation*

matical model that takes into account the details of this thermodynamics. Here we use the same model to simulate the chamber pressure. In this model the following simplifying assumptions were made:

- The gas is ideal.

- Pressures and temperature within the chamber are homogeneous.

- Kinetic and potential energy terms are negligible.

Three main principles are used in this model,

Ideal gas law:

$$p = \rho R T \tag{6.7}$$

continuity equation:

$$\dot{m}_{in} - \dot{m}_{out} = \dot{\rho}V + \rho\dot{V} \tag{6.8}$$

and the energy equation:

$$q_{in} - q_{out} + kC_v(\dot{m}T_{in} - \dot{m}_{out}T) - \dot{W} = \dot{U} \tag{6.9}$$

The parameters used in these three equations are described in table

Table 6.19 *Parameter description for Eqs 6.7, 6.8, 6.9*

Parameter	Description (value/unit)	Parameter	Description (value/unit)
R	Ideal Gas Constant 287 $J/(kg°K)$	q_{in}	Input Heat (J)
ρ	Density of the gas inside the Chamber (kg/m^3)	q_{out}	Output Heat (J)
T	Temperature of the gas inside the Chamber $(°K)$	T_{in}	Temperature of the incoming gas flow $(°K)$
$\dot{m}_{in}$	Input Mass Flow (kg/s)	$\dot{W}$	rate of change in the work (J/s)
$\dot{m}_{out}$	Output Mass Flow (kg/s)	$\dot{U}$	the change of Internal Energy (J/s)
V	Chamber Volume	k	the Specific Heat Ratio (1.4)
C_v	Specific Heat for Constant Volume process (0.718 $kJ/kg.°K$)		

These researchers concluded that if the incoming flow is already at the temperature of the gas in the chamber*, the pressure inside chamber can be calculated using the following equation:

Figure 6.25 *Measuring dead volume of chmaber B of a cylinder*

$$\dot{p} = \frac{RT}{V_0 + Ax}(\alpha_{in}\dot{m}_{in} - \alpha_{out}\dot{m}_{out}) - \alpha\frac{pA}{V_0 + Ax}\dot{x} \qquad (6.10)$$

Where V_0 is unused volume of the cylinder and α, α_{in} and α_{out} are heat transfer co-efficients with values between 1 and k for heat transfer during the piston movement, charge and discharge processes respectively. The closer the coefficient to k the more adiabatic the heat transfer is calculated as opposed to values close to 1 which gives the isothermal heat transfer. In this formula T is the operating temperature of the chamber which is assumed as a constant value, however the effect of Temperature change is taken into account using the heat transfer coefficients.

According to these researchers' work, the charging process is nearly an adiabatic process while the discharging is best modelled as an isothermal process. Furthermore α_{in} should be selected close to k and α_{out} close to 1. These values will be verified later via cross-checking the experimental and simulation results. In their work they state that Al-Ibrahim and Otis [2] concluded that expansion/compression resulted by piston movement is best modelled with $\alpha = 1.2$.

*In this project the cylinders always do full cycles and the dead volumes and the end of the chambers are very small so this assumption can be considered to be always true without causing any significant errors.

The dead volume value is measured by filling it (when the piston is completely at one end) with a viscous oil and measuring the amount of oil it takes to completely fill, figure 6.25.

The Simulink model for a single chamber, figure 6.26, uses Eq 6.10 and integrates the outcome to calculate the pressure inside the chamber. The operating temperature is set as a parameter in this subsystem's mask however it is also exported for convenience to form vector of pressure and temperature.
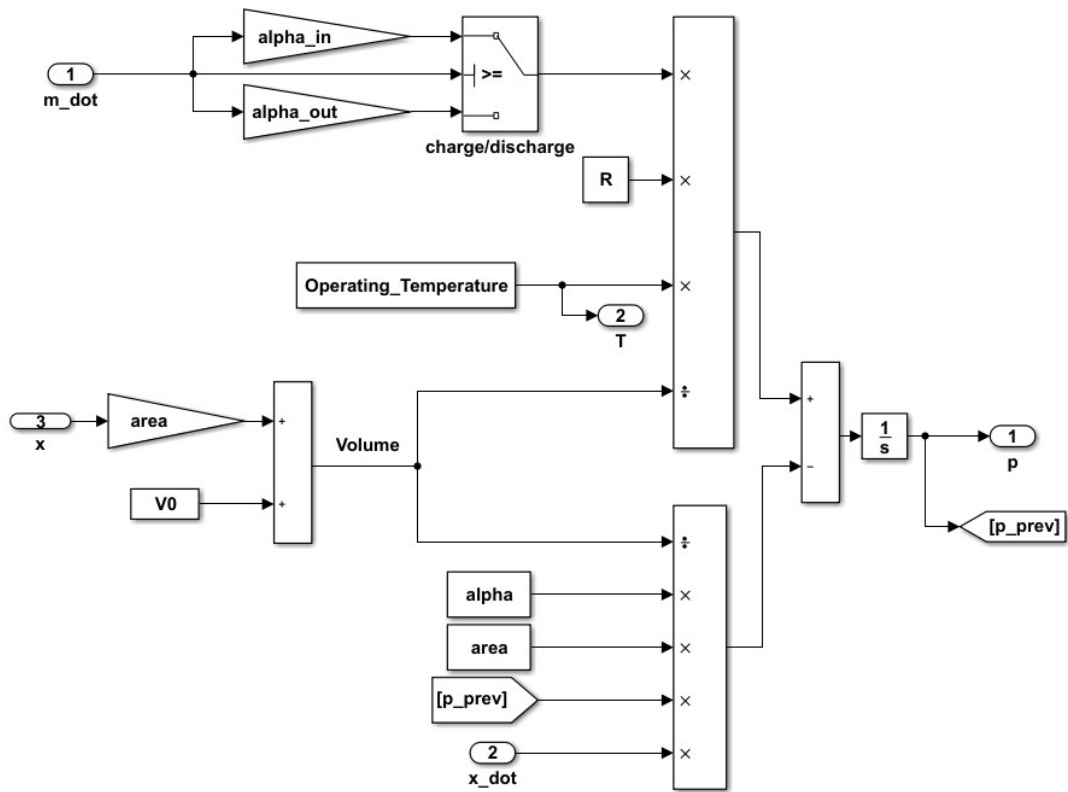
Figure 6.26 *Single Chamber Simulation diagram*

6.3.3 Cylinder Leakages

Regarding the rubber type seals used in the cylinders and relatively low differential pressure, the leakage was assumed to be negligible in the simulation.

6.4   Friction mathematical model of Magni

Modeling friction in pneumatic cylinders is one of the challenging parts of the simulation which its characteristics have to be defined properly. This is of high importance in automation and industries where a precise model is needed to predict the dynamic and steady state behavior of the system accurately enough. Unfortunately, in contrast with hydraulics where the friction models are developed properly and the models are simpler, in pneumatic the proposed models are more complicated and the friction coefficients are hard to identify.

6.4.1   Mathematical modeling

A study is carried out by Belforte et al [4] where the authors' main focus is on steady state behavior of the cylinder friction. They have studied the behavior of specific cylinders in different velocities and working pressures and repeated the test for different cylinder sizes. They have concluded that the pressure is the second important factor alongside the velocity, that has remarkable effect on friction force and it increases almost linearly with the raise in working pressure and non-linearly with the raise in velocity. Unfortunately, no mathematical model was proposed by them.

Among various friction models proposed so far, LuGre friction model (Canudas de Wit C) has been accepted globally as a precise model. However, this model is only suggested when the working pressure at both chambers are set to 0 bars. For being able to use this model for accurate modeling and simulation purposes, a study is carried out by Hao Liu et al [15] where the friction characteristics were examined by studying the influence of differential pressure and working pressure on both steady state and dynamic behavior of the system. The results showed that the pressure has remarkable effect on steady state friction in contrast with dynamic behavior. Comparing the results with the luGre friction model and the results in reference condition, The changes were nearly linear so modified LuGre model is suggested in applications with varying chamber pressures.

The proposed model

For steady state condition, the friction model can be represented using the LuGre model where the Eq 6.11 and 6.12 are representing dynamic and steady state friction model respectively. [15]

$$F = \sigma_0 z + \sigma_1 \frac{dz}{dt} + \sigma_2 v \tag{6.11}$$

$$F_{ss}(v) = F_c sgn(v) + (F_s - F_c)e^{-(\frac{v}{vs})^2} + \sigma_2 v \tag{6.12}$$

Here the steady state coefficients F_c, F_s, v_s and σ_2 in Eq 6.12 can be identified when the velocity of the piston is held constant. However the dynamic friction coefficients need much more complicated tests and are harder to be identified. The coefficients of the original LuGre model are corrected using equations 6.13 to 6.16 in order to obtain the modified friction model.

$$F_c = F_{c0} + k_1 p_s + k_2 \Delta p \tag{6.13}$$

$$F_s = F_{s0} + k_3 p_s + k_4 \Delta p \tag{6.14}$$

$$v_s = v_{s0} + k_5 p_s + k_6 \Delta p \tag{6.15}$$

$$\sigma_2 = \sigma_{20} + k_7 p_s + k_8 \Delta p \tag{6.16}$$

where the parameters $F_{c0}, F_{s0}, v_{s0}, \sigma_{20}$ and σ_{10} can be identified experimentally when the pressure in both chambers are kept constant at ambient pressure.

6.4.2 Magni friction characteristics

The friction in cylinders which is due to seals and rod bearings, is not only dependent on the velocity of the rod. As stated previously, it is also dependent on both the working pressure of cylinder and the differential pressure over the cylinder chambers. Considering this fact, it is needed to study the behaviour of Magni in different pressure conditions to obtain a suitable model.

Friction characterization approach

It is possible to determine the friction characteristics of Magni either by studying a cylinder alone or by considering the Magni as one module and study its behavior as a distinct system. Following are the reasons for going through the second approach:

- Studying the cylinders alone requires complicated set-ups in order to maintain the speed of cylinder constantly. It requires a hydraulic cylinder with position feedback in order to control the speed of cylinder rod which is a complicated project itself and is ignored due to time and hardware limitations.

- The final objective of friction parameter determination is to model the friction force inside the Magni module, not the cylinder itself. Since we are able to keep Magni module to work at constant working rpm, it is reasonable to study the behaviour of the whole module instead of each cylinder separately.

- Magni has a reciprocating (dynamic) behaviour were some hidden mechanical factors might be ignored if we consider each cylinder separately.

- The proposed models for friction in pneumatic cylinders considers both dynamic and steady state behaviour and is comprised of complicated mathematical models which its dynamic coefficients are hard to define. Considering the behaviour of friction in pneumatic cylinders, it is expectable to observe similar behaviour when three cylinders are connected in parallel.

Table 6.20 shows the steps for implementing different tests.

Table 6.20 *Friction characterization approach*

Title	Objectives	Conditions
Inertia calculation	Determine inertia in order to calculate the cylinder friction	In any working pressure or differential pressure
Effect of working pressure	Study the relation between friction and working pressure	Both chambers of all cylinders must be in the same pressure
Effect of differential pressure	Study the relation between friction and differential pressure	Chamber with bigger area must be set to a specific pressure and the pressure on other chamber must vary
Base friction equation	Derive a suitable friction equation in atmospheric condition	Both chambers must be in exhaust mode
Base model modification	Adapt the base model to work in different pressure circumstances	-
Verification	Validate the derived model	Experimental data and modelled plot must be fit quite properly with negligible error

Limitations

1. The ideal condition is to keep the chamber pressures in certain values. However due to the geometry of valve orifice, there is a resistance to flow especially in high rpms that causes pressure fluctuation.

2. With the available hardware, we are able to monitor only the pressure changes in two chambers (cylinder 2). Since the rpm change rate is a not considerable, cylinders are assumed to have similar pressure trends.

3. Response time of the pressure sensor is not mentioned in the catalog. By looking into the response of pressure sensor in experimental data, and determining how long it does take for the chambers to reach the line pressure after valve opening command, it is observable that there is only about 30 milliseconds delay which is fairly close to the valve's response time. It can be concluded that any possible error due to pressure sensor is negligible.

4. Due to high vibration caused by the consumer module (mainly flywheel), the read torque has a fluctuating nature which is eliminated using proper filters before data processing.

Data Smoothing Filters

In order to eliminate the effects of vibrations and shaft misalignment which is emerging as sinusoidal torque read on load-cell, it is necessary to utilize proper filters. Two Matlab filters are used in order to achieve the desired output:

1. A moving average filter: y = movmean(x, window_length)

2. Savitzky-Golay filter: y = sgolayfilt(x, order, frame_length)

First a Sgolay filter is used to filter the data vector followed by a 20 sample wide moving average filter. The result is shown in figure below for an arbitrary logged torque data. It can be observed in the figure 6.27 that the filters have kept the trend of changes as well as eliminating the effects of vibrations.

Torques caused by the chamber pressures

In order to study the effect of torques caused by the pressurized air inside the chambers, it is necessary to monitor the pressure in the cylinders. In the experiments done in this section, chambers are connected to the constant pressure air tanks, however due to reciprocating behaviour of Magni, and the change in the piston velocity, a positive or negative torque is imposed to the main shaft. Hence, it is necessary to calculate the generated torque since even a small deviation in pressure can impose a tangible torque to the system.
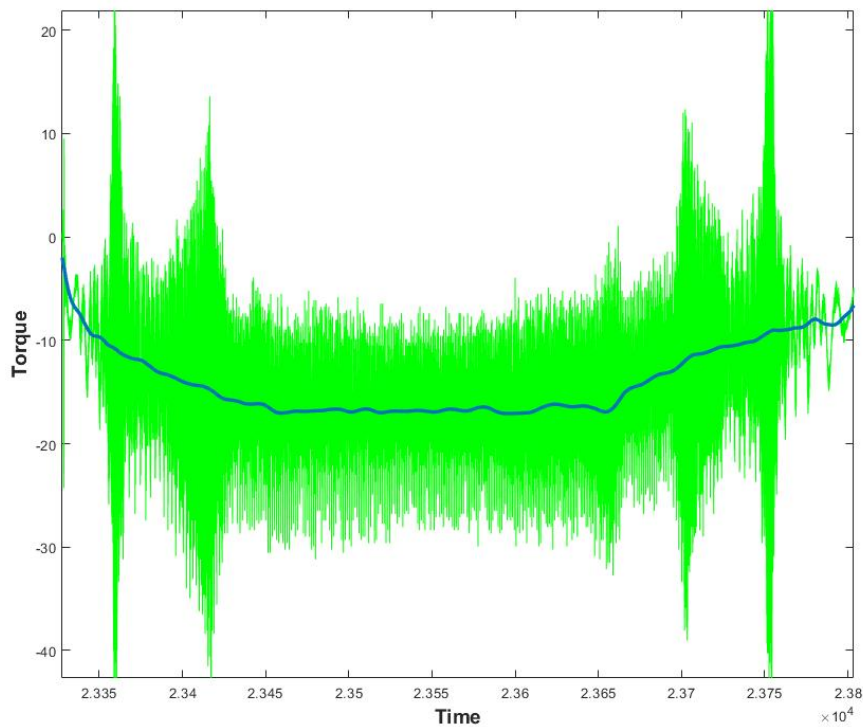
Figure 6.27 *Data noise filtering*

Due to the triangular geometry of Magni, each chamber has 120 degrees of phase shift with another one. The pressure fluctuations in the chambers increase with the rise of rpm, however since the increase rate of rpm is not significant and in some cases it is zero, it is possible for the other chambers to inherit the pressures trends from cylinder 2 in one cycle before or after their current phase according to their phase shift. This is summurized in table 6.21.

Table 6.21 *Chamber phase shifts*

ID	Phase shift with respect to cylinder 2 chamber A	Phase shift with respect to cylinder 2 chamber B	Inherit from
Cyl 1 A	+120	-	One cycle after C2_A
Cyl 3 A	-120	-	One cycle before C2_A
Cyl 1 B	-	+120	One cycle after C2_B
Cyl 3 B	-	-120	One cycle before C2_B

The code below is developed that is based on the phase shift between chambers, and looks for the next or previous step where the cylinder chambers has the same phase and inherits their corresponding pressure samples.

chamber's pressures transfers

```
for j=1:length(rpm)
    for i=j:length(rpm)
        if abs(c1_A_ang_pos(j)-c2_A_ang_pos(i))<2
            c1_A_p(j,1)=c2_A_p(i);
            break;
        end
    end
end
```

According to the geometry of Magni, each chamber based on whether it is at a phase between [0-180] or [180-360], imposes a positive or negative torque respectively. Utilizing simple "sine rule" and equation 6.17 that describe the relation between edges and angles in a triangle, the driving force is calculated by decomposing the force which is applied in the direction of cylinder. Lastly, the torque is calculated by multiplying the calculated force by crank length as it can be seen in the figure 6.28.
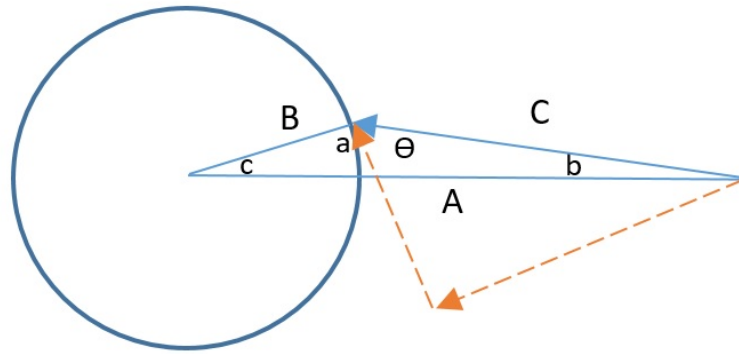
Figure 6.28 *driving torque of cylinders*

$$C = \sqrt{A^2 + B^2 - 2.A.B.cos(c)} \tag{6.17}$$

$$sin(\alpha) = A.\frac{sin(c)}{c} \tag{6.18}$$

$$\tau = F.B.cos(\theta) \tag{6.19}$$

$$cos(\theta) = sin(90 + \theta) = sin(a) \tag{6.20}$$

$$\tau = F.B.sin(\alpha) = p.pist\_area.B.sin(\alpha) \tag{6.21}$$

In the above equations, angle c in the equations is equivalent to the phase of each chamber. Once the torque in each chamber has been calculated in every step, the resultant torque on the main shaft imposed by the pressurized chambers can be calculated using the following scripts:

Torque imposed due to pressurized chambers

```
for k=1:1:length(rpm)
        theta_c=c1_A_ang_pos(k);
        C=sqrt(A^2+B^2-2*A*B*cos(theta_c*2*pi/360));
        sin_a=A*sin(theta_c*2*pi/360)/C;
        c1_A_trq(k)=1e5*c1_A_p(k)*ch_A_area*B*sin_a;
end
```

The resultant torque of all cylinders together

```
for k=1:1:length(rpm)
        torque_sum(k)=c1_A_trq(k)+c1_B_trq(k)+...
        c2_A_trq(k)+c2_B_trq(k)+c3_A_trq(k)+c3_B_trq(k);
end
```

Magni's inertia effect on load-cell data

Inertia of Magni module consisting of cylinders, crank, shaft and pulley can be obtained using either from the Simscape multi-body (inertia of each single component is calculated and added to the model previously) or by experimental data. The dominant term in Magni's inertia is the pulley connected to the main shaft, which its inertia is calculated in Solid Works automatically which is equal to 0.1 $kg.m^2$.

To be able to extract the friction data from read torque by the means of load-cell, it is necessary to subtract the effect of inertia when there is an accelerating or decelerating motion. In case of the tests that have been done in order to observe the behavior of friction, the acceleration of Magni and the inertia is negligible. As a result, the residual torque caused by the inertia in acceleration mode is negligible compared to the friction values and the read torque can be used a friction data with reasonable accuracy.

6.4.3 Friction experiments and results

From the experiments that has been mentioned in table **??** the tests with the conditions mentioned in the figure 6.29 have been done in order to study the friction characteristics. These test conditions are able to demonstrate the maximum deviations from the reference conditions.

Note: a pre-tension is added to the load-cell to be able to measure the force on both direction. Consequently, the more negative torque read in the collected data, means

(a) A and B chambers set to 0 bars

(b) As 7 bars and Bs 0 bars

(c) As 0 bars and Bs 7 bars

(d) A and B chambers set to 7 bars
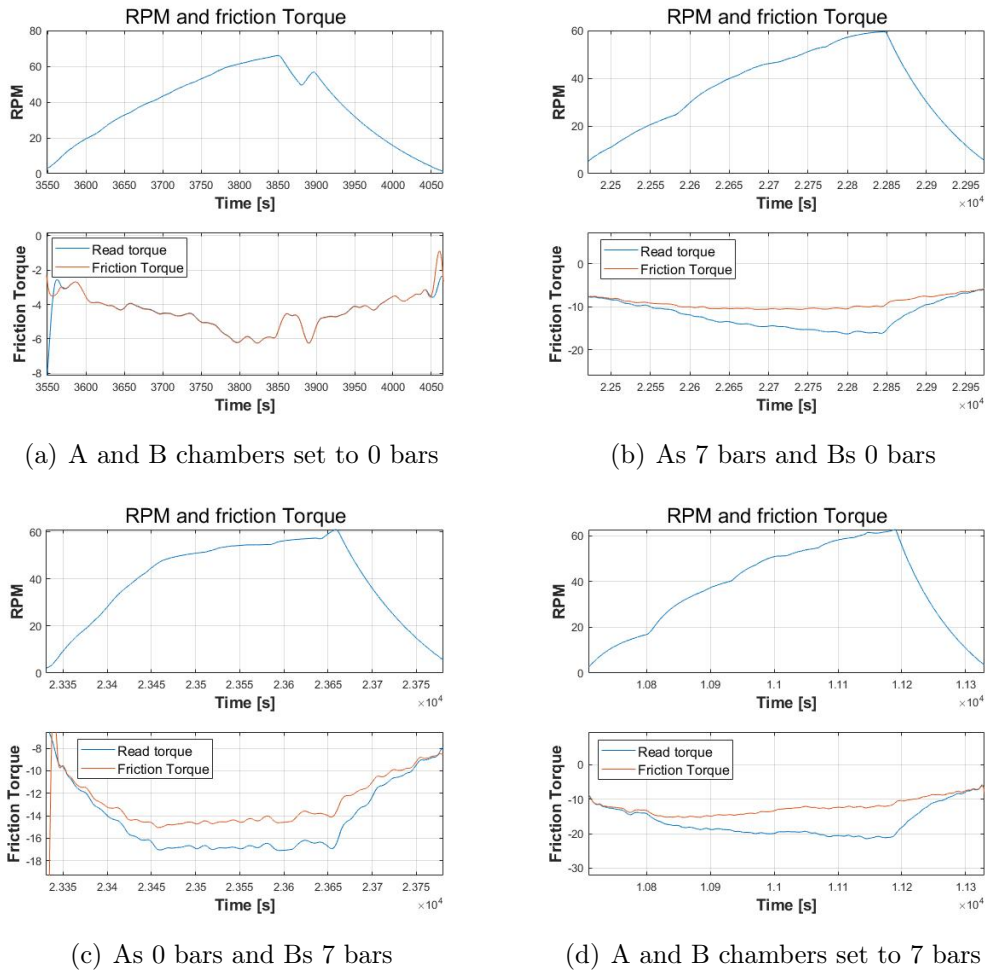
Figure 6.29 *Magni module frictional torques in different chamber pressures*

greater torque.

The conditions in which the test have been performed are as below:

- the rpm is increasing up to 60 rpm and it decreases again by connecting all the valves to the exhaust line and turning off the motor.

- The motor is operating with approximately constant current (torque).

- Since the inertia of Magni is negligible and acceleration is not remarkable, it does not impose negative resistance to the acceleration, hence it is possible to neglect the effect of inertia in acceleration part. As a result, the read torque is of accepted to be due to friction only.
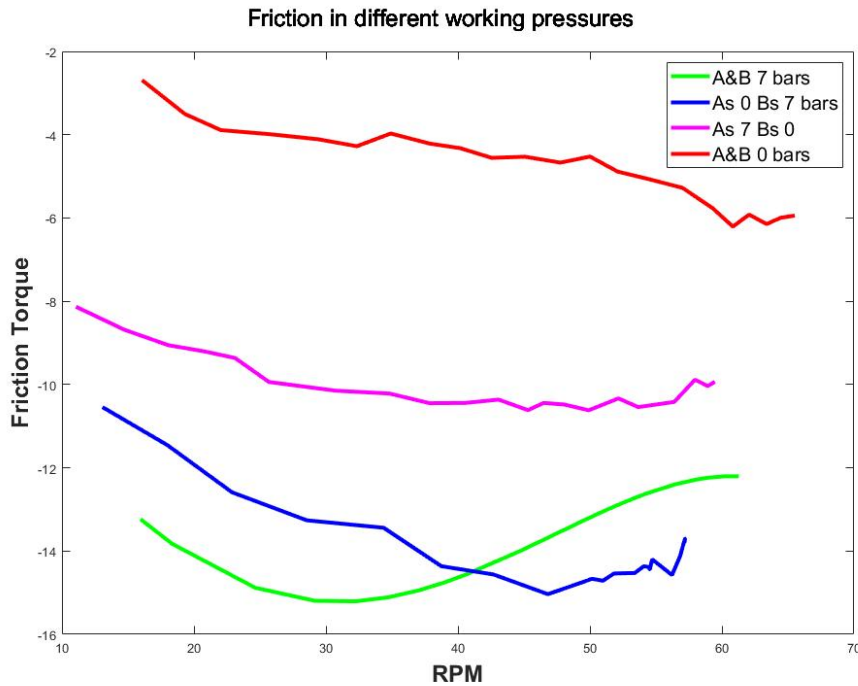
Figure 6.30 *Torque vs rpm in different working pressures*

Test results

Figures 6.29(a) to 6.29(d) are the generated residual torques via magni modules. As it can be seen in the figure 6.29(a), since the chambers are connected to exhaust, the pressure does not affect the generated torque and the curves are overlapping. However, in other conditions a notable deviation from the read torque is observable which grows with the rise in the rpm.

In order to obtain the relation between frictional torques and the working conditions, friction data is plotted with respect to the rpm in different working pressures and differential pressures as it can be seen in the figure 6.30. The results from the test can be summarized in table 6.22.

Uncertainities

As it was expected, the friction ranges and its behaviour is dependent on both rpm and pressure in chambers, however the trend of its change is not similar to viscous friction which can be related to temperature change inside the chambers. The following experiments were done in order to observe the effects of temperature on the friction:

Table 6.22 *Magni friction results in different working pressures*

Test Condition of the chambers	Observations
A&B at ambient pressure	• The friction torque is increasing from 2.5 Nm in lower rpms to 6 Nm in higher rpms almost linearly. • In deceleration part, the friction shows symmetric behavior. • the friction increases with the rise in rpm as it is expected
A&B at 7 bars pressure	• A residual torque is added to the main shaft which increases in higher rpms due to pressure inside chambers. • The friction in low rpms increases with rpm, however it is revers in after 30 rpm. • The friction in deceleration mode continues to decrease in deceleration mode which is not as expected. • The read torque and the pressure hindering torque both have similar shapes. Meaning that the read torque is affected mostly by the pressure.
A at 7 bars, B at ambient pressure	• The same behavior is observable as the condition when A and B chambers are at 7 bars pressure. • In this case the decreasing part starts after 45 rpm.
A at ambient pressure, B at 7 bars	• The same behavior is observable as the condition when A and B chambers are at 7 bars pressure. • In this case the decreasing part starts after 50 rpm.

- The motor was let to work at a constant rpm and the friction torque was read after 20 minutes to let the cylinder exchange heat. The temperature had changed about 5 degrees and the resulted friction torque has decreased, however this reduction was not significant.

- The current I_c to the motor increased manually to a certain value until Magni settled at a certain rpm. This time the current decreased manually to settle in a lower rpm. However after a few minutes, the rpm started to increase slightly again. This can be explained by the temperature rise followed by friction reduction after working for some minutes. (since the pressurized air inside chambers are not going back to the tank and is doing forward and backward movement inside chambers, it starts to get warmer)

The temperature change was read at the tubes that have significantly lower temperatures than inside the chambers due to energy losses. However even with greater temperature changes, the torques were not changing significantly with respect to temperature so the unexpected behaviour of Magni friction is related to uncertainties. Since after each test a residual stress remains at the connecting point of consumer module and load sensor, there is always ±5 Nm shift in the read data which is observable in the plotted data. Besides that, there is always some torque shifts related to the shaft misalignment that makes it impossible to read the friction

accurately.

Conclusion and final friction model

The friction formula 6.22 is concluded from the observations and test results based on the following information:

- In all the cases there is 3 Nm difference between the maximum and minimum values of friction and only the extremum is moving from test to test.

- Whatever the reason for this behaviour of friction inside Magni module is, it requires a complicated and wide range of tests in order to achieve a very precise model.

- Since there are hidden uncertainties related to the torque reading beside the unexpected friction behaviour in chambers, the reference friction equation at ambient pressure is used in the simulation model. Although it can not be a precise representative of friction model, it is an acceptable approximation for the purpose of this study.

$$F_{r\_magni} = 0.051 \times RPM + 2.25 \tag{6.22}$$

7. RESULTS AND DISCUSSION

The parameters which measuring them are the interest of this study and are the main features if the prototype are Efficiency, Torque generation Ability and Power density. In this chapter experiments through which these parameters are measured and their outcome are going to be explained. In the final section of this chapter a brief review over thewhole procedure and possible improvements will be discussed.

7.1 Efficiency

As explained in 5.3, for achieving the best efficiency, the air loss has been eliminated by intelligently controlling the charge phase. In this section, the following experiment has been conducted in order to evaluate the round trip efficiency of Magni.

1. Air tank is initially set to 2.5 bars pressure.

2. DC motor accelerates the Magni to 60 rpm while Magni is in free rotating mode and is neither using compressed air nor compressing.

3. After stage 2, The compression starts in order to keep the rpm at 60 rpm and resist against imposed torque by the DC motor. This will continue until the pressure inside the tank reached 8 bars.

4. The Dc motor torque is decreased via electrical adjustments and as a result Magni controller switched to the expansion mode in order to maintain the rpm using the energy stored in the air tank.

5. During the expansion, the imposed torque by DC motor was manipulated so that the Magni module generates nearly equal torque for maintaining the rpm as it was absorbing during the compression stage.

Figure 7.1 is the results obtained from the experiment above. As it can be seen, the rpm during the experiment is kept constant at 60 rpm and the torque is also kept close to 26 Nm.
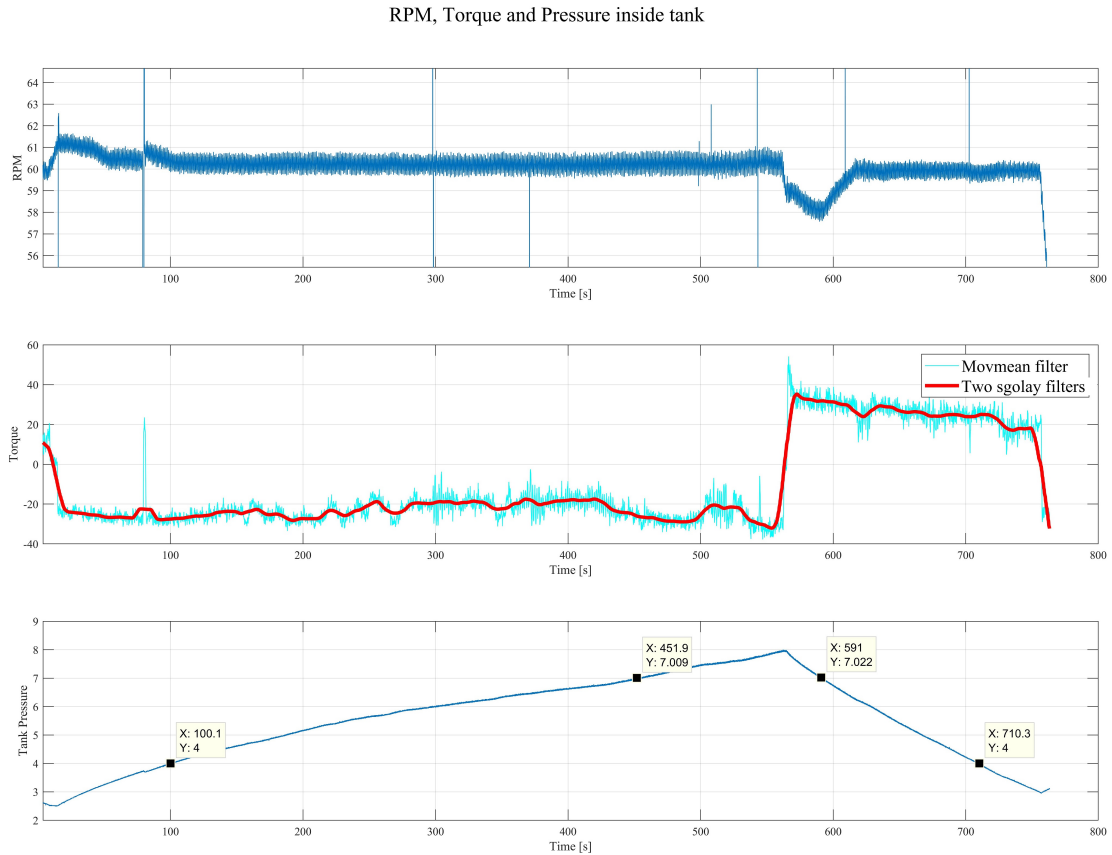
Figure 7.1 *Efficiency test results*

In order to calculate round-trip efficiency, The work that CM has done to compress the air from 4 to 7 bars in 60 rpm has been calculated as well as the work that Magni has done to maintain the Magni at 60 rpm until the pressure inside tank return to 4 bars.

The results is a calculated efficiency of 39 percent using Eq 7.1 with the mentioned conditions.

$$\frac{\int AngularSpeed * Torque * dt : During\ Expansion}{\int AngularSpeed * Torque * dt : During\ Compression} \tag{7.1}$$

however the following should be considered regarding this value:

- In theory, the torque sensor has a resolution of 0.2 N.m and the measured angular speed and time are accurate to 0.1 rpm and milliseconds respectively. In practice because of the mechanical constraints and involved uncertainties the torque is measured with $\pm 1\,N.m$ accuracy which is consequently extended to the efficiency value.

- Since the expansion started immediately after compression, it is expected to achieve slightly lower efficiency when there is a time gap between two stages and the tank have exchanged heat with the ambient.

- One of major reasons for efficiency loss is the friction resistance which is present at both stages and does not change significantly with the capacity usage i.e at different torque generation points the resisting friction is almost the same. Since efficiency is measured at a certain torque capacity of the machine, it is expected that in higher capacity usages Magni shows higher efficiency and in lower capacities become less efficient.

7.2   Torque Generation Ability

An important feature of a CAES is the ability to generate useful amount of torque in a wide range of supply pressures. This is necessary so more of the stored CM can be converted to output power before the next storage cycle. This property of Magni was tested via the following steps:

- Tank was filled with the compressed air from the lab's utility air supply.

- The system was sped up to over 35 rpm by the DC motor in free rotating mode.

- The rpm set-point was set to 60 so the controller always uses highest charge-phase possible.

- Manipulating the CM's input torque to the system in a way that the speed does not increase and the previous condition is preserved.

- Starting the expansion mode so Magni starts to use the compressed air inside the tank and generates torque until pressure drops below 2 bars.

As it is observable in figure 7.2, while the pressure inside the tank declines, the charge phase controller changes the maximum charge phase dynamically to make sure highest torque is possible without loosing any pressurized air. Figure 7.3 shows that while a high pressure of 6 bars is available, system can deliver up to 30 Nm and at half of that pressure still 2/3 of that output is available. This is while the temperature inside the tank has dropped from 22°C to 16°C.

Max Ch-Phz and Tank p & T
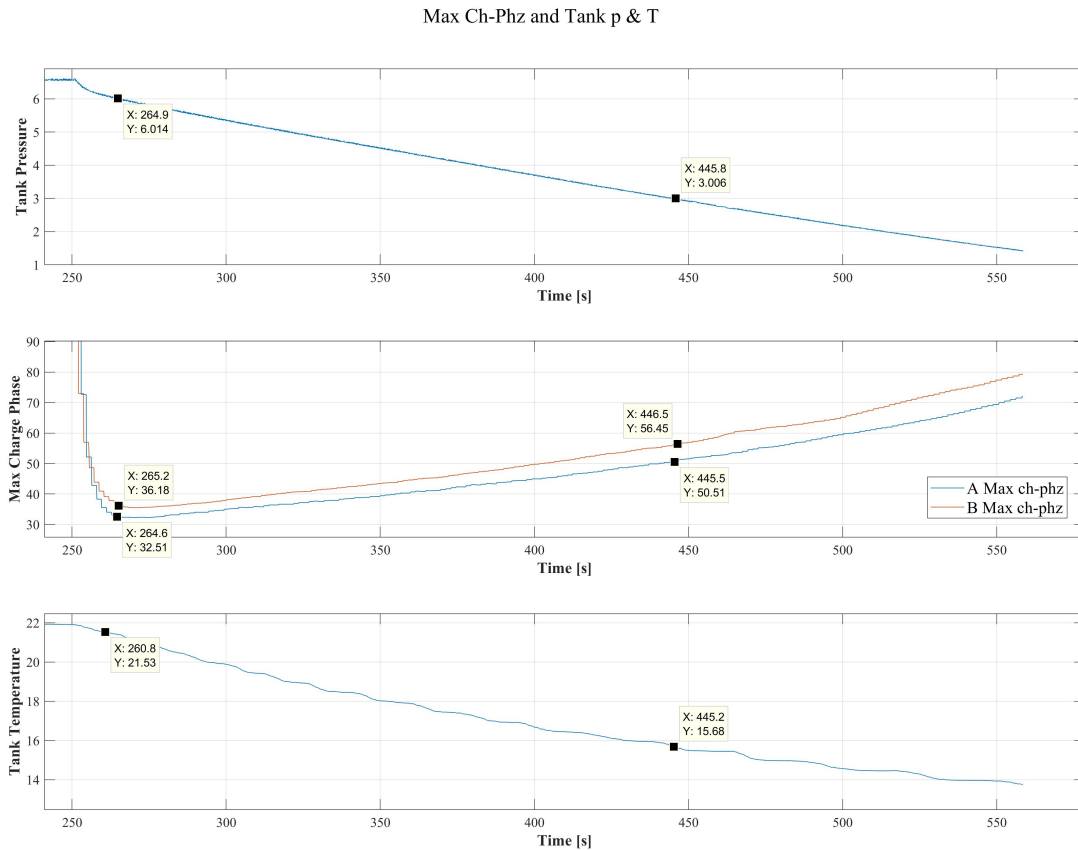
*Figure **7.2** Torque generation test results*

7.3 Power Density

During the expansion stage of the efficiency test, figure 7.4, Magni generates an average of 25Nm with constant speed of 60 rpm while the tank pressure gradually decreases from 7 to 3 bars. This numbers translate to 157W of average output power which is delivered in a 160s time-span which are equal to 7Wh of total deliverable energy.

7.4 Discussion

The goals of this study were designing, simulating and building a SC-CAES prototype and measure its performance. For each of these steps there are sub-steps that went particularly well and there are others for which there is room for improvement in order to generate faster and more reliable results.

The design process of the physical configuration reached an optimal shape after a few iterations. This is partially owed to benefit of using the 3D modeling software,

RPM, Torque and Pressure inside tank

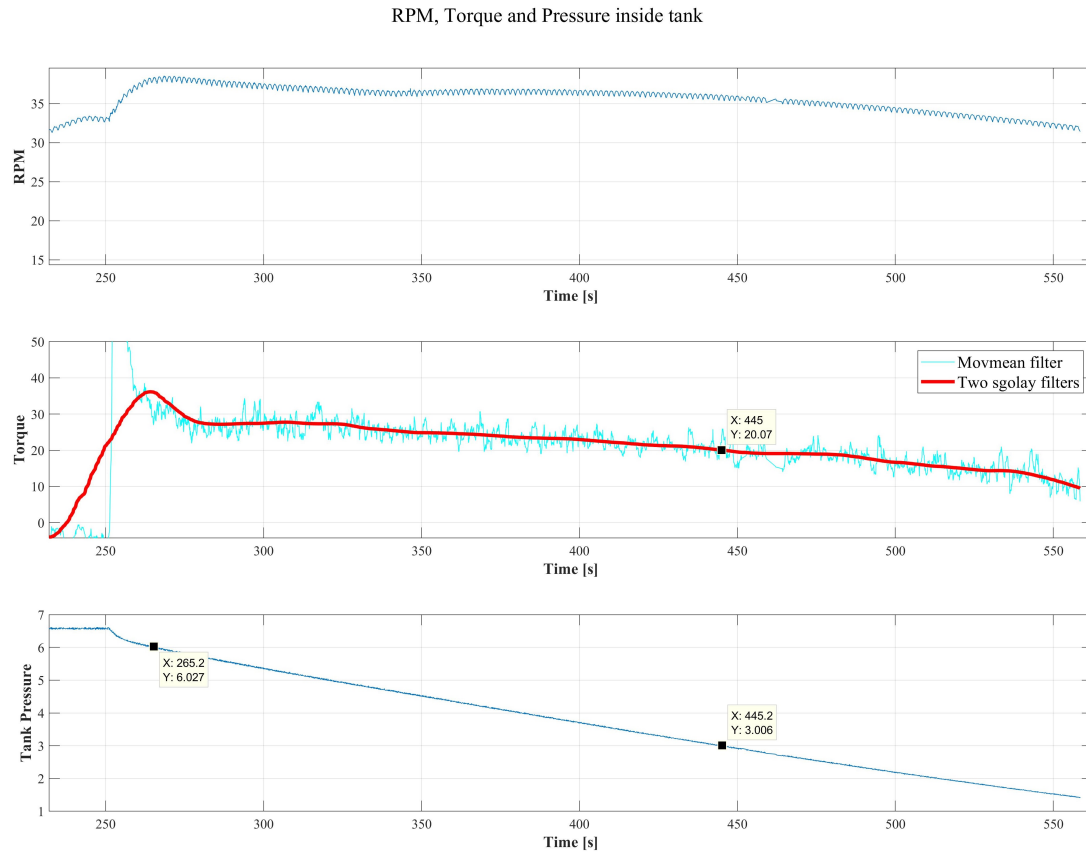***Figure*** **7.3** *Torque generation test results*

Solidworks which is a significant help in envisioning the final product. Another option that could be considered in the design stage was to use a ready made reciprocating compressor and modify its components.

The final control hardware of this prototype is significantly economic with equipment value of less than 100 euros and the result frequency, accuracy, flexibility and reliability are satisfactory for the scope of this study however multiple time consuming approaches as mentioned in sec 4.2 were examined beforehand. Employing this method from the beginning can save other researchers a significant amount of time.

The simulation of this machine was done with attention to details and the final results show good compliance with the actual experiments however regarding the complicated nature of friction in pneumatic cylinders there is a lot of uncertainty in the results that prevents complete reliance on them. In cases where an accurate simulation of a similar machine is required, a thorough study must be carried out to eliminate the uncertainties of friction behavior in different pressures and temperatures.

RPM, Torque and Pressure inside tank
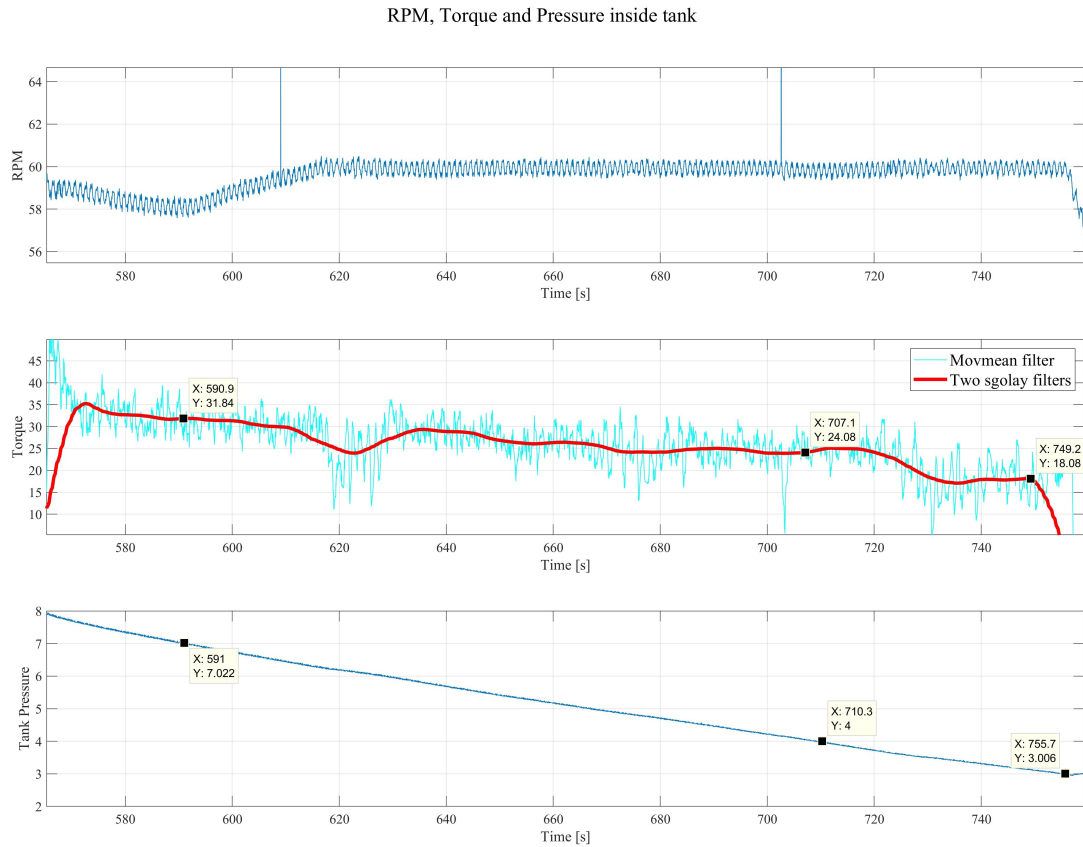
Figure *7.4 Power Density Graph*

The torque over the main shaft is one of the most important parameters to measure in this work and while suspending the Consumer Module and using a single force sensor is a creative and practical way to measure it, using a dedicated torque sensor on the shaft will deliver faster and more accurate results. Another cheaper alternative is to use a soft coupling between Magni and CM and have two force sensors under the CM.

8.   CONCLUSIONS

The main goal in this thesis was to design and build an actual SC-CAES and use it as a test stand to study the possibilities that this technology offers. Throughout the duration of this work, multiple mechanical designs were considered for the target device and one was built along with necessary complementary mechanical, electrical and electronic devices using standard parts available on the market. Also a considerable amount of work was done on developing an effective control algorithm to ensure highest torque and efficiency achievable by the hardware is attained.

In order to evaluate the results of this study first the technical properties of the prototype are going to be reviewed. These parameters are summarized in table 8.1. Magni falls into diabatic CAES category and it does not store and recover the generated heat during the compression stage. Regarding this fact, the efficiency is very satisfying and shows promise for further study.

Table 8.1 Magni Technical properties

Parameter	Value	Parameter	Value
Nominal speed	60 rpm	Generated torque available in working pressure range	20 Nm
Operating pressure	3 to 7 bars	Max generated torque	32 Nm
Tank capacity	45 liter	Output power range	125W -220W
Roundtrip efficiency	39 %	Total available energy delivery	7 Wh

On the other hand the energy density is considerably low for a machine that occupies 0.3 cubic meters of space and is only able to deliver as little as a few Watt-hours. Magni is able to generate higher torques than the ranges stated in the table at the expense of efficiency which means using higher charge-phases resulting in venting pressurized air to the atmosphere. As a ESS this practice is not favorable however, in cases where this machine is used as an rpm regulation device, the ability counts as a positive feature. The tank used for this machine is relatively small and increasing the storage volume is expected to increase the total energy capacity linearly however this would not improve the energy density significantly.

8.1 Improvement Areas

While Magni is a machine that is able to successfully store energy in form of compressed air and recover it, its performance can be improved in many areas by taking proper measures. These areas and possible enhancements are as follows:

- **Efficiency:** During both compression and expansion stages, a considerable amount of torque is wasted only to overcome the internal friction of cylinders. Using components with lower friction will effectively improve the total efficiency of the system. Moreover adding means to store the generated heat during storage and reusing the same heat can increase the round-trip efficiency significantly.

- **Power Capacity:** Both Operating pressure and speed of this machine are significantly lower than the operational CAES power-plants. Increasing this parameters will boost the amount of deliverable power. Increasing the pressure range also will lead to higher temperatures in the system which leads to more effective heat storage in case the target is a AA-CAES.

- **Energy Density:** The remedies mentioned in the two previous items will also increase the ratio of stored energy to footprint of the device. In other words having higher efficiency and power delivery simply translates to more energy density.

8.2 Future Developments

Magni is a SC-CAES prototype made of widely available components on the market and building this machine was done without having to deal with tight manufacturing tolerances and high accuracy production procedures. The fact that this machine has achieved satisfactory performance as the first of its line shows promise that this technology can be developed to a completely working product usable in many applications including households, small factories, stand-alone wind-turbines, etc.

Further study to find more suitable components and implementing the improvements mentioned in this thesis will surely lead to higher performance and possibly lower costs in next iterations. In addition, next prototypes will shed light on more enhancement possibilities and writers of this are confident that next generations of this machine in near future are going to be finished products with high demand in today's market.

BIBLIOGRAPHY

[1] "Pneumatic fluid power determination of flowrate characteristics of components using compressible fluids," International Organization for Standardization, Geneva, Switzerland, Standard ISO 6358-1:2013(E), May 2013.

[2] A. M. Al-Ibrahim, *Transient air temperature and pressure measurements during the charging and discharging processes of an actuating pneumatic cylinder*. University of Wisconsin–Madison, 1991.

[3] E. Barbour, I. G. Wilson, I. G. Bryden, P. G. McGregor, P. A. Mulheran, and P. J. Hall, "Towards an objective method to compare energy storage technologies: development and validation of a model to determine the upper boundary of revenue available from electrical price arbitrage," *Energy & Environmental Science*, vol. 5, no. 1, pp. 5425–5436, 2012.

[4] G. Belforte, G. Mattiazzo, S. Mauro, and L. Tokashiki, "Measurement of friction force in pneumatic cylinders," *Tribotest*, vol. 10, no. 1, pp. 33–48, 2003.

[5] B. B. Boveri, "Huntorf air storage gas turbine power plant," *Energy Supply, Publication# D GK*, vol. 90202, 1983.

[6] T. K. Brekken, A. Yokochi, A. Von Jouanne, Z. Z. Yen, H. M. Hapke, and D. A. Halamay, "Optimal energy storage sizing and control for wind power applications," *IEEE Transactions on Sustainable Energy*, vol. 2, no. 1, pp. 69–77, 2011.

[7] H. Chen, T. N. Cong, W. Yang, C. Tan, Y. Li, and Y. Ding, "Progress in electrical energy storage system: A critical review," *Progress in Natural Science*, vol. 19, no. 3, pp. 291–312, 2009.

[8] K. Divya and J. Østergaard, "Battery energy storage technology for power systems: An overview," *Electric Power Systems Research*, vol. 79, no. 4, pp. 511–520, 2009.

[9] B. Dunn, H. Kamath, and J.-M. Tarascon, "Electrical energy storage for the grid: a battery of choices," *Science*, vol. 334, no. 6058, pp. 928–935, 2011.

[10] L. Evans, G. Guthrie, and A. Lu, "The role of storage in a competitive electricity market and the effects of climate change," *Energy Economics*, vol. 36, pp. 405–418, 2013.

[11] J. Goodwin and J. Derby, "Compressed air batteries," *Energetix. Gr*, 2011.

[12] E. Jannelli, M. Minutillo, A. L. Lavadera, and G. Falcucci, "A small-scale caes (compressed air energy storage) system for stand-alone renewable energy power plant for a radio base station: A sizing-design methodology," *Energy*, vol. 78, pp. 313–322, 2014.

[13] S. Koohi-Kamali, V. Tyagi, N. Rahim, N. Panwar, and H. Mokhlis, "Emergence of energy storage technologies as the solution for reliable operation of smart power systems: A review," *Renewable and Sustainable Energy Reviews*, vol. 25, pp. 135–165, 2013.

[14] C. Krupke, J. Wang, J. Clarke, and X. Luo, "Modeling and experimental study of a wind turbine system in hybrid connection with compressed air energy storage," *IEEE Transactions on Energy Conversion*, vol. 32, no. 1, pp. 137–145, 2017.

[15] H. Liu, J. Chen, and G. Tao, "Parameters identification and analysis of pneumatic cylinders friction model based on experiments," in *Symposium on Fluid Power*, vol. 2011, 2011.

[16] X. Luo, J. Wang, M. Dooner, and J. Clarke, "Overview of current development in electrical energy storage technologies and the application potential in power system operation," *Applied Energy*, vol. 137, pp. 511–536, 2015.

[17] X. Luo, J. Wang, M. Dooner, J. Clarke, and C. Krupke, "Overview of current development in compressed air energy storage technology," *Energy Procedia*, vol. 62, pp. 603–611, 2014.

[18] A. Poullikkas, "A comparative overview of large-scale battery systems for electricity storage," *Renewable and Sustainable Energy Reviews*, vol. 27, pp. 778–788, 2013.

[19] E. Richer and Y. Hurmuzlu, "A high performance pneumatic force actuator system: Part 1 - nonlinear mathematical model," *Journal of dynamic systems, measurement, and control*, vol. 122, no. 3, pp. 416–425, 2000.

[20] S. Samir, "Large energy storage systems handbook (compressed air energy storage), fs barnes and jg levine," pp. 112–152, 2011.

[21] R. Sebastián and R. P. Alzola, "Flywheel energy storage systems: Review and simulation for an isolated wind power system," *Renewable and Sustainable Energy Reviews*, vol. 16, no. 9, pp. 6803–6813, 2012.

[22] S. Succar, R. H. Williams, *et al.*, "Compressed air energy storage: theory, resources, and applications for wind power," *Princeton environmental institute report*, vol. 8, 2008.

[23] Z. Yang, J. Zhang, M. C. Kintner-Meyer, X. Lu, D. Choi, J. P. Lemmon, and J. Liu, "Electrochemical energy storage for green grid," *Chemical reviews*, vol. 111, no. 5, pp. 3577–3613, 2011.

[24] B. Zakeri and S. Syri, "Electrical energy storage systems: A comparative life cycle cost analysis," *Renewable and Sustainable Energy Reviews*, vol. 42, pp. 569–596, 2015.